Aus der Abteilung Experimetelle Pharmakologie, European Center for Angioscience,

der Medizinischen Fakultät Mannheim

(Direktor: Prof. Dr. Thomas Wieland)

Modulation of hERG channel in human-induced pluripotent stem cell-derived cardiomyocytes from a patient with short QT syndrome type 1

Inauguraldissertation

zur Erlangung des Doctor scientiarum humanarum (Dr. sc. hum.)

der

Medizinischen Fakultät Mannheim

der Ruprecht-Karls-Universität

zu

Heidelberg

vorgelegt von

Xin Li

aus

Sichuan, China

2021

Dekan: Prof. Dr. med. Sergij Goerdt

Referent: Prof. Dr. rer. nat.Thomas Wieland

CONTENTS

ABBREVIATIONS

AF: Atrial fibrillation

AP: Action potential

APA: Amplitude of action potential

APD: Action potential duration

APD50: Action potential duration at 50% repolarization

APD90: Action potential duration at 90% repolarization

ARVC: Arrhythmogenic right ventricular cardiomyopathy

BrS: Brugada syndrome

CCh: Carbachol

CHO: Chinese hamster ovary

Cm: Membrane capacitance

CRP: C-reactive protein

DAD: Delayed afterdepolarization

DCM: Dilated cardiomyopathy

EAD: Early afterdepolarization

EAG: *ether-à-go-go*

ECG: Electrocardiogram

ELK: eag-like K^+ channel

Epi: Epinephrine

ERG: eag-related gene

ESCs: Embryonic stem cells

HCM: Hypertrophic cardiomyopathy

HEK: Human embryonal kidney

hERG: Human ether a´-go-go-related gene

hESCs: Human embryonic stem cells

hiPSCs: Human-induced pluripotent stem cells

hiPSC-CMs: Human-induced pluripotent stem cell-derived cardiomyocytes

HQ: Hydroquinidine

ICD: Implantable cardioverter defibrillator

I_{Ca-L}: L-type calcium channel current

iPSCs: Induced pluripotent stem cells

I_{Na}: Sodium current

I_{NCX}: Na/Ca exchanger current

I_{K1}: Inward rectifier potassium channel current

I_{KATP}: ATP-sensitive potassium channel current

I_{Kr}: Rapidly activating delayed rectifier potassium current

I_{Ks}: Slowly activating delayed rectifier potassium current

I_{SK}: Calcium-activated small conductance potassium channel current

Iso: Isoprenaline

I/R: Ischemia/reperfusion

LPS: Lipopolysaccharide

LQTS: Long QT syndrome

NAC: N-Acetyl-L-cysteine

NADPH: Nicotinamide adenine dinucleotide phosphate

NCX: Na/Ca exchanger

PKA: Protein kinase A

PKC: Protein kinase C

QT: QT interval

QTc: QT interval (corrected)

ROS: Reactive oxygen species

RP: Resting potential

Rs: Series resistance

SCD: Sudden cardiac death

SQTS: Short QT syndrome

SQTS1: Short QT syndrome type 1

SQTS2: Short QT syndrome type 2

SQTS3: Short QT syndrome type 3

SQTS4: Short QT syndrome type 4

SQTS5: Short QT syndrome type 5

SQTS6: Short QT syndrome type 6

TTS: Takotsubo syndrome

Vmax: Maximal depolarization velocity of action potential

VF: Ventricular fibrillation

VT: Ventricular tachycardia

WT: Wild type

1. INTRODUCTION

1.1. Short QT syndrome

Short QT syndrome (SQTS) is a rare, genetic channelopathy representing short QT interval (QTc) and sudden cardiac death (SCD). The first clinical cases of the SQTS were reported in 2000, showing that four patients with short QT interval suffered from atrial fibrillation (AF) and/or SCD caused by ventricular tachycardia (VT) or ventricular fibrillation (VF) [1]. SQTS is diagnosed usually in asymptomatic adults with a family history of SCD. About 250 cases and nearly 200 families worldwide have been reported [2]. Due to the limited number of reported cases and the possibility of overlooking SQTS cases, the real prevalence of SQTS is difficult to be determined in the world population. However, recent studies suggest a prevalence between 0.02 and 0.1% in adults and 0.05% in pediatric population [3]. Iribarren et al. stated that the prevalence of short QT interval (<300 ms) in Africa Americans was highest (5.8 per 100,000), followed by Caucasians (3.2 per 100,000), Latinos (1.8 per 100,000), and Asian/Pacific Islanders (1.6 per 100,000 persons)[4]. Lethal events may occur in both genders, but a slight male predominance probably exists. Data from analyzing 145 patients diagnosed with SQTS between 2000 and 2017 showed that male patients presented syncope more often than females [5]. This suggests that higher testosterone levels in male may contribute to QTc interval regulation [6, 7]. Arrhythmogenic events associated with SQTS were documented in ages from infants to 80-year-old patients, but the first year of life seems to be the most risk with a 4% rate of cardiac arrest [2, 8]. The chance of a first syncope, is nearly 40% by age 40. It was suggested that there exist two high-risk peaks of SCD: (1) in the first year of life and (2) from 20 to 40 years old [9].

Clinical manifestations associated with SQTS include asymptomatic (around 40% of cases) feature, dizziness, AF, ventricular arrhythmias, syncope and even SCD [2]. Clinical symptoms may be severe, especially in children, and can cause SCD in infants. Since it is a genetic disease, diagnosed patients frequently have a family history of syncope or SCD in a young, first or second-degree relative [2]. Hence, clinical examination is recommended in all family members. Asymptomatic patients carrying a pathogenic variant associated with SQTS are also at high risk because the first manifestation of the disease can be the SCD [2, 10].

The SQTS diagnosis criteria have been debated since the last decade. The main question in clinical diagnosis is how to define the cut off value at the lower end of the QTc. In guidelines/consensus established in 2011 [11] and 2013 [12], the SQTS was defined as: "*a genetic arrhythmogenic disorder characterized by a short and uniform QT/QTc intervals (<330 ms) on the ECG, with absent or minimal ST segments, with an interval from J point to T wave peak (Jp-Tp) measured in the precordial lead with the T wave of greatest amplitude<120 ms, possible tall T waves with narrow base similar to the T wave of moderate hyperkalemia ("desert tent T waves"), frequent early repolarization pattern, prolongation of T peak-T end interval, and possible presence of prominent U waves in the absence of structural heart disease and others disturbances that cause repolarization abnormalities*" [2]. Currently, according to the European Society of Cardiology (ESC) guidelines in 2015 [13], a clinical diagnosis of SQTS can be made by a QTc<340 ms, or a QTc≤360 ms accompanied by one or more of the following: A. a confirmed pathogenic mutation; B. a family history of SQTS; C. a family history of sudden death at age 40 years; D. survival from a VT/VF episode in the absence of heart disease. Importantly, SQTS could be overlooked in ECG, therefore caution is required, especially in case of unclear syncope, arrhythmia, or the presence of paroxysmal or persistent atrial fibrillation in young patients [14].

For the treatment of SQTS, implantable cardioverter defibrillator (ICD) is the first choice for prevention and treatment of SCD in SQTS patients. It is recommended for those, who are surviving cardiac arrest or at high risk of SCD. However, ICD has numerus disadvantages, such as an increased risk of inappropriate shock due to sinus tachycardia, T-wave oversensing or lead failure and AF [15-17]. Therefore, drug therapy is required, especially for young patients who rejected or are contraindicated with ICD implantation, as an alternative therapy.

So far, a few drugs such as disopyramide, nifekalant, quinidine, flecainide, sotalol, ibutilide and propafenone have been used in vivo studies on SQTS [18], among which only quinidine was shown to be effective for the treatment [19-23]. Hydroquinidine (HQ) was shown to prolong the QTc interval and to be effective in preventing ventricular tachyarrhythmias during long-term follow-up [20, 23, 24]. It can be considered in SQTS patients, who refuse to receive or cannot receive ICD.

Roles of genetic mutations and pathophysiological mechanisms that underlie the SQTS development remain unclear. The ability to identify specific gene mutations in individual cases of SQTS is of great importance in determining causality and potential treatments. SQTS is inherited autosomal dominant with genetic heterogeneity. So far, different types of SQTS have been described. Three genes encoding potassium channels (KCNH2, KCNQ1, KCNJ2) and three genes encoding calcium channels (CACNA1C, CACNB2, CACNA2D1) were found to be associated with SQTS, which are called SQTS type 1 to 6, respectively [8]. In addition, SCN5A gene was also linked to a subclinical phenotype Brugada syndrome (BrS) and short QT interval in ECG [25]. This was described as SQTS7 [2, 23, 26]. In 2017, Thorsen et al described a mutation in the anion exchanger Solute Carrier Family 4 Member 3 (SLC4A3) gene, encoding a Cl^-, HCO_3^- exchanger (AE3), as a novel genetic etiology for SQTS [27]. This mutation could change the function of AE3 and increase intracellular pH (pHi) and reduce intracellular Cl^- concentration ($[Cl^-]i$). High pHi and low $[Cl^-]i$ shorten cardiac action potential in zebrafish embryos [28], which confirmed functional association of AE3 with SQTS. Currently, although a large number of mutations have been reported to be possibly related to SQTS, only a small part of them have been investigated experimentally to explore their functional significance. Using data from the literature, Campuzano et al. analyzed the significance of all reported gene variants detected in SQTS-patients and revealed that only 28.12% of reported variants has a conclusive pathogenic role for SQTS [29].

SQTS type 1 (SQTS1) is the most frequently described form. SQTS1 was firstly reported by studying three families with hereditary SQTS in 2004 [30]. In the three families, 2 different missense mutations that lead to the same amino acid change (N588K) at the S5-Pore loop region of the cardiac hERG (KCNH2) channel were detected. The genetic mutations in hERG attenuate the inactivation and increase hERG channel current (I_{Kr}) leading to shortening of the repolarization and QT intervals [29, 31]. A second mutation (C1853T) in the KCNH2 gene, resulting in an amino acid change of T618I, was found in a Chinese family with a markedly short QT interval (QTc=316 ± 9 ms) and a strong family history of sudden death [32]. Both mutations cause a gain-of-function (an increase in channel current) of hERG channels.

SQTS type 2 (SQTS2) is caused by a gain-of-function mutation in KCNQ1 gene encoding slowly activating delayed rectifier K channel (I_{Ks}). A mutation with the G>C

substitution at nucleotide 919 in the KCNQ1 gene, which results in the substitution of the valine at position 307 by leucine (V307L), was detected in SQTS2-patients [33]. Another mutation, KCNQ1-V141M, was linked to APD-shortening and bradyarrhythmia [34, 35]. An additional rare variant R259H has been identified as being potentially associated with SQTS 2 [36].

Inward rectifier potassium (I_{K1}, Kir2) channels are linked to SQTS type 3 (SQTS3). Priori et al. reported this form of SQTS, which was associated with a D172N substitution in the Kir2.1 channel and characterized by asymmetrical T waves. The mutation in the KCNJ2 gene (encoding Kir2 channels) significantly increases the outward component of I_{K1}, which was exhibited by transfecting Chinese Hamster Ovarian (CHO) cells with Kir2.1 WT- or D172N-mutant DNA [37]. Furthermore, another KCNJ2 gain-of-function mutation, M301K, was also shown to be associated with SQTS3 [38]. In addition, it was described that the E299V mutation and the V93I mutation in KCNJ2 gene are associated with AF but not with VT/VF in SQTS, although the reason for these findings needs to be further analyzed [39-41].

SQTS type 4-6 (SQTS4 and SQTS5 and SQTS6) are caused by loss-of-function of L-type Ca^{2+} channels. In 2007, Antzelevitch et al. reported missense mutations in CACNA1C (A39V and G490R) gene coding the α subunit and CACNB2b (S481L) gene coding the β subunit of the Ca^{2+} channel as being linked to SQTS type 4 and SQTS type 5 overlapped with Brugada syndrome (BrS) [2, 42]. In 2011, Templin et al identified SQTS type 6 (SQTS 6) as being related to a variant in CACNA2D1 gene encoding the ɣ-subunit of the voltage-dependent L-type Ca^{2+} channel. They found that the heterozygous transition c.2264G>C in CACNA2D1 gene predicting replacement of serine by threonine at position 755 (p.Ser755Thr) is associated with SQTS [43].

A mixed SQTS and BrS phenotype caused by a heterozygous missense mutation R689H in SCN5A gene was first reported in 2012 [25]. The patient with a short QT interval (QT of 320 ms at 71 beats min^{-1}) was found to have a Brugada-like ECG and biophysical analysis showed that SCN5A protein containing the R689H mutation was unable to mediate I_{Na}, indicating loss-of-function of Na$^+$ channels. However, there is no conclusive data with respect to the association of this variant with SQTS.

In spite of rapid progress in searching for genetic factors in SQTS, a convincing proof of genotype-phenotype correlation remains lacking for most SQTS forms. Functional roles of most gene mutations or variants associated with SQTS have not clarified. Of note, only around 30% SQTS-patients have been proven to carry the disease-associated gene mutation and arrhythmias appear only under certain conditions even in patients carrying a clear pathogenic mutation, suggesting roles of environmental factors. Studies regarding roles of environmental factors in occurrence of arrhythmias of SQTS remain spars. Whether the SQTS-associated mutation can influence effects of environmental factors in cardiac electrophysiology is unknown.

Since SQTS1 results from an increased (a gain-of-function) hERG channel (I_{Kr}) current, an I_{Kr} inhibitor should prolong QT interval or suppress the occurrence of arrhythmias in SQTS1-patients. However, some typical I_{Kr} inhibitors such as sotalol and ibutilide showed no effect on QTc in SQTS1-patients [23, 24], indicating possible roles of the I_{Kr} channel mutation for drug drugs. It is known that some drugs like sotalol and ibutilide exert effect on I_{Kr} only when the channel is inactivated and the mutation leads to an inactivation defect and in turn decrease drug effects on I_{Kr} [44]. Quinidine has effects on both the activated and inactivated I_{Kr} channels and can still reduce I_{Kr} even when the channel inactivation is impaired. Hence, several studies investigated influences of mutations on channel sensitivity and/or affinity of hERG channels to drugs, but the change of sensitivity may not be the only reason for the change of drug effects. For instance, amiodarone, propafenone and quinidine suppressed N588K-I_{Kr} with a similar efficacy, but only quinidine can prolong APD/QTc or reduce arrhythmic events in SQTS1-patients or SQTS1-cardiomyocytes [44, 45], suggesting that extra mechanisms might also play critical roles for drug effect in SQTS1-patients. Thus, we expect that besides the drug affinity the channel gating kinetics may be also critical for the efficacy of a drug. It is known that the N588K mutation in the I_{Kr} channel can change drug effects by impairing the channel inactivation, but it is not known whether N588K also change other gating parameters of I_{Kr} and in turn change drug effects.

1.2. The hERG channel

The *ether-à-go-go* (EAG; Kv10–Kv12) channels encoded by KCNH genes belong to a superfamily of voltage-gated K⁺ channels (figure 1A). The EAG gene was first discovered in *Drosophila melanogaster* [46, 47]. It was identified in a mutant that exhibited

rhythmic leg shaking under ether anesthesia, reminiscent of a go-go dance [47, 48]. Thereafter, eight mammalian EAG channel subtypes encoded by the *KCNH* gene family have been discovered (figure 1A) [46]. According to sequence similarities, the EAG channels were divided into three subfamilies including two EAG (Kv10), three ERG (eag-related gene; Kv11) and three ELK (eag-like K$^+$ channel; Kv12) channel members [49]. The diversity of EAG channels can be increased further by the formation of heteromeric channels, which is possible within each subfamily [46, 50-52]. The human ether a´-go-go-related gene (hERG or KCNH2) was originally cloned from a human hippocampal cDNA library by homology to Drosophila EAG [49]. The hERG gene encodes the pore-forming subunit of the rapidly activating delayed rectifier potassium channel (I_{Kr}, also called hERG or Kv11.1 channel).
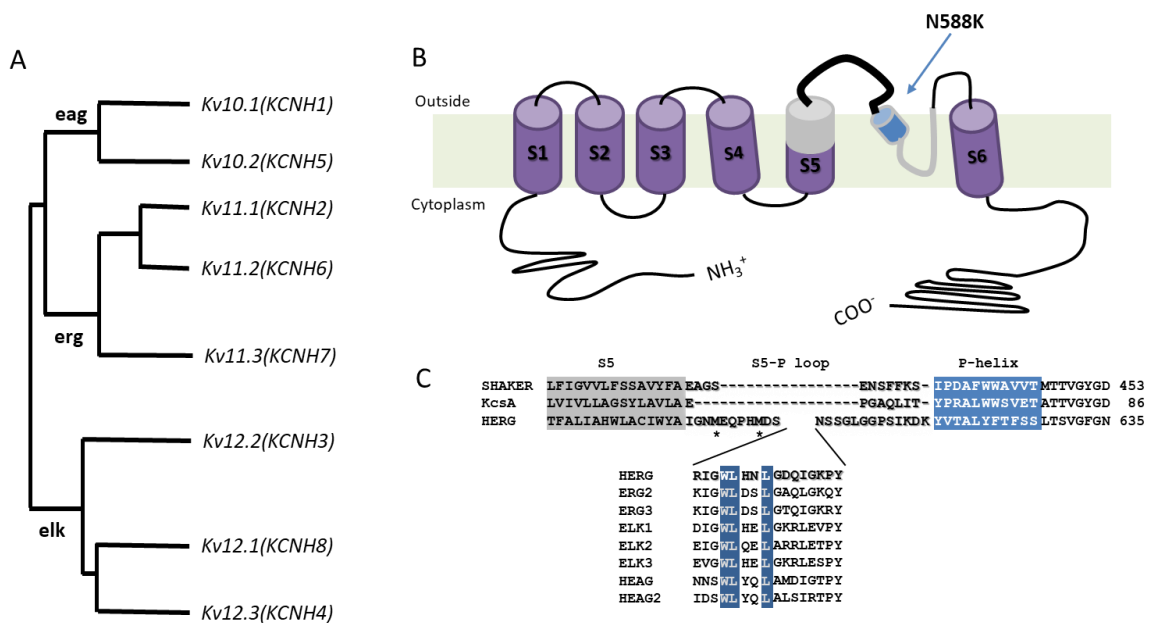
Figure 1. (A) Phylogenetic tree of the EAG superfamily members. (B) The hERG structure. (C) The sequence of pore region of hERG channel comparing with other channels.

The hERG channel is mainly expressed in cardiac tissue, but exists also in other tissues including the hippocampus neurons [49], jejunal smooth muscle [53] and pancreatic β-cells [54]. In addition, increasing evidences show that hERG is up-regulated in several animal and human tumors and tumor cell lines [55, 56].

The hERG channel plays a critical role in the repolarization of cardiac action potentials (APs) [57, 58]. The ventricular action potential duration (APD) reflects the QT interval (QT) on an electrocardiogram (ECG). Inhibition of hERG channel current can prolong APD/QT and lead to LQTS, which may cause fatal ventricular arrhythmia torsades de pointes and sudden death [59, 60]. Numerus loss-of-function mutations in hERG have been detected in humans, which reduce the hERG current and lead to type 2 genetic LQTS [61]. Inhibition of hERG channel current may also cause acquired LQTS. For instance, many drugs can inhibit hERG and hence lead to drug-induced LQTS [59]. Moreover, a reduction in the serum K^+ concentration (hypokalemia) can suppress hERG function and expression, resulting in LQTS [62]. On the other hand, gain-of-function mutations in hERG channel have been identified SQTS-patients [2]. Increase in hERG channel current, either by genetic factors or environmental factors or by drugs, can shorten APD/QT and cause SQTS, either genic or acquired.

The hERG channel is a member of the family of voltage-gated potassium channels, which contain six transmembrane segments (S1–S6) and a pore helix that is interposed between S5 and S6 (figure 1 B). The positively charged S4 acts as the voltage sensor for the channel activation [49, 63]. Unlike other members of the voltage-gated K^+ channel family, the hERG channel possess the feature of slow activation, very rapid voltage-dependent inactivation and rapid recovery from inactivation [57, 64, 65]. Four hERG α-subunits assemble with a modulatory subunit MiRP1 (encoded by KCNE2, stoichiometry unknown) to form a functional channel, which underlie the rapidly activating delayed rectifier potassium current (I_{Kr}). The hERG channel functions as an inward rectifier, i.e., it conducts small outward currents at but large inward currents [63].

The inactivation of the hERG channel is caused by conformational changes in the outer pore region [65-67] and involves so-called "collapse of the pore" [63, 68]. The pore region of hERG, including the pore helix, a selectivity filter, and S6, is highly homologous to that of other members of the voltage-dependent K^+ channel family [49, 69] and also to the bacterial K^+ channel KcsA (figure 1 B-C) [67, 70]. This feature provides the possibility to construct homology models of hERG channels based on the KcsA structure [70]. However, the extracellular loop connecting the pore helix to the top of S5 (S5-pore loop) in hERG is very different from that in other voltage-dependent K^+ channel family members. First, the S5-pore linker of the hERG channel is unusually long (43 amino

acids) compared with the linkers of other voltage-gated K⁺ channels (10–23 amino acids) [63, 71]. Second, many mutations in the S5-pore loop disrupt the inactivation process in hERG [67, 72]. Third, it possesses the binding site for scorpion toxins (*e.g.* BeKm-1) that selectively block hERG channel [73]. Therefore, the S5-pore loop of hERG is a critical region of the protein for channel functions.

Numerous genetic mutations in hERG gene have been reported as possible modulator of hERG channels. Most mutations were identified in patients with long QT syndrome (LQTS) [74]. The mutations detected in LQTS-patients are associated with a change called loss-of-function of the channel, i.e., a reduction of the hERG channel current, which prolong APD in cardiomyocytes and QT interval in ECG. Some mutations such as N588K[30], T6181[31, 32], R1135H[75], Glu50Asp[76], I560T[34] in hERG gene have been identified in SQTS patients. Functional studies showed that these mutations increased the hERG channel current, implying they lead to gain-of-function of hERG channel.

Besides genetic mutations, the hERG channel can be regulated by some intracellular signaling factors. It was shown that PKA and PKC activation can inhibit the hERG channel current, but not through phosphorylation of the channel, instead, through ROS-induced signaling [77]. However, other studies showed that the inhibition was mediated by direct phosphorylation of the channel protein [78-80]. On the contrary, it was also shown that PKA activation by cAMP can enhance hERG channel current by phosphorylation of the channel [81]. It was shown that diacylglycerol potently inhibited the hERG current, which is mediated by a protein kinase C-evoked endocytosis of the channel protein and dependent on the dynein-dynamin complex [82]. High-glucose caused hERG channel deficiency via the inhibition of channel trafficking [83]. Data showed that hERG channels interact with caveolin-1 and are negatively regulated by this interaction [84]. It was reported that when hERG channels were expressed in Xenopus oocytes with β-catenin, a multifunctional protein regulating the expression of a wide variety of genes relevant for cell proliferation and cell survival, the hERG channel activity and protein level in cell membrane were enhanced [85]. Hypoxia can reduce hERG channel current and mature hERG channel expression through calpain up-regulation [86]. Extracellular pH value can modulate hERG channel gating kinetics [87, 88]. The body temperature can also change the hERG channel gating [89, 90]. Besides, many drugs target the hERG channel, inhibit hERG channel current, and lead to acquired LQTS [91]. Drug-induced SQTS has been rarely reported [92, 93]. Together, the

hERG channel can be modulated by some environmental factors via either direct effect on the channel or indirect regulation through different intracellular signaling. However, whether and how a genetic mutation can influence the regulation of hERG channels by environmental factors are unclear so far.

1.3. Human-induced pluripotent stem cell-derived cardiomyocytes

Embryonic stem cells (ESC), a type of cells with properties of self-renewal and pluripotency, were reported for the first time in the study of Evans et al. in 1981 [94]. ESCs were successfully derived from human blastocysts in 1998 [95]. Although ESCs provide advantages for basic researches and clinical applications, destroying the early embryos in the process of ESC preparation causes ethical problems. In addition, the tissue rejection also limits the use of human ESCs. Shinya Yamanaka's research group improved the situation by generating induced pluripotent stem (iPS) cells. They found that somatic cells from mice and humans could be reprogrammed to a pluripotent state through introduction of four transcription factors (OCT-4, SOX-2, KLF-4 and C-MYC) [96, 97]. The iPS cells generated from somatic cells possess the properties of unlimited self-renewal and pluripotency character like ESCs, and they avoid the ethical issues caused by embryo destruction and may reduce tissue rejection by using iPSC cells generated from the same patient. Nowadays, iPS cells that can differentiate to specific cell types are commonly used in studies in different fields by different differentiation methods.

In 2008, Narazaki et al successfully differentiated iPS cells into cardiomyocytes [98]. Since then, human iPS cell-derived cardiomyocytes (hiPSC-CMs) have been wildly used for studies regarding disease modeling, pathogenesis and drug testing for toxic or therapeutic effects. hiPSC-CMs possess properties and ion channel expression profiles similar to native cardiomyocytes [99]. Strikingly, they can recapitulate some important features of some cardiac diseases such as long QT syndrome (LQTS) [100, 101], Brugada syndrome (BrS) [15, 102, 103], arrhythmogenic right ventricular cardiomyopathy (ARVC) [104, 105], dilated cardiomyopathy (DCM) [106], hypertrophic cardiomyopathy (HCM) [107], Takotsubo syndrome (TTS) [108] and septic cardiomyopathy [109]. Hence, hiPSC-CMs provide a good opportunity for studying human cardiomyocyte properties in cell culture models, including physiology, pathophysiology and drug testing.

Human mature cardiomyocytes are optimal for studying ion channel functions or their roles for human heart diseases. However, the availability and ethical issues limit the experimental studies using human cardiomyocytes, especially, the ventricular cardiomyocytes. Therefore, animal models or animal cells have been widely used for such studies. Given the differences between humans and animals, animals or animal cells are far from optimal for studying human cardiac diseases. Besides animal cells, some heterologous expression systems, like HEK293, CHO and HeLa cells, have been employed for studying ion channel functions [110, 111]. These non-cardiac cells are also far from being optimal as they cannot generate APs and they obviously lack some signaling proteins that are important for regulating ion channel functions in cardiomyocytes. Therefore, in this study we used hiPSC-CMs as the most relevant study platform.

1.4. Aims of the Study

Since the modulation of hERG channel gating kinetics by the mutation of N588K and the influence of the mutation on the channel modulation by environmental factors are unclear, we hypothesized that (1) the mutation N588K detected in the SQTS patient might affect the channel gating in addition to the inactivation, (2) the mutation might enhance modulatory effects of some environmental factors and (3) the mutation might change some drug effects on hERG channel gating kinetics.

To test our hypotheses, we designed the experimental setups to investigate:

(1) The hERG channel gating kinetics in hiPSC-CMs from healthy donors and a SQTS-patient carrying the mutation N588K in the hERG channel.

(2) The modulation of the hERG channel current and gating kinetics by some environmental factors in hiPSC-CMs from healthy donors and the SQTS-patient carrying the mutation N588K in the hERG channel.

(3) The Influence of the N588K mutation on drug effects with respect to hERG channel gating kinetics.

In general, the study aimed to clarify whether a) the N588K mutation change hERG channel gating kinetics besides inactivation, b) whether some important factors including adrenergic and muscarinic stimulation, frequency, pH value, hyperthermia

and inflammatory factors can modulate hERG channel current and gating, c) whether the mutation change the modulation of hERG channel by environmental factors and d) whether the mutation change drug effects on hERG channel gating kinetics. Thus, the study may provide new insights into the arrhythmogenic potential of hERG channels and might identify new therapeutic targets for the treatment of SQTS1.

2. METHODS AND MATERIALS

2.1. Ethics statement

The written informed consents were obtained before skin biopsies from the healthy donors and SQTS1-patient. The study was approved by the Ethical Committee of the Medical Faculty Mannheim, University of Heidelberg (approval number: 2018-565N-MA) and by the Ethical Committee of University Medical Center Göttingen (approval number: 10/9/15). The study was performed following the approved guidelines and conducted in accordance with the Helsinki Declaration of 1975, as revised in 1983.

2.2. Study design

To investigate possible modulations of hERG channel gating kinetics in SQTS1-hiPSC-CMs, the flowing experiments were designed (figure 2). First, the hERG channel current and gating kinetics were analyzed in healthy donor cells (D-hiPSC-CMs) and SQTS1-hiPSC-CMs to explore the modulation of hERG channel gating by the mutation N588K. Second, possible regulatory effects of some environmental factors including adrenergic and muscarinic stimulator, frequency, pH value, hyperthermia and inflammatory factors on hERG channel gating were investigated and compared between healthy and diseased cells to explore roles of the mutation for the channel modulation by environmental factors. Third, drug (quinidine, ivabradine, ajmaline, amiodarone, mexiletine, flecainide and ranolazine) effects on hERG channel gating were investigated and compared between healthy and diseased cells to explore roles of the mutation on drug effects.
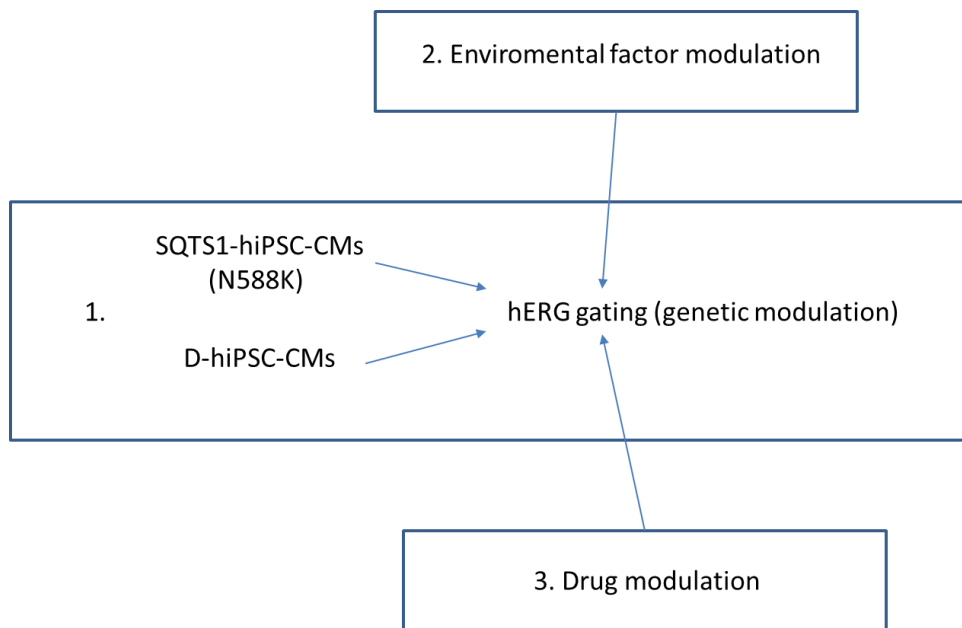
Figure 2. Schematic plan of the study.

2.3. Generation of human iPS cells

The human induced pluripotent stem cells (hiPSCs) were generated from primary human fibroblasts derived from skin biopsies. The hiPSC line from healthy donor 1 (D1) was generated by using lentiviral particles carrying the transactivator rtTA and an inducible polycistronic cassette containing the reprogramming factors OCT4, SOX2, KLF4, and c-MYC. The hiPSC lines from healthy donor 2 (D2) and donor 3 (D3) were generated in feeder-free culture conditions using the integration-free episomal 4-in-1 CoMiP reprogramming plasmid (Addgene, #63726) with the reprogramming factors OCT4, KLF4, SOX2, c-MYC, and short hairpin RNA against p53, as previously described with modifications [112]. Generated hiPSCs were cultured under feeder free conditions. For examining the pluripotency, hiPSCs were subjected to a teratoma-formation assay.

The SQTS1 cell lines were generated from fibroblasts from a patient with SQTS carrying the mutation N588K in hERG channel. Three hiPSC lines isSTQSa1.7 (GOEi091-A.7, the SQTS1 cell line used in the study), isSQTSa1.8 (GOEi091-A.8) and isSQTSa1.15 (GOEi091-A.15) were generated from fibroblasts with the integration-free CytoTune-iPS 2.0 Sendai Reprogramming Kit (Thermo Fisher Scientific, #A16517) containing the reprogramming factors OCT4, KLF4, SOX2, c-MYC following

manufacturer's instructions with some modifications. Shortly, 1.5×10^4 early passage fibroblasts were plated in two wells of a Matrigel-coated 24-well plate with HFBM medium two days before transduction. Cells were transduced at 40-50% confluence with Sendai virus cocktail (hKOS: hc-Myc: hKlf4) at a MOI of 10:10:6 depending on the counted cell number of extra well (typically 2.5×10^4 cells/well) in HFBM. Virus was removed after 24 h and HFBM was changed every two days.

At day 7 after transduction/transfection, cells were replated in different density in Matrigel-coated 6-well plates in HFBM supplemented with 500 µM sodium butyrate and 2 µM Thiazovivin. From day 8 on, medium was changed to E8 medium (Thermo Fisher Scientific, #A1517001) supplemented with 500 µM sodium butyrate (day 8-day 11) and the medium was changed every day. Cells were detected for morphology change and appearance of colonies (typically after 2-3 weeks). Individual colonies with iPSC-like morphology were picked mechanically in Matrigel-coated 12-well plates in E8 medium supplemented with 2 µM Thiazovivin. Generated iPSC lines were passaged with Versene solution (Thermo Fisher Scientific, #15040066) and cultured in E8 medium supplemented with 2 µM Thiazovivin. After at least ten passages, iPSC cells were used for pluripotency characterization and differentiation experiments.

To examine pluripotent characteristics of generated hiPSCs, cell morphology, alkaline phosphatase activity, expression of endogenous pluripotency markers and spontaneous differentiation potential were assessed. The hiPSC lines from the healthy donor and SQTS1 patient displayed a typical morphology for human pluripotent stem cells and were positive for alkaline phosphatase. Comparing with fibroblasts, generated hiPSC lines showed expression of endogenous pluripotency markers SOX2, OCT4, NANOG, LIN28, FOXD3 and GDF3 at mRNA level measured by RT-PCR. Human embryonic stem cells (hESCs) were used as positive control, mouse embryonic fibroblasts (MEFs) were used as negative control. The expression of pluripotency markers OCT4, SOX2, NANOG, LIN28, SSEA4 and TRA-1-60 was detected in generated iPSC lines. Spontaneous differentiation potential of iPSC lines was examined by embryoid body (EB) formation. Germ layer-specific genes like α-fetoprotein (AFP) and albumin (ALB) (endoderm), cTnT and α-MHC (mesoderm), and tyrosine hydroxylase (TH) and MAP2 (ectoderm) were detected in a developmental manner during differentiation of EBs (days 0, 8, or 8+25), while endogenous OCT4 expression was reduced during spontaneous differentiation. Immunocytochemical

staining of spontaneously differentiated hiPSC lines showed expression of endodermal marker AFP, mesodermal-specific α-SMA and ectodermal βIII-tubulin. All data together confirmed the pluripotency and differentiation potential of generated hiPSCs.

The above process was conducted in the Stem Cell Unit, Clinic for Cardiology and Pneumology, University Medical Center Göttingen. The iPS cell lines were then transported to our lab and stored in the liquid nitrogen tank.

2.4. Generation of hiPSC-CMs

Frozen aliquots of hiPSCs were thawed and cultured without feeder cells and differentiated into hiPSC-CMs as described with some modifications [113].

For the differentiation, the following steps were performed.

One day before thawing cells, a T-25 flask coated with Matrigel was put in the incubator.

Mix medium (13 ml E8 medium + 6.5 ul from 10 mM stock solution of Rock inhibitor) was prepared. 2.5ml mix medium was added in the T-25 flask and put into incubator. Frozen hiPS cells were taken out from liquid nitrogen tank and thawed in hand until only small lumps of ice exist. Then, the cell suspension was transferred to a 50 ml-falcon prepared with 5 ml of mixed medium. The cell suspension was centrifuged at 250 x g (1200 rpm), 4 min, 20 °C. The supernatant was discarded and 2.5 ml mix medium was added. After 4x pipetting up and down, the cell suspension was transferred into the T-25 flask with 2.5 ml mix medium. The flask stayed into incubator until the next day.

On the next day, the medium in T-25 flask was changed to E8 medium without ROCK inhibitor. Then, the E8 medium was changed every two days. 2 to 4 days later, when cells reached 85-95% confluence, the differentiation was started.

First, cells were treated with EDTA and dissolved in E8 Medium. Then, the cells were counted and plated on Matrigel / Geltrex coated plates (optimal cell density for plating is cell line dependent; 15.000 cells/cm^2 - 26.000 cells/cm^2 = 150.000-260.000 cells per 6-well). Lastly, E8 medium was added to final volume (3 ml per 6-well with 5 µM ROCK inhibitor). The plate was shaken and then incubated at 37°C with 5% CO_2.

Day -x to -1: daily medium change with E8 medium was performed.

Day 0: when cell density reached 85-95% confluence, the medium was changed to cardiac medium (consisting of RPMI, 1% sodium pyruvate, 1% Pen / Strep, 2% B27 and 200 uM ASC) freshly enforced with 1 uM CHIR, 5 ng / ml BMP4, 9 ng / ml activin A, 5 ng / ml FGF.

Day 2: after around 48h, the medium was changed to cardiac medium freshly enforced with 5 uM IWP4.

Day 4 and later: the medium was changed every 2-3 days to cardiac medium only.

Normally, on day 8 of differentiation some cells start to beat.

Day 13: the cardiac medium was changed to selection medium (consisting of RPMI without glucose and glutamine ,1% Pen / Strep) freshly added with 440 mM Sodium Lactate Stock and 50 mM 2-mercaptoethanol. The selection medium was changed every day for 4-7 days.

Day 18: the selection medium was changed to cardiac medium (consisting of RPMI, 1% sodium pyruvate, 1% Pen / Strep, 2% B27 and 200 uM ASC) and then the cardiac medium was changed every 2-3 days.

From Day 40: cells were ready for experiments.

2.5. Calcium transient measurement

To measure the intracellular Ca^{2+} transients, cells were loaded with the fluorescent Ca^{2+}-indicator Fluo-3 AM. First, 1.5 ml PSS (see below) was added into a petri dish with hiPSC-CMs cultured for 2 to 4 days. The following steps were executed in a dark room due to the light sensitivity of the fluorescent Ca^{2+} indicator Fluo-3. 50 μg of the membrane permeable acetoxymethyl ester derivative of Fluo-3 (Fluo-3 AM) was dissolved in 44 μl of the Pluronic F-127 stock solution (20% w/v in DMSO) to get a 1 mM Fluo-3 AM stock solution, which can be stored at -20 °C for a maximum of 1 week. Next, 15 μl of the Fluo-3 AM stock solution were added into 1.5 ml PSS resulting in a final concentration of 10 μM Fluo-3 and the dish was agitated carefully. The cells were incubated at room temperature for 10 minutes. Thereafter, the PSS was carefully sucked out and discarded and the cells were washed with PSS for 4-5 times. Finally, the cells in PSS were kept at room temperature for about 30 minutes for de-

esterification before measurements. After de-esterification, the fluorescence of the cells was measured by using Cairn Optoscan calcium imaging system (Cairn Research, UK). The fluorescence is excited by 488 nm and emitted at 520 nm. The rhythm of calcium transients and arrhythmic events like EAD (early afterdepolarization)- or DAD (delayed afterdepolarization)-like or trigger activity events were analyzed. The measurement was carried out at 37°C.

2.6. Single cell contraction measurement

Single-cell shortening was recorded by a single cell contraction system (MyoCam-S™ ION OPTIK). The shortening of spontaneously beating cells was recorded in PSS (see below) at 37°C. To enhance the occurrence of arrhythmic events, epinephrine of 300 µM was added, which can more frequently induce arrhythmic events. The rhythm and arrhythmic events like extrasystoles, EAD-or DAD-like events were analyzed in absence and presence of a drug.

2.7. Patch-clamp

Whole-cell patch clamp recording was used to measure the action potentials (APs) and hERG channel current (I_{Kr}). Borosilicate glass capillaries (MTW 150F; world Precision Instruments, Inc., Sarasota, FL) were pulled to form patch electrodes by using a DMZ-Universal Puller (Zeitz-Instrumente Vertriebs GmbH, Martinsried, Germany) and then filled with pipette solution (see below) before measurements. Current and AP recordings were performed at 37 °C with an EPC-7 amplifier (HEKA Elektronik), connected via a 16-bit A/D interface to a Pentium IBM clone computer. The signals were sample at 5 kHz after low-pass filtered at 1 kHz. The ISO-3 multitasking patch-clamp program (MFK M. Friedrich) was used for data acquisition and analysis.

To establish whole-cell recording configurations, patch-pipettes with resistances ranged from 1–2 MΩ (for current measurements) and 3-4 MΩ (for AP-measurements) were used. The electrode offset potentials were zero-adjusted before the patch pipette touched the cell. After the patch pipette was slowly moved on the cell surface by a micromanipulator, a gentle suction was given to obtain high-resistance (Giga-Ohm) seal between cell membrane and the pipette wall (Giga-seal). Then, the fast capacitance current was compensated and the membrane in the pipette tip was disrupted by a stronger suction to establish the whole-cell configuration. In order to

examine the cell capacitance, a voltage pulse from −80 to −85 was given to record the capacitance transient current for calculating the membrane capacitance (Cm). Thereafter, the Cm and series resistance (Rs) were compensated (60–80%). The liquid junction potentials were not corrected. To reduce the influence of rundown of recorded currents on experimental results, we carefully checked the time-dependent change of ion channel currents. Recordings were started when currents reached a steady state, normally within 1 to 3 minutes.

APs were recorded in the current-clamp mode. The duration of APs at 50% (APD50) and 90% repolarization (APD90) were analyzed (figure 3).
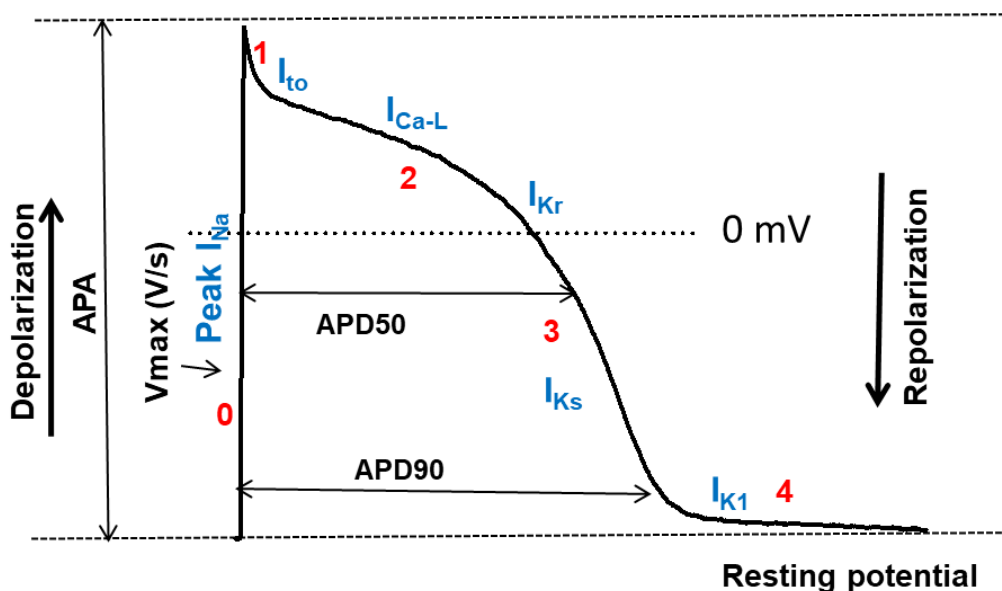
Figure 3. Parameters and corresponding ion channel currents in action potentials. The numbers in red present the phases of action potentials, 0 (phase 0), 1 (phase 1), 2 (phase 2), 3 (phase 3) and 4 (phase 4). APA: amplitude of action potentials. Vmax: the maximal velocity of depolarization. APD50: action potential duration at 50% repolarization. APD90: action potential duration at 90% repolarization. I_{Na}: peak Na$^+$ channel current. I_{Ca-L}: L-type Ca^{2+} channel current. I_{to}: transient outward K$^+$ channel

current. I_{Kr}: rapidly activating delayed rectifier K$^+$ channel (hERG) current. I_{Ks}: slowly activating delayed rectifier K$^+$ channel current. I_{K1}: inward rectifier K$^+$ channel current.

The action potential is divided into five phases, which contain contributions of different ion channel currents (figure 3). Phase 0 is a rapid depolarization of the cell membrane from a negative resting potential to a positive potential, caused by peak I_{Na} resulting mainly from the activation of Na$^+$ (Na$_v$1.5) channel. Phase 1 is short and rapid repolarization due to inactivation of the Na$^+$ channels and activation of the transient outward current (I_{to}) channel. Phase 2 is also known as plateau period, which is determined by the inward currents, mainly the L-type calcium channel current (I_{Ca-L}), and outward currents, mainly the rapidly activating delayed rectifier K$^+$ current (I_{Kr}). Phase 3 is the rapid repolarization phase due to increased outward K$^+$ channel currents including I_{Kr} and I_{Ks} (the slowly activating delayed rectifier K$^+$ current). Phase 4 (the resting potential) is mainly determined by the inward rectifier potassium current (I_{K1}). The depolarization velocity (V_{max}) of APs predominantly determines the speed of excitation conduction. A reduction of peak I_{Na} can cause conduction defect and hence arrhythmias, for example, in Brugada syndrome. The repolarization velocity mainly determines the duration of APs (APD) and in turn the QT interval in ECG. An increase in inward current (I_{Ca-L} or late I_{Na}) or a decrease in outward current (I_{to}, I_{Kr}, I_{Ks}) can prolong APD/QT, resulting in LQTS. By contrast, a decrease in the inward or an increase in the outward current will shorten APD/QT, leading to SQTS.

The hERG channel gating includes 5 processes, i.e., resting state, activation, inactivation, recovery from inactivation and deactivation (figure 4). When cell membrane potential is depolarized (from p1 to p2, figure 4), the channel will be activated (the activation gate is opened, current increases) and immediately inactivated (inactivation gate is closed, current decays). When the potential is repolarized (from p2 to p3, figure 4), first, the inactivated channel will recover from inactivation (the inactivation gate is open, tail current increases) and then the recovered channel will deactivate (the activation gate is closed, tail current decays). Of note, all the process are voltage- and time-dependent. It means that at different levels (potentials) of depolarization or repolarization, different amounts of channels are opened or closed, resulting in different amplitude of current; besides, each gating process needs certain time, depending on the speed of a process. Therefore, analyzing the I_{Kr} at different potentials of depolarization or repolarization and the time

constants of I_{Kr} increasing or decaying over time can examine physical properties of hERG channel gating kinetics.
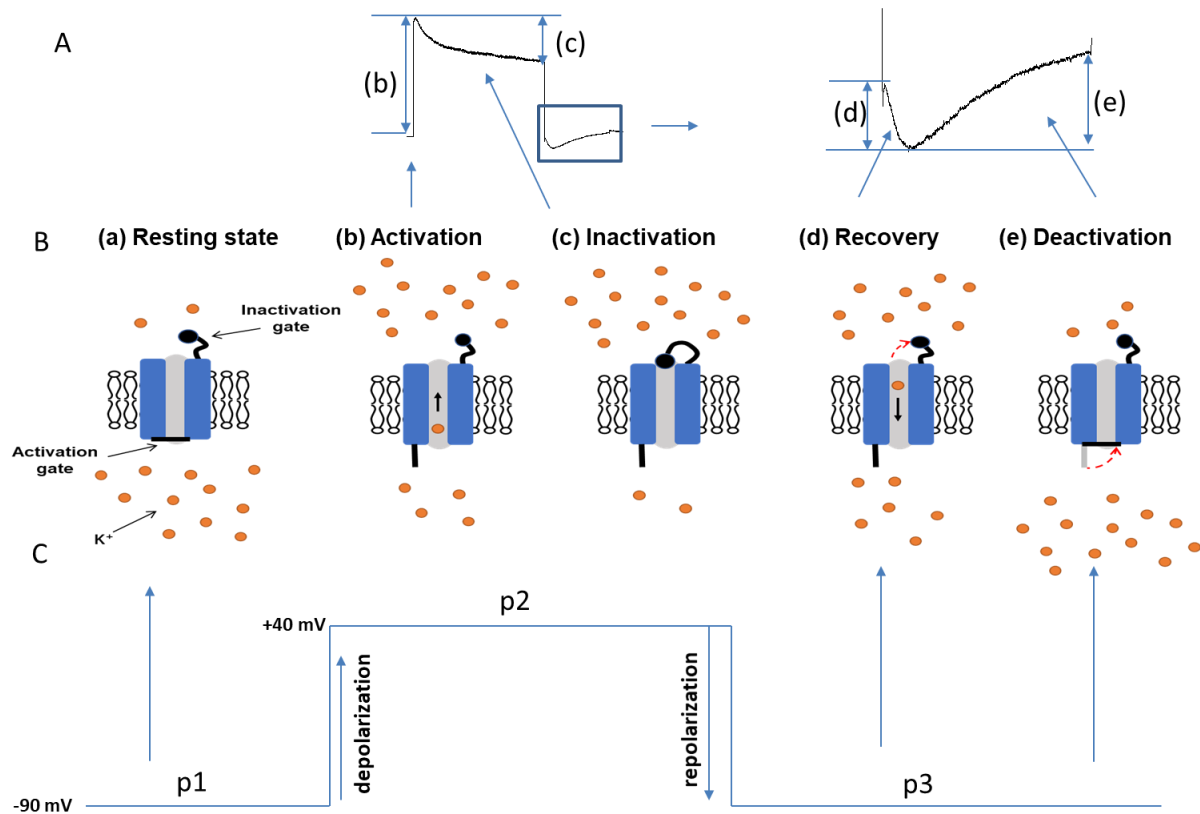
Figure 4. Schematic representation of hERG channel gating states. (A) Example of current trace showing the activation (b) and inactivation (c) as well as the recovery (d) and deactivation (e). (B) Gating states of hERG channel including resting state (activation gate is closed, a), activation (activation gate opens and an outward current appears, b), inactivation (inactivation gate closes and the outward current decays, c), recovery (inactivation gate opens and an inward tail current appears, d) and deactivation (activation gate closes and the inward tail current decays, e). Of note, when the channel is open, the direction of ion flow (either inward or outward) depends on the driving force. In depolarization, the driving force facilitates outward current, while

in repolarization to -90 mV (or lower than the ion reverse potential) the driving force facilitates inward current. (C) Protocol for changing membrane potential from resting potential (p1) to depolarization (p2) and then back to resting potential (repolarization, p3), which induce the gating changes of hERG channels.

The bath solution (PSS) for AP measurements contained (mmol/l): 5.9 KCl, 130 NaCl, 11 glucose, 2.4 $CaCl_2$, 10 HEPES, 1.2 $MgCl_2$, pH 7.4 (NaOH). The pipette solution contains (mmol/l): 6 NaCl, 126 KCl, 1.2 $MgCl_2$, 5 EGTA, 10 HEPES, 11 glucose and 1 MgATP, pH 7.2 (KOH).

To separate the I_{Kr} from other currents, the Cs^+ currents conducted by hERG channels were measured. The bath solution contains (mM): 140 CsCl, 2 MgCl2, 10 HEPES, 10 Glucose, pH=7.4 (CsOH). The pipette solution is same as the bath solution.

2.8. Drugs

H_2O_2 (Fisher Scientific) stock solution of 30% H_2O_2 was diluted to achieve the final concentrations used in this study. A fresh solution was prepared for each experiment and protected from light to prevent degradation. LPS (Lipopolysaccharides from E. coli, source strain ATCC 12740, serotype 0127: B8, gel filtrated, gamma irradiated, cell culture tested, Sigma L 4516) was dissolved in water. N-acetylcysteine (NAC), chelerythrine chloride were dissolved in DMSO. Phorbol 12-myristate 13-acetate (PMA), chelerythrine chloride, ivabradine, flecainide, amiodarone, mexiletine, quinidine, and ranolazine were from Sigma, ajmaline from MP Biomedicals, Sp-8-Br-cAMPS from Biolog. The tested concentrations were selected according to literatures and our previous studies in hiPSC-CMs.

2.9. Statistics

Data are shown as mean ± SEM and were analyzed using InStat© (GraphPad, San Diego, USA) as well as SigmaPlot 11.0 (Systat GmbH, Germany). By analyzing the data with the Kolmogorov Smirnov test, it was decided whether parametric or non-parametric tests were used for analysis. Unpaired Student's t-test was used for

comparisons of two independent groups with normal distribution. The paired t-test was used for comparison before and after application of a drug. For parametric data of more than two groups, one-way ANOVA with Holm-Sidak post-test for multiple comparisons (all treated groups versus control) was performed. $P < 0.05$ (two-tailed) was considered significant.

3. RESULTS

3.1. Phenotypic features were recapitulated by hiPSC-CMs from the patient of SQTS1

To examine whether hiPSC-CMs from the patient with SQTS1 carrying the N588K mutation in hERG channel could recapitulate disease features, the action potentials and beating rhythm were analyzed in cells from three healthy donors and the SQTS1-patient. The results showed that the action potential duration at 50% repolarization (APD50) and at 90% repolarization (APD90) were shortened in cells from the patient (SQTS1-hiPSC-CMs) (figure 5 A-C). Strikingly, SQTS1-hiPSC-CMs displayed more arrhythmic events like EAD (early afterdepolarization), DAD (delayed afterdepolarization) and trigger activity (figure 5 D-E). Since the changes of action potential duration (APD) reflect changes of ECG at organ level (QT interval) and the main phenotypic changes in SQT-patients are shortening of QT interval and occurrence of arrhythmias, the data imply that the SQTS1-hiPSC-CMs recapitulated the main phenotypic features of SQTS.
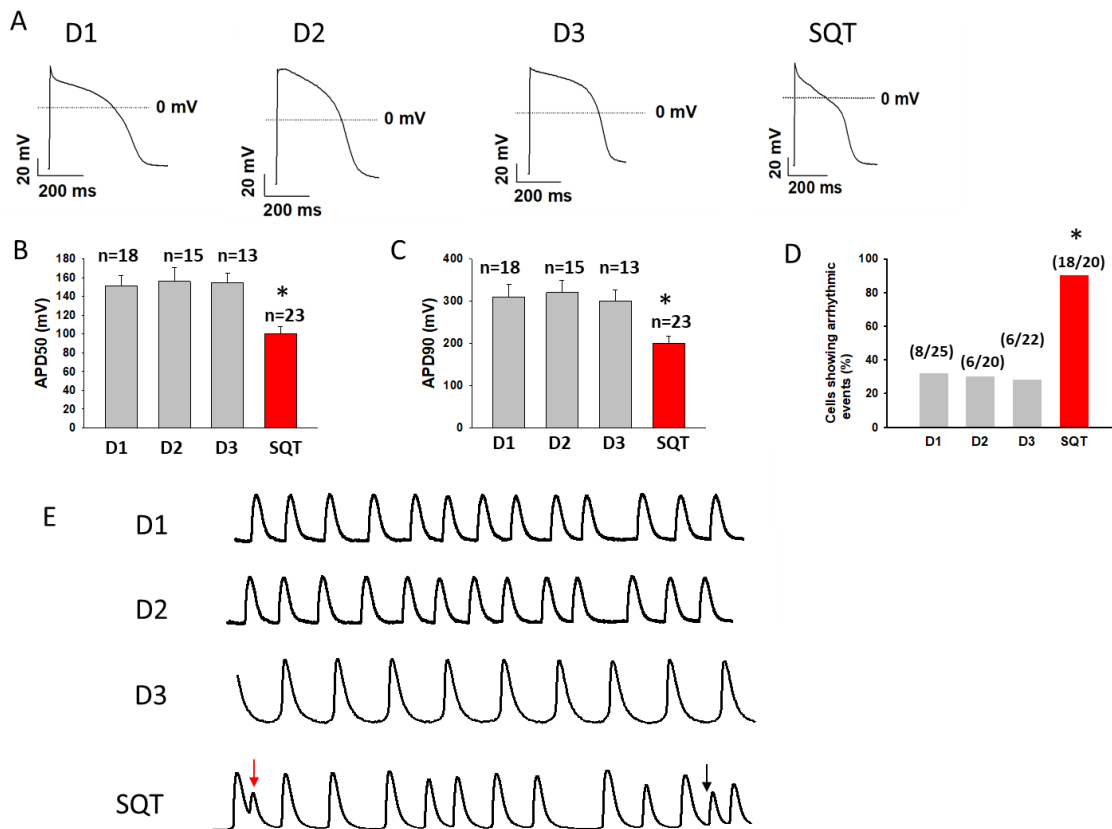
Figure 5. APD shortening and arrhythmic events in SQTS1-hiPSC-CMs. Action potentials in cells paced at 1 Hz were recorded by patch clamp whole cell recording technique. To detect arrhythmic events, calcium transients in spontaneously beating cells were recorded. (A) Representative action potentials recorded in hiPSC-CMs derived from healthy donors (D1, D2 and D3) and the SQTS1-patient (SQT). (B)-(C) Mean values of action potential duration at 50 % repolarization (APD50) and at 90 % repolarization (APD90) in healthy and the diseased hiPSC-CMs. (D) Percentage of cells showing arrhythmic events such as early afterdepolarization (EAD)-like (red arrow in E) or delayed afterdepolarization (DAD)-like events (black arrow in E). (E) Representative calcium transients recorded in control (D1, D2 and D3) and the SQTS1-hiPSC-CMs (SQT). The arrows indicate arrhythmic events. The n number in B and C present the numbers of measured cells, the numbers in D present the numbers of cells showing arrhythmic events versus totally measured cells. *$P<0.05$ versus D1 according to one-way ANOVA with Holm-Sidak post-test (B, C) or Fisher-test (D).

3.2. Gain-of-function of hERG channels in SQTS1-hiPSC-CMs

The SQTS1-patient recruited for the study carries a mutation (N588K) in hERG channels and previous studies showed that this mutation could enhance the hERG channel current in CHO cells [44]. We checked whether this mutation exerts the same

effect in cardiomyocytes. Indeed, the hERG channel currents in SQTS1-hiPSC-CMs were much larger than that in cells from the healthy donors (D-hiPSC-CMs) (figure 6), suggesting that the mutation N588K caused a gain-of-function of hERG channels in SQTS1-hiPSC-CMs.

Of note, the basal electrical features including action potentials and hERG channel current (I_{Kr}) were very similar in hiPSC-CMs from the three healthy donors, indicating the individual variability is not large under our experimental conditions. Therefore, the following experiments used hiPSC-CMs from the first donor (D1) as healthy controls.
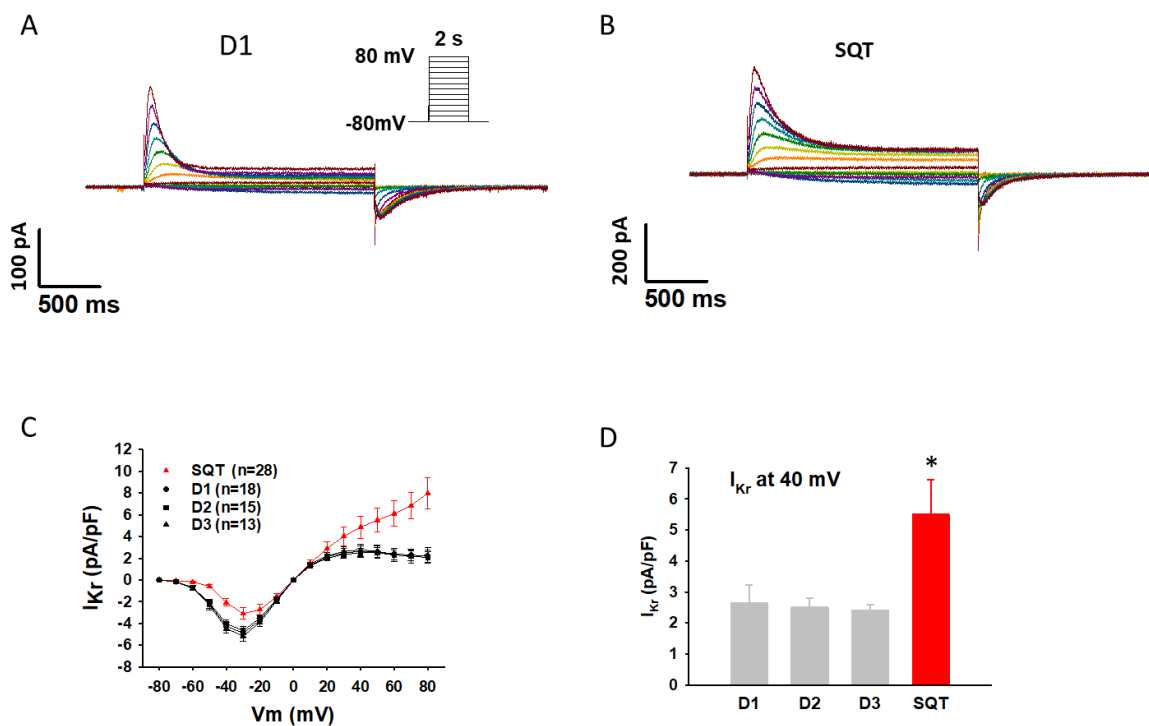
Figure 6. The hERG channel current was enhanced in SQTS1-hiPSC-CMs. The hERG channel current (I_{Kr}) was recorded by patch clamp whole cell recording technique with the protocol shown in A (inset). The steady state current was measured at the end of depolarizing pulse. (A) Representative traces of I_{Kr} recorded in a D1-hiPSC-CM. (B) Representative traces of I_{Kr} recorded in a SQTS1-hiPSC-CM (SQT). (C) Current-voltage relationship (I-V) curves of I_{Kr} in healthy (D1, D2 and D3) and the SQTS1-hiPSC-CM (SQT). (D) The mean values of I_{Kr} at 40 mV in healthy (D1, D2 and D3) and the SQTS1-hiPSC-CM (SQT). The n numbers given C present the numbers of measured cells for C-D. *P<0.05 versus D1 according to one-way ANOVA with Holm-Sidak post-test.

3.3. Effects of adrenergic stimulation on action potential and hERG channel current

Due to the importance of adrenergic/muscarinic regulation for heart electrophysiology, we examined whether the hERG-N588K mutation influences their regulatory effect on cardiomyocytes. For this purpose, we used isoprenaline (Iso, 10 µM) and carbachol (CCh, 10 µM) to mimic the adrenergic and muscarinic stimulation and analyzed their effects on APs and hERG channel currents. The results showed that Iso shortened APD in both healthy and SQTS1-cells (figure 7 A, C-D), whereas CCh had no effect (figure 7 B E-F). However, Iso failed to inhibit I_{Kr} in both SQTS1- and D-hiPSC-CMs (figure 7 G-H). CCh showed no effect either (figure 7 I-J).
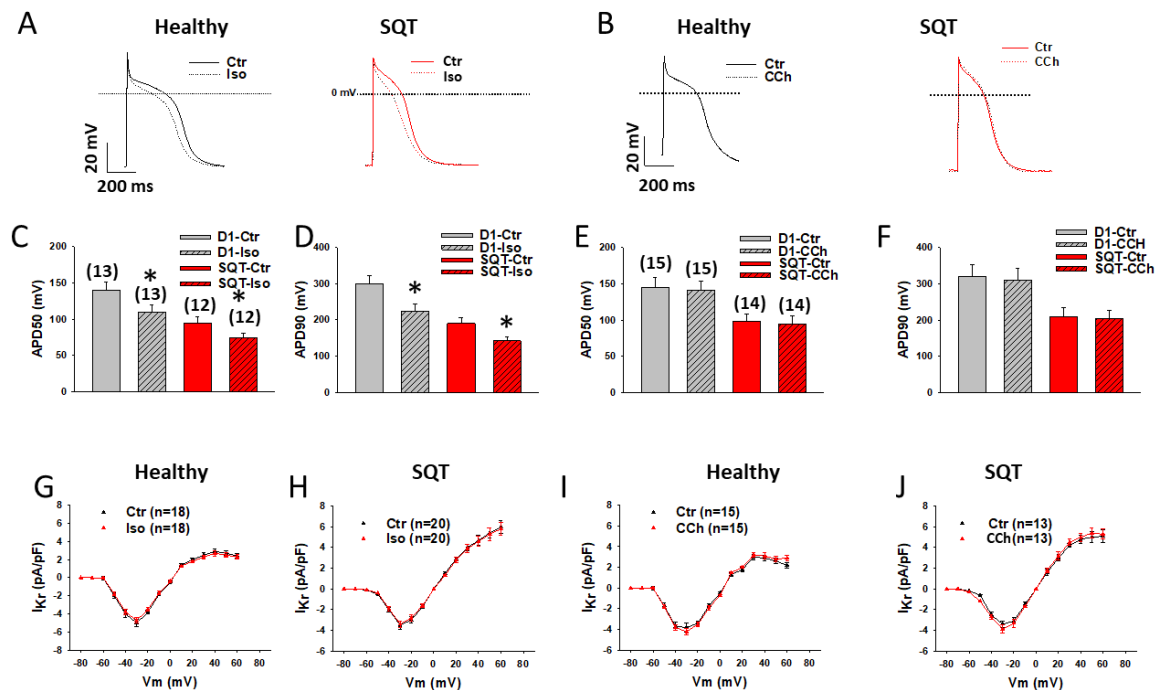
Figure 7. Effects of adrenergic and muscarinic stimulation on action potential and hERG channel current. To simulate adrenergic and muscarinic stimulation of cardiomyocytes, isoprenaline (Iso, 10 µM) or carbachol (CCh, 10 µM) was applied to hiPSC-CMs. Action potentials (APs) and the hERG channel current (I_{Kr}) were recorded by patch clamp whole cell recording technique. (A) Representative traces of APs recorded at 1 Hz in donor cells (Healthy)

and SQTS1-hiPSC-CMs (SQT) before (Ctr) and after application of Iso. (B) Representative traces of APs recorded in donor cells (Healthy) and SQTS1-hiPSC-CMs (SQT) before (Ctr) and after application of CCh. (C) Mean values of action potential duration at 50 % repolarization (APD50) in healthy and the diseased hiPSC-CMs before (D1-Ctr and SQT-Ctr) and after application of Iso (D1-Iso and SQT-Iso). (D) Mean values of action potential duration at 90 % repolarization (APD90) in healthy and the diseased hiPSC-CMs before (D1-Ctr and SQT-Ctr) and after application of Iso (D1-Iso and SQT-Iso). (E) Mean values of action potential duration at 50 % repolarization (APD50) in healthy and the diseased hiPSC-CMs before (D1-Ctr and SQT-Ctr) and after application of CCh (D1-CCh and SQT-CCh). (F) Mean values of action potential duration at 90 % repolarization (APD90) in healthy and the diseased hiPSC-CMs before (D1-Ctr and SQT-Ctr) and after application of CCh (D1-CCh and SQT-CCh). (G) Current-voltage relationship (I-V) curves of I_{Kr} recorded at 0.2 Hz in D1 (Healthy) hiPSC-CMs before (Ctr) and after application of Iso. (H) I-V curves of I_{Kr} in SQTS1 (SQT) hiPSC-CMs before (Ctr) and after application of Iso. (I) I-V curves of I_{Kr} in D1 (Healthy) hiPSC-CMs before (Ctr) and after application of CCh. (J) I-V curves of I_{Kr} in SQTS1 (SQT) hiPSC-CMs before (Ctr) and after application of CCh. The numbers given present the numbers of measured cells. The numbers given in C and E present the numbers of measured cells also for D and F. *$P<0.05$ versus Ctr according to paired t-test.

3.4. Effects of stimulation frequency on action potential and hERG channel current

It is known that in SQTS-patients the adaptation of QT interval to the frequency of heart beats is attenuated, which may be a substrate for occurrence of arrhythmias. To examine whether this phenomenon can be mimicked in SQTS1-hiPSC-CMs, APs were measured in cells stimulated by electrical pulses at different frequencies. We observed that in hiPSC-CMs from healthy donors, the APD shortened when the stimulation frequency was increased from 1 to 3 Hz (figure 8 A-B). In SQTS1-hiPSC-CMs, however, APD only slightly shortened (figure 8 A-B), suggesting that the adaptation of APD to the increase in frequency was reduced.

Further, the effect of stimulation frequency on I_{Kr} was assessed. Higher frequency increased I_{Kr} in healthy donor hiPSC-CMs (figure 8 C), but failed to increased I_{Kr} in SQTS1-hiPSC-CMs (figure 8 D).
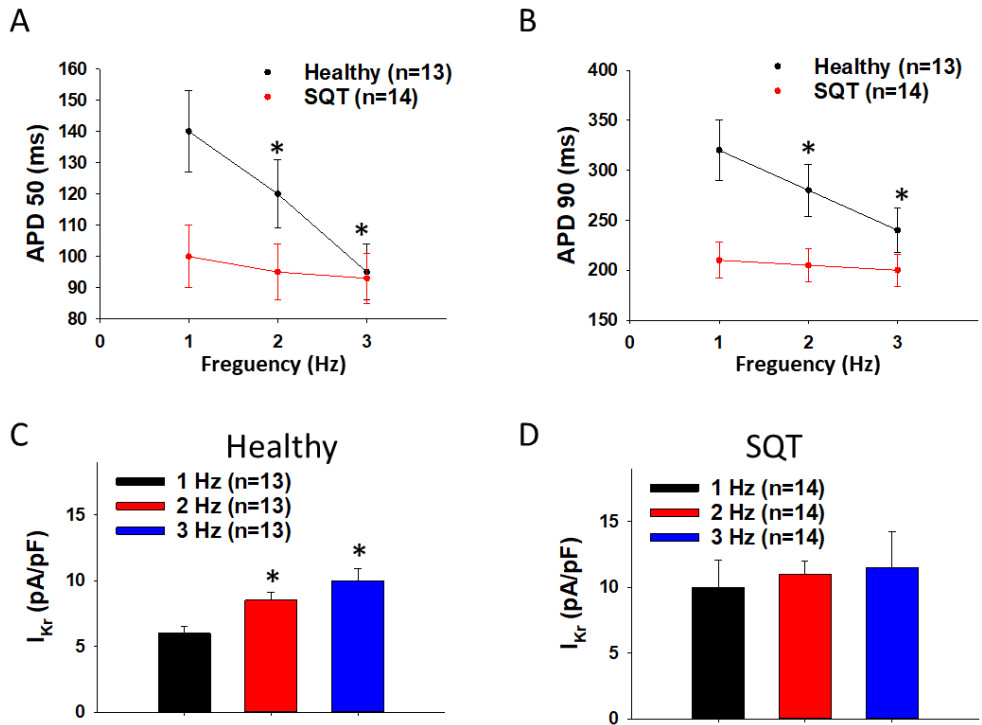
Figure 8. Effects of frequency on the action potential duration and hERG channel current. Action potentials (APs) and the hERG channel current (I_{Kr}) in cells paced by electrical pulses at 1 Hz, 2 Hz and 3 Hz were recorded by patch clamp whole cell recording technique. (A) Mean values of action potential duration at 50 % repolarization (APD50) in healthy donor (Healthy) and the SQTS1-hiPSC-CMs (SQT) paced at 1 Hz, 2 Hz and 3 Hz. (B) Mean values of action potential duration at 90 % repolarization (APD90) in healthy donor (Healthy) and the SQTS1 hiPSC-CMs (SQT) paced at 1 Hz, 2 Hz and 3 Hz. (C) Mean values of I_{Kr} at 60 mV in healthy hiPSC-CMs paced at 1 Hz, 2 Hz and 3 Hz. (D) Mean values of I_{Kr} at 60 mV in SQTS1-hiPSC-CMs paced at 1 Hz, 2 Hz and 3 Hz. The n numbers given present the numbers of measured cells. *$P<0.05$ versus 1 Hz according to one-way ANOVA with Holm-Sidak post-test.

3.5. Effects of pH values on action potential and hERG channel current

The intra- and extracellular pH value is important for cell functions including cardiac electroactivities, which led us to examine whether the N588K mutation can change effects of acidosis in SQTS1 patient cells. In healthy donor and SQTS1-hiPSC-CMs, acidosis (pH=6) shortened APD (figure 9 A-C) and the extent of APD shortening in both cell lines was similar (figure 9 F). Surprisingly, the acidosis inhibited I_{Kr} in both healthy donor and SQTS1 patient cells (figure 9 D-E), The inhibition was also similar in healthy donor and SQTS1 patient cells (figure 9 F).
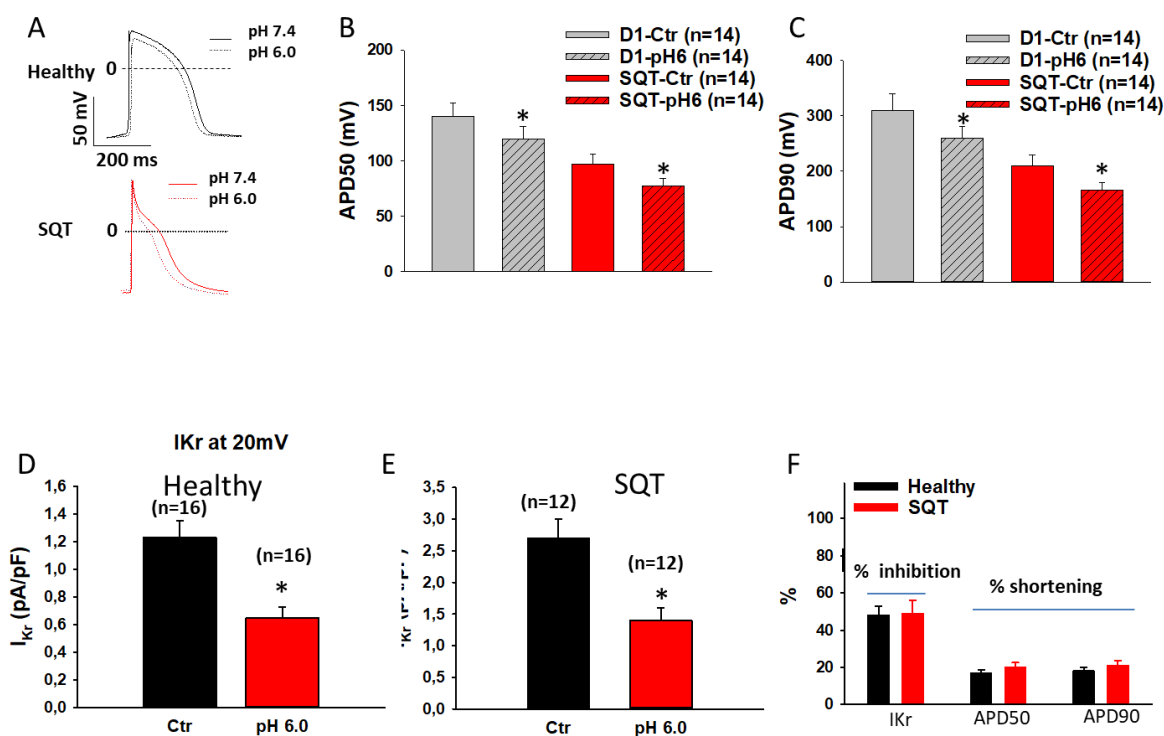
Figure 9. Effects of extracellular pH on the action potential duration and hERG channel current. Action potentials (APs) and the hERG channel current (I_{Kr}) were recorded by patch clamp whole cell recording technique. The pH value of extracellular solution was changed from 7.4 (Ctr) to 6.0. APs and I_{Kr} were recorded before (pH 7.4) and after solution change (pH 6) in same cells. (A) Representative traces of APs recorded in a cell from healthy donor (Healthy) and an SQTS1-hiPSC-CM (SQT) in solution with pH value of 7.4 and 6.0. (B) Mean values of action potential duration at 50 % repolarization (APD50) in healthy (D1) and the SQTS1-hiPSC-CMs (SQT) in solution with pH value of 7.4 (D1-Ctr, SQT-Ctr) and 6.0 (D1-pH6, SQT-pH6). (C) Mean values of action potential duration at 90 % repolarization (APD90) in healthy (D1) and the SQTS1-hiPSC-CMs (SQT) in solution with pH value of 7.4 (D1-Ctr, SQT-Ctr) and 6.0 (D1-pH6, SQT-pH6). (D) Mean values of I_{Kr} at 20 mV in healthy donor hiPSC-CMs in solution with pH value of 7.4 (Ctr) and 6.0 (pH 6.0). (E) Mean values of I_{Kr} at 20 mV in SQTS1-hiPSC-CMs in solution with pH value of 7.4 (Ctr) and 6.0 (pH 6.0). (F) Percent inhibition of I_{Kr} and percent shortening of APD 50 and APD90 induced by pH 6.0. The percent inhibition or shortening was calculated as: %=(V7.4-V6.0)/V7.4*100, where V7.4 is the value at pH 7.4, V6.0 is the value at pH 6.0. The data in F resulted from calculations of the data from B-E. The n numbers given present the numbers of measured cells. *P<0.05 versus Ctr according to paired t-test.

3.6. Effects of hyperthermia on hERG channel current

It is known that fever can be a trigger for arrhythmias in some cardiac disorders such as Brugada syndrome and it was reported that fever can influence I_{Kr} [114]. Thus, possible effects of hyperthermia on SQTS phenotype features were investigated in the current study. As expected, I_{Kr} was enhanced when the temperature of bath solution of measured cells was elevated from 37 °C to 40 °C (figure 10 A-B). Compared to healthy donor hiPSC-CM, in SQT1-hiPSC-CMs, a stronger effect was detected (figure 10 C).
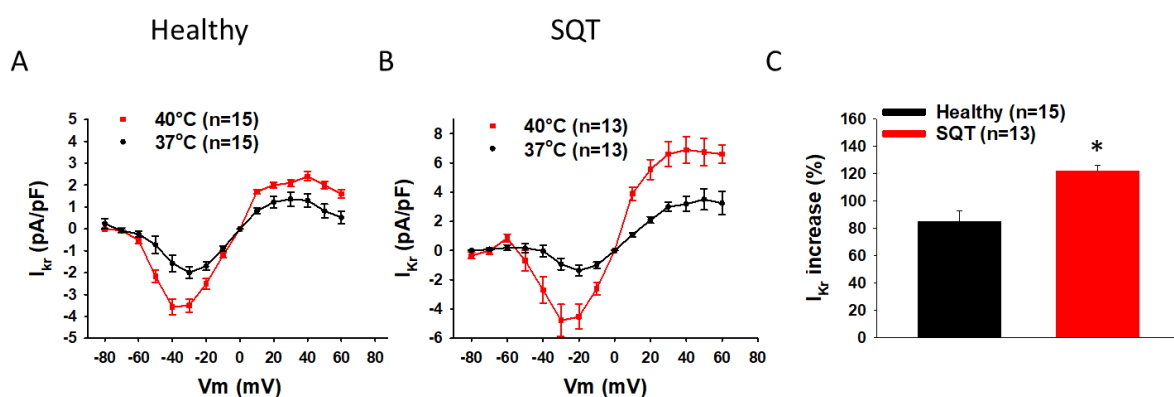
Figure 10. Temperature sensitivity of hERG channel current in healthy and SQTS1-hiPSC-CMs. The hERG channel current (I_{Kr}) in cells paced by electrical pulses at 0.2 Hz were recorded by patch clamp whole cell recording technique at 37 °C and 40 °C. (A) I-V curves of I_{Kr} recorded in healthy donor (Healthy) hiPSC-CMs at 37 °C and 40 °C. (B) I-V curves of I_{Kr} recorded in SQTS1-hiPSC-CM (SQT) at 37 °C and 40 °C. (C) Percent increase of I_{Kr} at +40 mV induced by increasing temperature to 40 °C. The n numbers given present the numbers of measured cells. *P<0.05 versus Healthy according to t-test.

3.7. Effects of LPS on hERG channel current

Inflammation can cause arrhythmias, which led us to examine whether inflammation effects can be enhanced in SQTS patients. Cells were treated for 24 hours with 2 µg/ml lipopolysaccharide (LPS), an endotoxin existing as a glycolipid component of the outer cell wall of gram-negative bacteria, to mimic a bacterial infection. LPS increased I_{Kr} in

healthy and SQT1-hiPSC-CMs (figure 11 A-B). Notably, the LPS effects in SQTS1 cells were lager than that in healthy donor cells (figure 11 C).
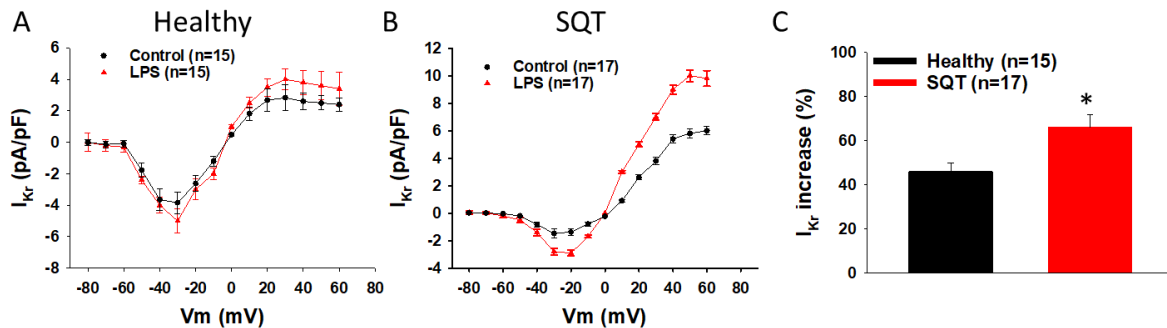
Figure 11. LPS increased hERG channel current in healthy and SQTS1-hiPSC-CMs. The hERG channel current (I_{Kr}) in cells paced at 0.2 Hz were recorded by patch clamp whole cell recording technique in absence (Control) and presence of LPS (2 µg/ml for 24 h). (A) Current-voltage relationship (I-V) curves of I_{Kr} recorded in healthy donor (Healthy) hiPSC-CMs in absence (Control) and presence of LPS. (B) I-V curves of I_{Kr} recorded in SQTS1-hiPSC-CM (SQT) in absence (Control) and presence of LPS. (C) Percent increase in I_{Kr} at +40 mV induced by LPS. The n numbers given present the numbers of measured cells. *P<0.05 versus Healthy according to t-test.

3.8. Roles of ROS for LPS effect on hERG channel current

Sine reactive oxygen species (ROS) are important signaling factors related to inflammation, possible roles of ROS for arrhythmogenesis in SQTS1 were explored. First, a ROS blocker N-Acetyl-L-cysteine (NAC, 1 mM) was applied together with LPS for 24 h treatment of hiPSC-CMs, and then I_{Kr} was analyzed. Interestingly, in the presence of NAC, LPS did not enhance, instead, slightly but not significantly inhibited I_{Kr} (figure 12 A-C). Next, cells were treated for 2 hours with 100 µM H_2O_2, which is the main form of endogenous ROS. H_2O_2 enhanced I_{Kr} in healthy donor and SQTS1-hiPSC-CMs (figure 12 D-E). The effects of H_2O_2 in SQTS1 cells were larger than that in healthy donor cells (figure 12 F).
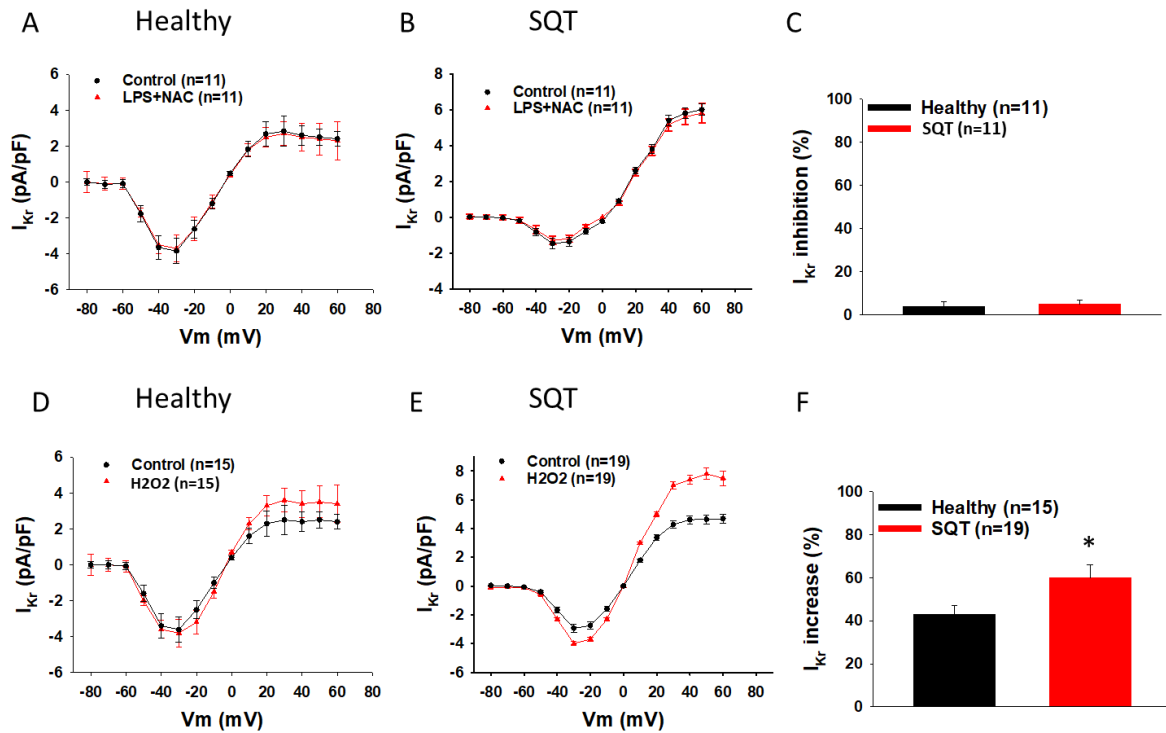
Figure 12. NAC abolished and ROS mimicked LPS effect on hERG channel currents in healthy and SQTS1-hiPSC-CMs. To examine possible role of ROS (reactive oxygen species) in LPS effect, a ROS blocker N-Acetyl-L-cysteine (NAC, 1 mM) was applied together with LPS (2 µg/ml for 24 h) for the treatment of hiPSC-CMs. To confirm ROS effect, cells were treated with H_2O_2 (100 µM), the main form of endogenous ROS, for 2 h. The hERG channel current (I_{Kr}) in cells was recorded by patch clamp whole cell recording technique. (A) I-V curves of I_{Kr} recorded in healthy donor (Healthy) hiPSC-CMs in absence (Control) and presence of LPS plus NAC. (B) I-V curves of I_{Kr} recorded in SQTS1-hiPSC-CM (SQT) in absence (Control) and presence of LPS plus NAC. (C) Percent inhibition of I_{Kr} at +40 mV induced by LPS plus NAC. (D) I-V curves of I_{Kr} recorded in healthy donor (Healthy) hiPSC-CMs in absence (Control) and presence of H_2O_2. (E) I-V curves of I_{Kr} recorded in SQTS1-hiPSC-CM (SQT) in absence (Control) and presence of H_2O_2. (F) Percent increase of I_{Kr} at +40 mV induced by H_2O_2. The n numbers given present the numbers of measured cells. *P<0.05 versus Healthy according to t-test.

3.9. NADPH oxidases were involved in effects of LPS

Since ROS production is related to numerus intracellular signaling, we tried to identify a signaling factor responsible for the elevated ROS induced by LPS. It was

demonstrated that in some cardiovascular diseases, the production of ROS is related to the activation of NADPH oxidase [115]. So, we employed diphenyleneiodonium (DPI,10 µM), an inhibitor of NADPH oxidases, for treating hiPSC-CMs together with LPS. We observed that the DPI prevented the effects of LPS on I_{Kr} (figure 13). These data indicate that NADPH oxidases are involved in LPS induced ROS generation.
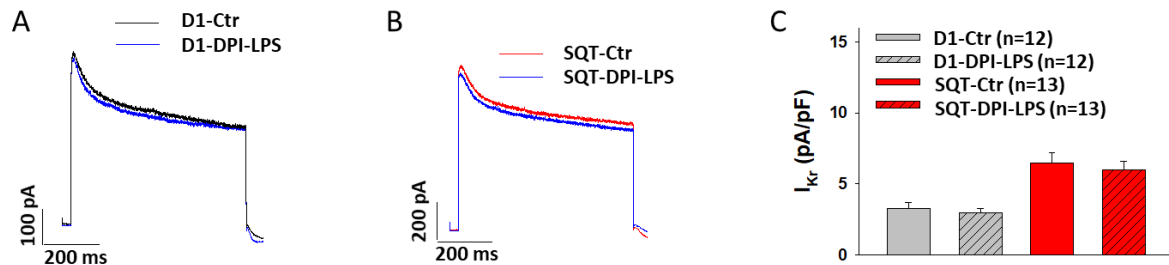
Figure 13. NADPH oxidases were involved in effects of LPS effect on hERG channel currents in healthy and SQTS1-hiPSC-CMs. DPI (10 µM) together with LPS (2 µg/ml) was used for the treatment (24h) of hiPSC-CMs. The hERG channel current (I_{Kr}) in cells was recorded by patch clamp whole cell recording technique. (A) Representative traces of I_{Kr} at 40 mV recorded in healthy donor (Healthy) hiPSC-CMs in absence (D1-Ctr) and presence of LPS plus DPI (D1-DPI-LPS). (B) Representative traces of I_{Kr} at 40 mV recorded in SQTS1-hiPSC-CMs in absence (SQT-Ctr) and presence of LPS plus DPI (SQT-DPI-LPS). (C) Mean values of I_{Kr} at +40 mV. The n numbers given present the numbers of measured cells.

3.10. Protein kinase C was involved in effects of LPS

Considering that protein kinase A (PKA) and protein kinase C (PKC) were reported to regulate I_{Kr} [77], we examined the possible role of PKA and PKC in the LPS effect on I_{Kr}. H89, an inhibitor of PKA and some other kinases (H89, 10 µM) failed to change LPS effect (LPS still increased I_{Kr}) (figure 14 A-B, I-J), whereas a broad range PKC-inhibitor (chelerythrine, 5 µM) suppressed the effects of LPS in both healthy and SQTS1-hiPSC-CMs (figure 14 C-D, I-J), suggesting a possible involvement of PKC in LPS effect. Next, a PKC activator phorbol-12-myristate-13-acetate (PMA) was applied to the cells and caused effects on I_{Kr} similar to that of LPS (figure 14 E-F, I-J). The effect of PMA was prevented by the treatment of cells with the chelerythrine (figure 14 G-J).
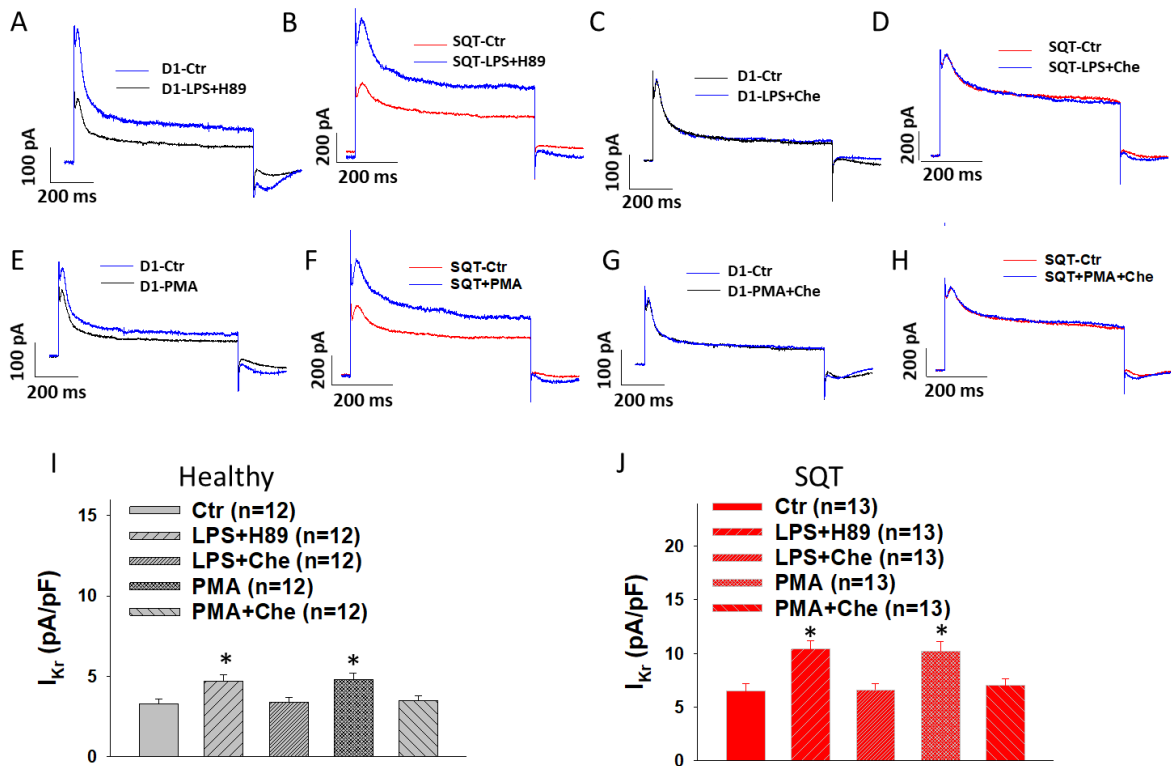
Figure 14. PKC likely mediates the LPS effect on hERG channel currents in healthy donor and SQTS1-hiPSC-CMs. Cells were treated with vehicle (Ctr) or LPS (2 µg/ml) plus H89 (10 µM) or LPS plus chelerythrine (Che, 10 µM) or with a PKC activator (PMA, 10 µM) or PMA plus chelerythrine (PMA+Che). The hERG channel current (I_{Kr}) in cells was recorded by patch clamp whole cell recording technique. (A) Representative traces of I_{Kr} at 40 mV recorded in healthy donor hiPSC-CMs in absence (D1-Ctr) and presence of LPS plus H89 (D1-LPS+H89). (B) Representative traces of I_{Kr} at 40 mV recorded in SQTS1-hiPSC-CMs in absence (SQT-Ctr) and presence of LPS plus H89 (SQT-LPS+H89). (C) Representative traces of I_{Kr} at 40 mV recorded in healthy donor hiPSC-CMs in absence (D1-Ctr) and presence of LPS plus chelerythrine (D1-LPS+Che). (D) Representative traces of I_{Kr} at 40 mV recorded in SQTS1-hiPSC-CMs in absence (SQT-Ctr) and presence of LPS plus chelerythrine (SQT-LPS+Che). (E) Representative traces of I_{Kr} at 40 mV recorded in healthy donor hiPSC-CMs in absence (D1-Ctr) and presence of PMA (D1-PMA). (F) Representative traces of I_{Kr} at 40 mV recorded in SQTS1-hiPSC-CMs in absence (SQT-Ctr) and presence of PMA (SQT-PMA). (G) Representative traces of I_{Kr} at 40 mV recorded in healthy donor hiPSC-CMs in absence (D1-Ctr) and presence of PMA plus chelerythrine (D1-PMA+Che). (H) Representative traces of I_{Kr} at 40 mV recorded in SQTS1-hiPSC-CMs in absence (SQT-Ctr) and presence of PMA plus chelerythrine (SQT-PMA+Che). (I) Mean values of I_{Kr} at +40 mV of each group in healthy donor hiPSC-CMs. (J) Mean values of I_{Kr} at +40 mV of each group in SQTS1-hiPSC-CMs. The n

numbers given present the numbers of measured cells. *P<0.05 versus Ctr according to one-way ANOVA with Holm-Sidak post- test.

3.11. Protein kinase C acted as a downstream factor of ROS

Considering that both ROS and PKC were involved in LPS effect on I_{Kr}, we tried to examine whether PKC is a downstream or upstream factor of ROS in LPS-relating signaling. Cells were challenged by H_2O_2 in presence and absence of chelerythrine or by PMA in absence and presence of NAC, and I_{Kr} was analyzed. The results showed that the chelerythrine suppressed the effects of H_2O_2 (Figure 15), whereas NAC had no effect on PMA effect, suggesting that PKC is a downstream signaling factor of ROS in the signal pathway.
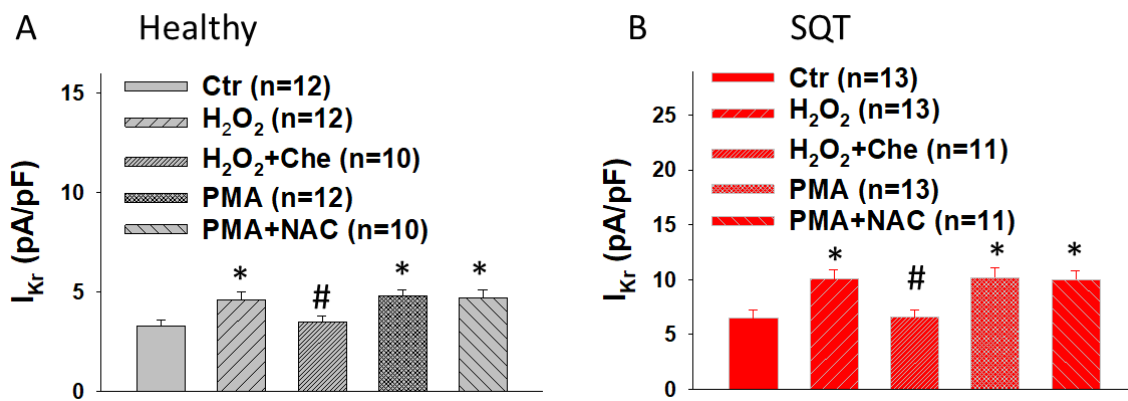
Figure 15. The ROS effect was attenuated by chelerythrine, but the PMA effect was not changed by NAC. Cells were treated for 2 h with vehicle (Ctr) or H_2O_2 (100 µM) or H_2O_2 plus 5 µM chelerythrine (H_2O_2 +Che) or 10 µM PMA or PMA plus 1 mM N-Acetyl-L-cysteine (PMA+NAC). The hERG channel current (I_{Kr}) in cells was recorded by patch clamp whole cell recording technique. (A) Mean values of I_{Kr} at +40 mV of each group in healthy donor hiPSC-CMs. (B) Mean values of I_{Kr} at +40 mV of each group in SQTS1-hiPSC-CMs. The n numbers given present the numbers of measured cells. *P<0.05 versus Ctr and #P<0.05 versus H_2O_2 according to one-way ANOVA with Holm-Sidak post- test.

3.12. Changes of hERG gating kinetics in SQTS1-hiPSC-CMs

To explore the mechanism underlying changes of hERG channel currents in SQTS1-hiPSC-CMs caused by the N588K mutation and environmental factors, the hERG channel gating kinetics including activation, inactivation, recovery from inactivation and deactivation were analyzed.

First, the difference between wild-type (healthy donor cells) and N588K (SQTS1 patient cells) channel activation was analyzed. The voltage-dependent activation evaluated by the values of voltage at 50% activation (V0.5) was slightly reduced, showing a slight shift of activation curve to a more positive potential (figure 16 A-B). In addition, the time-dependent activation evaluated by the time to peak of I_{Kr} was slowed, showing that longer time was needed to reach the peak of I_{Kr} in SQTS1-hiPSC-CMs (figure 16 C-D).
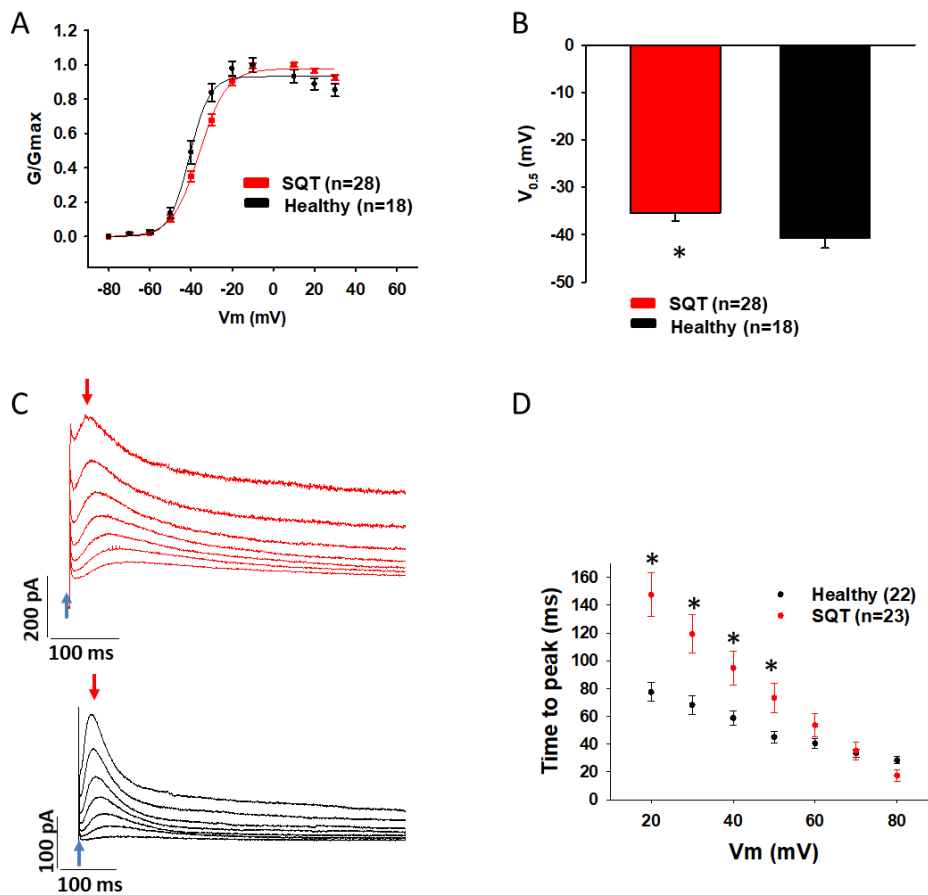
Figure 16. Change of hERG channel activation in SQTS1-hiPSC-CMs. The hERG channel currents (I_{Kr}) in cells were recorded by patch clamp whole cell recording technique with protocol as shown in figure 6A (inset). The conductance (G) was obtained by G=I/V, where I is the peak current of I_{Kr}, V is the voltage of pulses. G was normalized to the maximal value (Gmax) and then the activation curve was obtained by plotting G/Gmax against voltages of testing pulses. The activation curves were fitted by Boltzmann equation to obtain the voltage at 50% activation (V0.5). The time to peak was defined as the time between the pulse start (blue arrows) and

the peak of the current (red arrows). (A) Activation curves of I_{Kr} in healthy donor 1 (Healthy) and SQTS1 patient (SQT) hiPSC-CMs. (B) Mean values of voltages at 50% activation (V0.5) of I_{Kr} in healthy and SQTS1 patient hiPSC-CMs. (C) Representative traces of I_{Kr} in a healthy donor (black) and an SQTS1 (red) hiPSC-CM. (D) Mean values of time to peak of I_{Kr} at different potentials (from 20 to 80 mV). The n numbers given present the numbers of measured cells. *P<0.05 versus Healthy according to t- test.

An inactivation defect was detected in CHO cells expressing N588K-HERG channels [44]. We assessed both voltage- and time-dependent inactivation of I_{Kr} in hiPSC-CMs. We found that the inactivation was slowed (the time constant of inactivation was increased) in SQTS1 patient-cells (figure 17 B-D). Consistent with previously reported data, a large shift of voltage-dependent inactivation curve to a more positive potential was also detected in our SQTS1-hiPSC-CMs (figure 17 E-F), implying an inactivation defect.
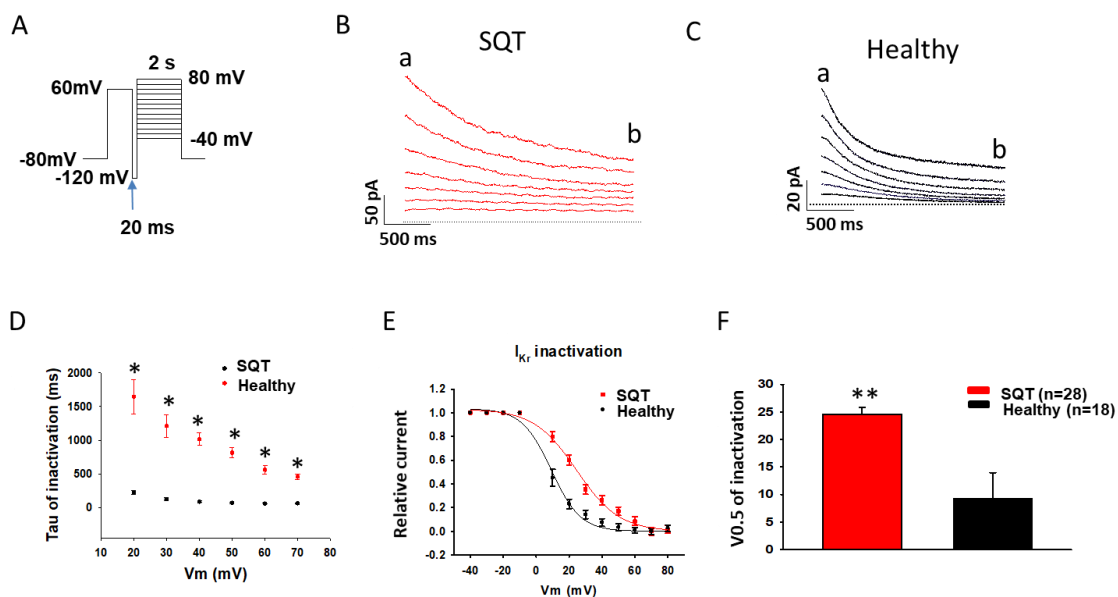
Figure 17. Change of hERG channel inactivation in SQTS1-hiPSC-CMs. The hERG channel current (I_{Kr}) in cells was recorded by patch clamp whole cell recording technique with the protocol as shown in A. A pre-pulse of 1 second from -80 mV (the holding potential) to +60 mV followed by a short (20 ms) repolarization to -120 mV was given for channel activation, inactivation and recovery to an open state. Before deactivation occurs, test pulses of 2 second from -40 mV to +80 mV (10 mV increments) were started to evaluate the inactivation of

channels. The time constant (Tau) of inactivation was obtained by fitting the current trace with single exponential decay fit. To analyze the fraction of inactivated I_{Kr} at different voltages, I_{Kr} was measured at the beginning (peak current, a) and end (steady current, b) of test pulses as shown in B and C. The current of inactivated channels (I_{inact}) was calculated as: $I_{inact} = I_a - I_b$, where I_a is the peak current, I_b is the steady current. When I_{inact} is larger than zero, it means inactivation occurred. When I_{inact} equals or is smaller than zero, it means no inactivation occurred. I_{inact} at different potentials were measured and normalized to the maximal current ($I_{inactMax}$). To plot the inactivation curves in a usual way (the curve decays with increasing voltages), the relative current was calculated by $I = 1 - I_{inact}/I_{inactMax}$. Finally, I was normalized to the maximal value I_{max} and plotted against voltages to obtain an inactivation curve. The inactivation curves were then fitted by Boltzmann equation to obtain the voltage value at half maximal inactivation (V0.5). (A) Protocol for measuring I_{Kr}. (B) Representative traces of I_{Kr} measured in an SQTS1-hiPSC-CM. (C) Representative traces of I_{Kr} measured in a healthy donor hiPSC-CM. (D) Mean values of time constant (Tau) of I_{Kr} inactivation in healthy donor (Healthy) and SQTS1 (SQT) hiPSC-CMs. (E) Inactivation curves of I_{Kr} in healthy donor (Healthy) and SQTS1 (SQT) hiPSC-CMs. (F) Mean values of voltage at 50% inactivation (V0.5) of I_{Kr} in healthy (Healthy) and SQTS1 (SQT) hiPSC-CMs. The n numbers given in F present the numbers of measured cells for D-F. *P<0.05 versus Healthy according to t- test.

Next, we assessed the recovery from inactivation of I_{Kr} in hiPSC-CMs. For this purpose, I_{Kr} was first evoked by a pulse from -80 mV to +80 mV for 2 second to let channels be activated and inactivated. Then, the pulse potential was repolarized to different potentials (from -20 mV to -100 mV) to let the inactivated channel to recover. The currents conducted by the recovered channels (the increased parts of the tail currents) were recorded and fitted by single exponential function to obtain the tau value of the recovery time course. The results showed that the recovery from inactivation of I_{Kr} was faster in SQT1 patient-hiPSC-CMs comparing with healthy donor hiPSC-CMs, significantly different at -20 mV to -80 mV (figure 18 F-G).
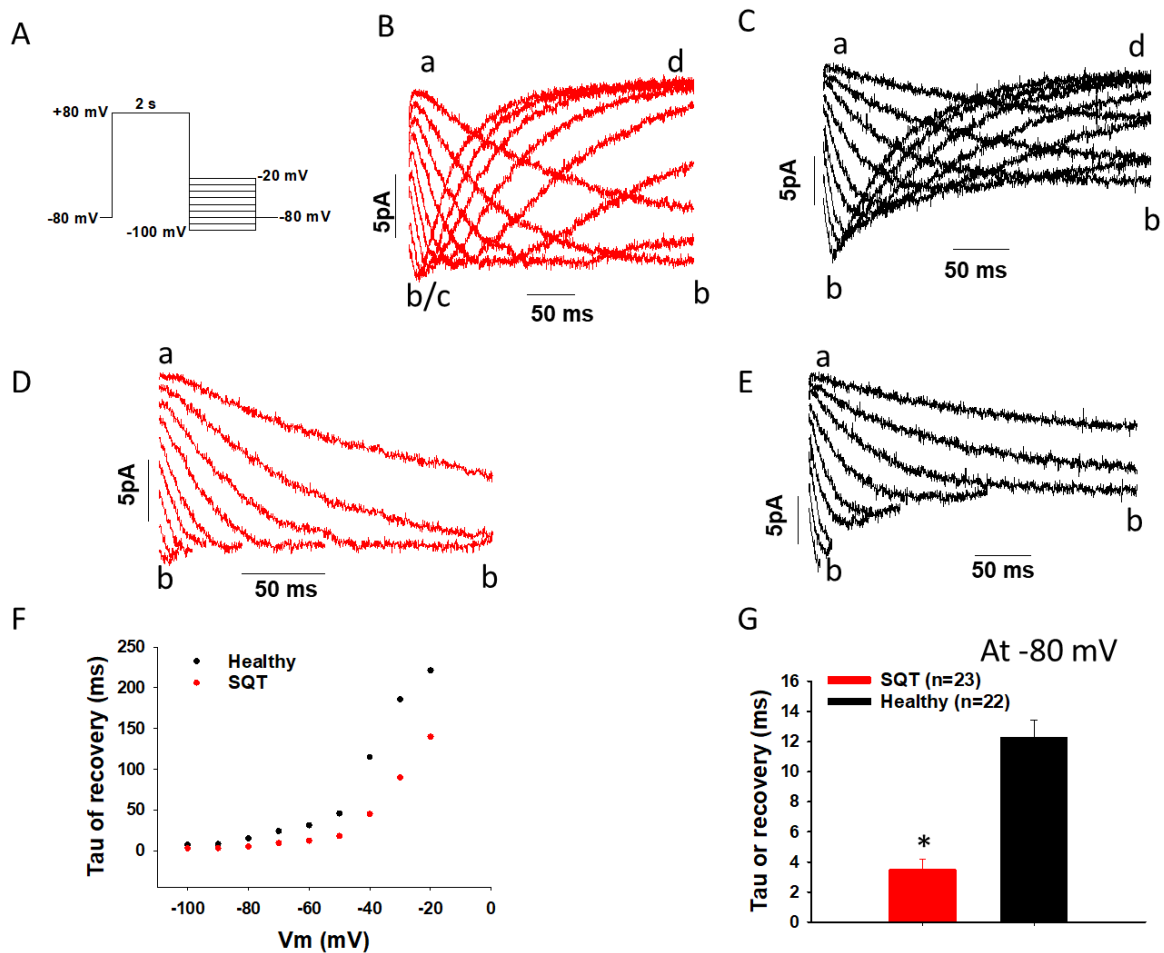
Figure 18. Change of hERG channel recovery from inactivation in SQTS1-hiPSC-CMs.
I_{Kr} was evoked by a 2 s-long pre-pulse from -80 mV to 80 mV to let hERG channels be activated and inactivated. Then, 500 ms test-pulses from -20 mV to -100 mV (10 mV increments) were started. Currents induced by test pulses (tail currents) were used for analyzing the recovery or deactivation of I_{Kr}. When the tail current increased, i.e., "b" is larger (more negative) than "a", the current was defined as recovered current. The curves were fitted by single exponential decay to obtain time constants (Tau) of recovery from inactivation. From -50 mV to -100 mV, deactivation became obvious. i.e., the current decrease again (the current at "d" is smaller than that at "c"). The change point "b/c" is defined as the end of recovery and the start of the deactivation. Of note, only the part of recovery of tail current as shown in D and E was fitted for obtaining the Tau of recovery. (A) Protocol for measuring I_{Kr}. (B) Representative traces of tail I_{Kr} evoked by the protocol in an SQTS1-hiPSC-CM. (C) Representative traces of tail I_{Kr} evoked by the protocol in a healthy donor hiPSC-CM. (D) The traces of tail I_{Kr} presenting the part of recovered current in an SQTS1 patient cell. (E) The traces of tail I_{Kr} presenting the part of recovered current in a healthy donor cell. (F) Mean values of Tau of I_{Kr} recovery from inactivation at different voltages in donor (Healthy) and SQTS1 (SQT) hiPSC-CMs. (G) Mean values of Tau of I_{Kr} recovery from inactivation at -80 mV in healthy donor (Healthy) and SQTS1

patient (SQT) hiPSC-CMs. Shown are mean ± SEM, n represents the number of measured cells. The statistical significance was examined by t-test, *$p < 0.05$ versus Healthy.

Next, we assessed the deactivation of I_{Kr} in hiPSC-CMs. For analysis of the deactivation, the same recording protocol as that used for analyzing the recovery was used. The difference is that only the decreased (less negative) part of the tail current, which resulted from the deactivation of hERG channels, was analyzed (figure 19 D-E). Strikingly, the deactivation of I_{Kr} was faster (Tau value is decreased) in SQTS1-hiPSC-CM than that in healthy donor cells (figure 19 F-G)
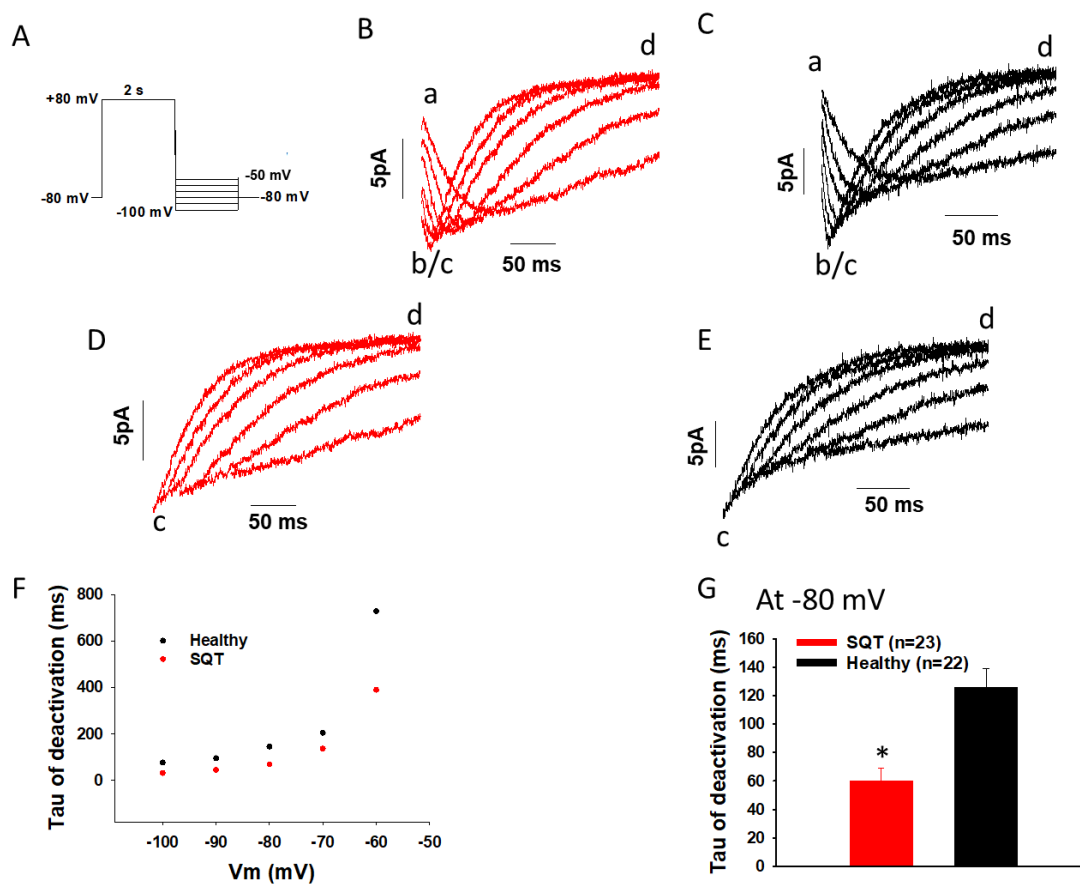
Figure 19. Change of hERG channel deactivation in SQTS1-hiPSC-CMs. I_{Kr} was evoked by using the protocol as in A, which is similar to that used in figure 18. Of note, only the part of the deactivated current as shown in D and E was fitted for obtaining time constant (Tau) of deactivation. (A) Protocol for measuring I_{Kr}. (B) Representative traces of tail I_{Kr} evoked by the protocol in an SQTS1-hiPSC-CM. (C) Representative traces of tail I_{Kr} evoked by the protocol in a healthy donor hiPSC-CM. (D) The traces of tail I_{Kr} presenting the part of the deactivated current in an SQTS1 patient cell. (E) The traces of tail I_{Kr} presenting the part of deactivated current in a healthy donor cell. (F) Mean values of Tau of I_{Kr} deactivation at different potentials in healthy donor (Healthy) and SQTS1 patient (SQT) hiPSC-CMs. (G) Mean values of Tau of

I_{Kr} deactivation at -80 mV in healthy donor (Healthy) and SQTS1 (SQT) hiPSC-CMs. Shown are mean ± SEM, n represents the number of measured cells. The statistical significance was examined by t-test, *$p<0.05$ versus Healthy.

3.13. Influence of N588K on modulation of hERG channel gating by environmental factors

Subsequently, the effects of some environmental factors on hERG channel gating kinetics were assessed and compared between wild-type and SQTS1-N588K cells. For comparison, changes of I_{Kr} gating parameters (delta values or values normalized to control) induced by a factor were calculated and analyzed statistically.

No factor except hyperthermia (40 °C) showed a significant effect on the time to peak. Increasing the temperature from 37 °C to 40 °C accelerated (reduced time to peak) I_{Kr} activation (figure 20 A-B). Acidosis (pH6) shifted the activation (V0.5) to more positive potential, while hyperthermia, LPS and ROS shifted the activation curve (V0.5) to more negative potentials in healthy donor and SQTS1-hiPSC-CMs (figure 20 C-D). Iso and CCh showed no significant effect on V0.5 of activation (figure 20 C-D).

Acidosis accelerated the inactivation (reduced the tau of inactivation) of I_{Kr} in both healthy and SQTS1 cells, whereas hyperthermia, LPS and ROS decelerated (increased the tau of inactivation) the inactivation only in SQTS patient cells (figure 20 E-F). Acidosis shifted the inactivation curve in healthy donor and in SQTS1 patient cells to a more negative potential, while hyperthermia, LPS and ROS shifted the V0.5 of inactivation curve to a more positive potential in both healthy donor and SQTS1 patient cells (figure 20 G-H).

An effect of hyperthermia on the recovery from inactivation of I_{Kr} was detected, by showing an acceleration (reduction of tau value) of the recovery in both healthy donor and SQTS1 patient cells (figure 20 I-J). All other factors had no influence on the time constant of recovery (figure 20 I-J). Finally, the time constant of deactivation of I_{Kr} was analyzed. Only significant effects of LPS and ROS in SQTS1 patient cells occurred, showing an acceleration (reduction of tau value) of the deactivation of I_{Kr} (figure 20 K-L).
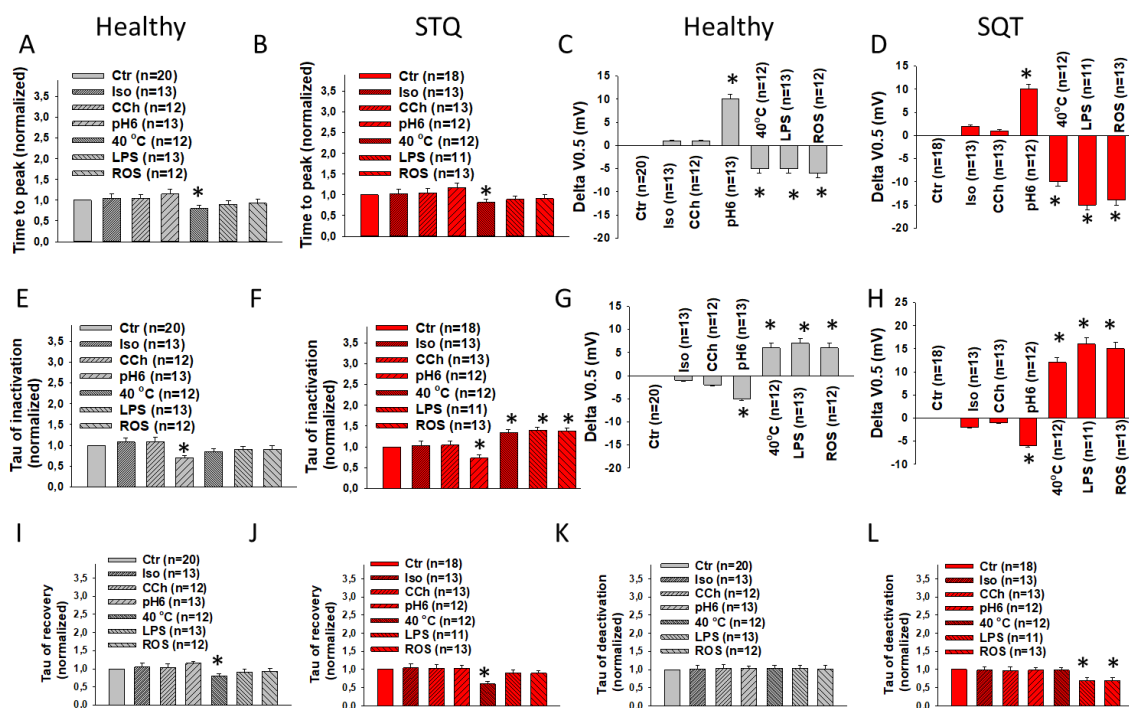
Figure 20. Effects of different factors on hERG channel gating kinetics in healthy and SQTS1-hiPSC-CMs. To examine effects of some factors including isoprenaline (Iso), carbachol (CCh), acidosis (pH6), hyperthermia ((40°C), lipopolysaccharide (LPS) and H_2O_2 (ROS) on I_{Kr} gating, the gating kinetic parameters including the time to peak, voltages of 50% (V0.5) activation and inactivation, time constants (Tau value) of inactivation, recovery and deactivation were analyzed. For comparison of time to peak and time constants, relative value (normalized to control value) was calculated as: Vf/Vc, where Vf is the value in presence of an experimental factor, Vc is the value in absence of the factor (control). For comparison of V0.5, the delta value was calculated as: Vf-Vc. (A) Effects of factors on the time to peak in healthy hiPSC-CMs. (B) Effects of factors on the time to peak in SQTS1 patient-hiPSC-CMs. (C) Effects of factors on V0.5 of activation (Delta value) in healthy donor hiPSC-CMs. (D) Effects of factors on V0.5 of activation (Delta value) in SQTS1-hiPSC-CMs. (E) Effects of factors on the time constant (Tau) of inactivation in healthy donor hiPSC-CMs. (F) Effects of factors on the time constant (Tau) of inactivation in SQTS1-hiPSC-CMs. (G) Effects of factors on V0.5 of inactivation (Delta value) in healthy donor hiPSC-CMs. (H) Effects of factors on V0.5 of inactivation (Delta value) in SQTS1-hiPSC-CMs. (I) Effects of factors on Tau of recovery from inactivation in healthy donor hiPSC-CMs. (J) Effects of factors on Tau of recovery from inactivation in SQTS1-hiPSC-CMs. (K) Effects of factors on the Tau of deactivation in healthy donor hiPSC-CMs. (L) Effects of factors on the Tau of deactivation in SQTS1-hiPSC-CMs. Shown are mean ± SEM, n represents the number of measured cells. The statistical significance was examined by one-way ANOVA with Holm-Sidak post-test, *$p < 0.05$ versus Ctr.

3.14. Effects of antiarrhythmic drugs on hERG channel gating in SQTS1-hiPSC-CMs

The aforementioned data showed that the hERG mutation N588K changed hERG channel gating kinetics and also modulated effects of some environmental factors on the channel gating, which suggest a possible modulation of drug effects in SQTS1 patient cells. Therefore, we examined effects of some clinically used drugs in healthy donor and SQTS1-hiPSC-CMs.

First, the influence of clinically used antiarrhythmic drugs on arrhythmic events were assessed in the hiPSC-CM model. Since at base line, not every cell of SQTS1-hiPSC-CMs showed arrhythmic events, 10 µM epinephrine (Epi) was applied to cells to induce arrhythmic events for establishing a cellular model of arrhythmias. Single cell contraction was measured to monitor arrhythmic events. Actually, many SQTS1-hiPSC-CMs but not healthy donor hiPSC-CMs treated with Epi showed arrhythmic events including EAD, DAD and trigger activity. In cells showing arrhythmic events, the drug to be tested was applied directly to the cell by a micro-perfusion system and its effect was analyzed. Strikingly, quinidine, ajmaline, ivabradine and mexiletine but not amiodarone, ranolazine and flecainide reduced arrhythmic events induced by Epi (figure 21).
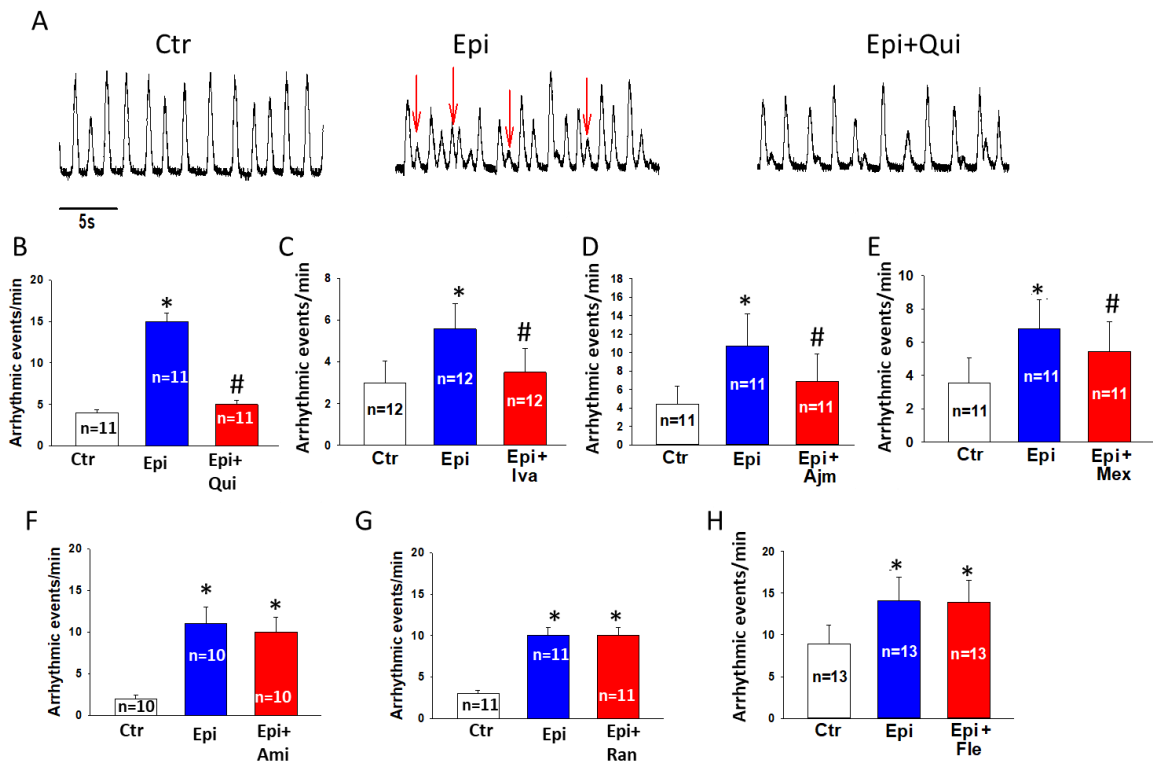
Figure 21. Effects of antiarrhythmic drugs on arrhythmic events induced by epinephrine in SQTS1-hiPSC-CMs. Single cell contraction was measured to monitor arrhythmic events. Epinephrine (10 µM) was applied to spontaneously beating SQTS1 patient-hiPSC-CMs to induce arrhythmic events (indicated by red arrows in A). In cells showing arrhythmic events, 10 µM quinidine (Qui),10 µM ivabradine (Iva), 30 µM ajmaline (Ajm), 100 µM mexiletine (Mex), 10 µM amiodarone (Ami), 30 µM ranolazine (Ran) or 30 µM flecainide (Fle) was applied to the measured cells. (A) Representative traces of single cell contraction measurements in SQTS1-hiPSC-CMs in absence (Ctr) and presence of epinephrine (Epi) and epinephrine plus quinidine (Epi+Qui). (B) Mean values of arrhythmic events in SQTS1-hiPSC-CMs in absence (Ctr) and presence of epinephrine (Epi) and epinephrine plus quinidine (Epi+Qui). (C) Mean values of arrhythmic events in SQTS1-hiPSC-CMs in absence (Ctr) and presence of epinephrine (Epi) and epinephrine plus ivabradine (Epi+Iva). (D) Mean values of arrhythmic events in SQTS1-hiPSC-CMs in absence (Ctr) and presence of epinephrine (Epi) and epinephrine plus ajmaline (Epi+Ajm). (E) Mean values of arrhythmic events in SQTS1-hiPSC-CMs in absence (Ctr) and presence of epinephrine (Epi) and epinephrine plus mexiletine (Epi+Mex). (F) Mean values of arrhythmic events in SQTS1-hiPSC-CMs in absence (Ctr) and presence of epinephrine (Epi) and epinephrine plus amiodarone (Epi+Ami). (G) Mean values of arrhythmic events in SQTS1-hiPSC-CMs in absence (Ctr) and presence of epinephrine (Epi) and epinephrine plus ranolazine (Epi+Ran). (H) Mean values of arrhythmic events in SQTS1-hiPSC-CMs in absence (Ctr) and presence of epinephrine (Epi) and epinephrine plus flecainide (Epi+Fle). Shown are mean ± SEM, n represents the number of measured cells. The statistical significance was

examined by one-way ANOVA with Holm-Sidak post-test, *p<0.05 versus Ctr, #p<0.05 versus Epi.

Next, to unveil the reasons for the difference among those drugs regarding their antiarrhythmic effects in SQTS1-hiPSC-CMs, three series experiments were performed to assess 1) their effects on action potential duration (APD), 2) their effects on hERG channel currents (I_{Kr}) and 3) their effects on hERG channel gating kinetics in both healthy donor and SQTS1-hiPSC-CMs.

We found that in healthy donor cells, quinidine, ivabradine, ajmaline, mexiletine and amiodarone significantly prolonged APD, whereas ranolazine, flecainide and mexiletine shortened APD (figure 22 A). In SQTS1-hiPSC-CMs, quinidine, ivabradine, ajmaline and mexiletine significantly prolonged APD to a similar extent, whereas amiodarone, flecainide and ranolazine did not alter APD (figure 22 B). All tested drugs inhibited I_{Kr}, but the extent of inhibition of all tested drugs (percent inhibition caused by a drug) was significantly smaller in SQTS1 patient cells than that in healthy donor cells (figure 22 C).
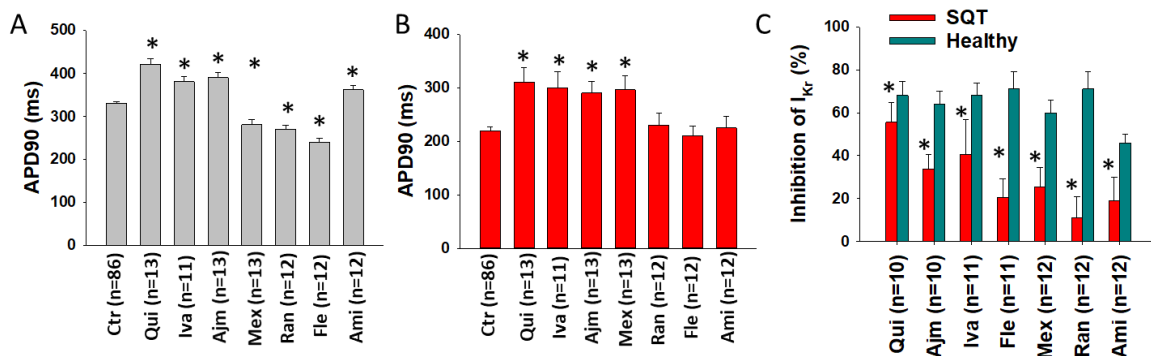
Figure 22. Drug effects on the action potential duration and I_{Kr} in healthy and SQTS1-hiPSC-CMs. Action potentials (APs) and I_{Kr} were recorded by patch clamp whole cell recording technique. 10 µM quinidine (Qui), 10 µM ivabradine (Iva), 30 µM ajmaline (Ajm), 100 µM mexiletine (Mex), 10 µM amiodarone (Ami), 30 µM ranolazine (Ran) or 30 µM flecainide (Fle) was applied to measured cells by a perfusion pipette. (A) Mean values of action potential duration at 90 % repolarization (APD90) in absence (Ctr) and presence of a drug in healthy donor hiPSC-CMs. (B) Mean values of APD90 in absence (Ctr) and presence of a drug in SQTS1-hiPSC-CMs. (C) Mean values of percent inhibition of I_{Kr} by a drug in healthy donor and SQTS1-hiPSC-CMs. Shown are mean ± SEM, n represents the number of measured cells.

The statistical significance was examined by one-way ANOVA with Holm-Sidak post-test (A-B) or t-test (C), *$p < 0.05$ versus Ctr (A-B) or Healthy (C).

In order to reveal mechanisms underlying the difference of effects of the tested drugs on APD and I_{Kr}, the drug effects on the channel gating kinetics were analyzed in both SQTS1 patient and healthy donor cells.

Ajmaline, amiodarone, ivabradine and ranolazine decelerated the I_{Kr} activation (increased the time to peak) in healthy donor and SQTS1-hiPSC-CMs (figure 23 A-B). Quinidine and mexiletine showed the opposite effect (figure 23 A-B). Flecainide increased the time to peak only in healthy donor cells (figure 23 A-B). In SQTS1-hiPSC-CMs, quinidine, ajmaline and ivabradine shifted the activation curve (V0.5) of I_{Kr} to more depolarized potentials, while ranolazine shifted the activation curve (V0.5) to more hyperpolarized potentials. Amiodarone, flecainide and mexiletine displayed no effect (figure 23 C). In healthy hiPSC-CMs, quinidine, ajmaline, amiodarone, ivabradine and mexiletine shifted the activation curves to more depolarized potentials, whereas ranolazine showed an opposite effect (figure 23 D). Flecainide showed no effect (figure 23 D).
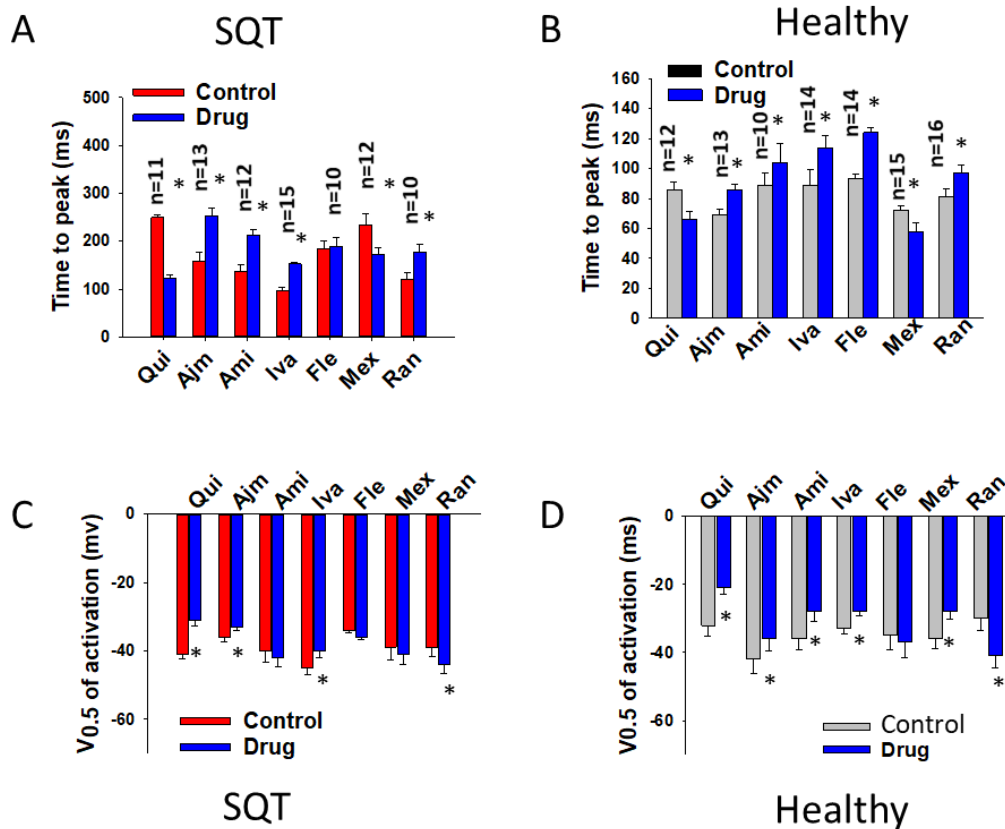
Figure 23. Drug effects on the activation of I_Kr in healthy and SQTS1-hiPSC-CMs. I_{Kr} in cells was recorded by patch clamp whole cell recording technique with the protocol as shown in figure 6. 10 µM quinidine (Qui), 10 µM ivabradine (Iva), 30 µM ajmaline (Ajm), 100 µM mexiletine (Mex), 10 µM amiodarone (Ami), 30 µM ranolazine (Ran) or 30 µM flecainide (Fle) was applied to measured cells by a perfusion pipette. Activation curve and time to peak were analyzed as described in figure 16. (A) Mean values of time to peak in absence (Control) and presence of drugs in SQTS1-hiPSC-CMs. (B) Mean values of time to peak in absence (Control) and presence of drugs in healthy donor hiPSC-CMs. (C) Mean values of V0.5 of activation in absence (Control) and presence of drugs in SQTS1-hiPSC-CMs. (D) Mean values of V0.5 of activation in absence (Control) and presence of drugs in healthy donor hiPSC-CMs. Shown are mean ± SEM, n represents the number of measured cells. The statistical significance was examined by paired t-test (comparison between before and after application of a drug), *p<0.05 versus Control. Numbers given in A and B present numbers of measured cells also for C and D, respectively.

To examine drug effects on I_Kr inactivation, the voltage-dependent inactivation curves of I_Kr and the time constant (Tau) of the current decay due to channel inactivation were analyzed. The inactivation curves (V0.5 values) were shifted to more hyperpolarized potentials by quinidine, ajmaline, ivabradine, mexiletine, and ranolazine but not

significantly changed by amiodarone and flecainide in SQTS1-hiPSC-CMs (figure 24 A-H). In healthy donor hiPSC-CMs, the inactivation curves were shifted to more hyperpolarized potentials by quinidine, ajmaline, flecainide, mexiletine and ranolazine and to more depolarized potentials by amiodarone and ivabradine (figure 24 I-P).
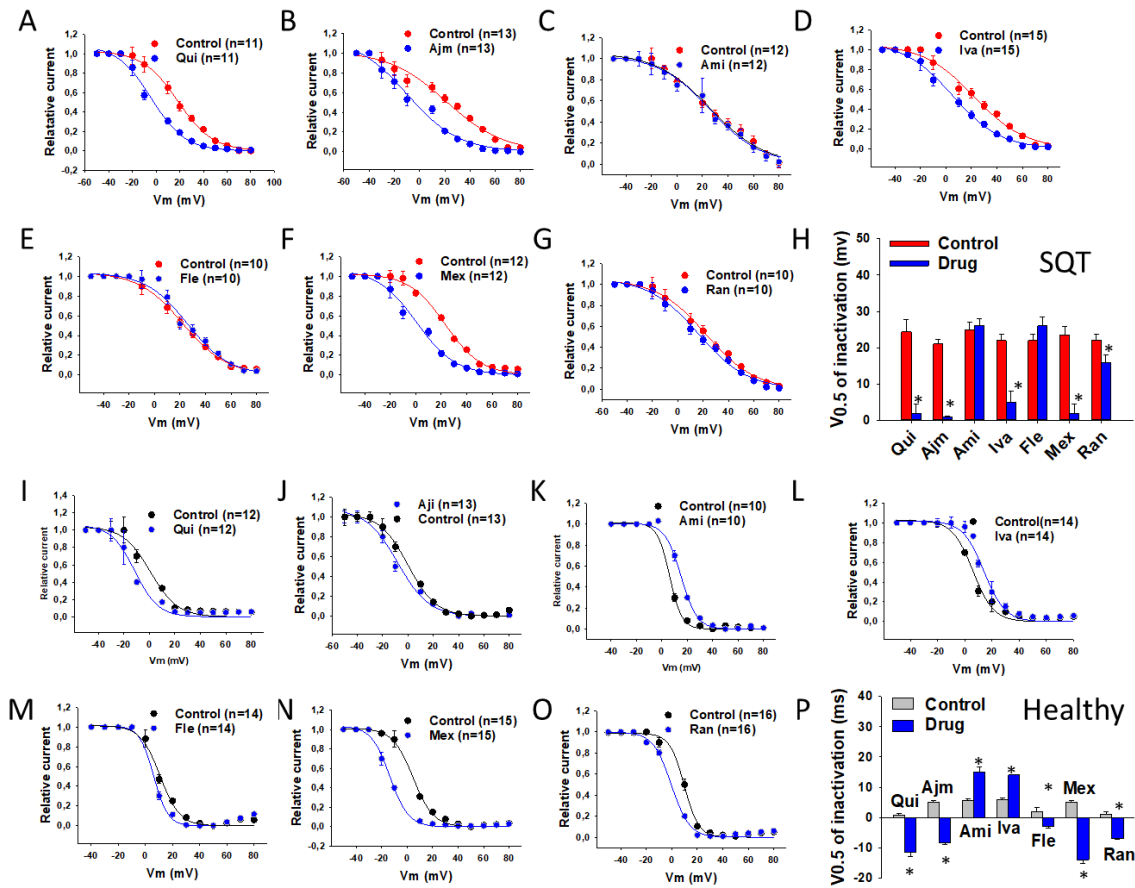
Figure 24. Drug effects on the inactivation of I_{Kr} in healthy and SQTS1-hiPSC-CMs. I_{Kr} in cells was recorded by patch clamp whole cell recording technique with the protocol as shown in figure 17. 10 µM quinidine (Qui), 10 µM ivabradine (Iva), 30 µM ajmaline (Ajm), 100 µM mexiletine (Mex), 10 µM amiodarone (Ami), 30 µM ranolazine (Ran) or 30 µM flecainide (Fle) was applied to measured cells by a perfusion pipette. The inactivation curves and V0.5 values were analyzed as described in figure 17. (A)-(G) Inactivation curves of I_{Kr} before (Control) and after application of a drug in SQTS1-hiPSC-CMs. (H) Mean values of V0.5 of inactivation curves before (Control) and after application of a drug in SQTS1-hiPSC-CMs. (I)-(O) Inactivation curves of I_{Kr} before (Control) and after application of a drug in healthy donor hiPSC-CMs. (P) Mean values of V0.5 of inactivation curves before (Control) and after application of a drug in healthy donor hiPSC-CMs. Shown are mean ± SEM, n represents the number of measured cells. The statistical significance was examined by paired t-test (comparison

between before and after application of a drug in same cells), *p<0.05 versus Control. Data in H and P are calculated from data in A-G and I-O, respectively.

Furthermore, in SQTS1-hiPSC-CMs, ajmaline, flecainide and ranolazine reduced the speed of the inactivation (the time constant was increased), whereas amiodarone and ivabradine accelerated it (figure 25 A-G). Quinidine and mexiletine had no significant effects (figure 25 A-G). In healthy donor hiPSC-CMs, quinidine, ajmaline, amiodarone and flecainide decelerated the inactivation (the time constant was increased), while ivabradine, mexiletine and ranolazine increased the speed of inactivation (the time constant was decreased) (figure 25 H-N).
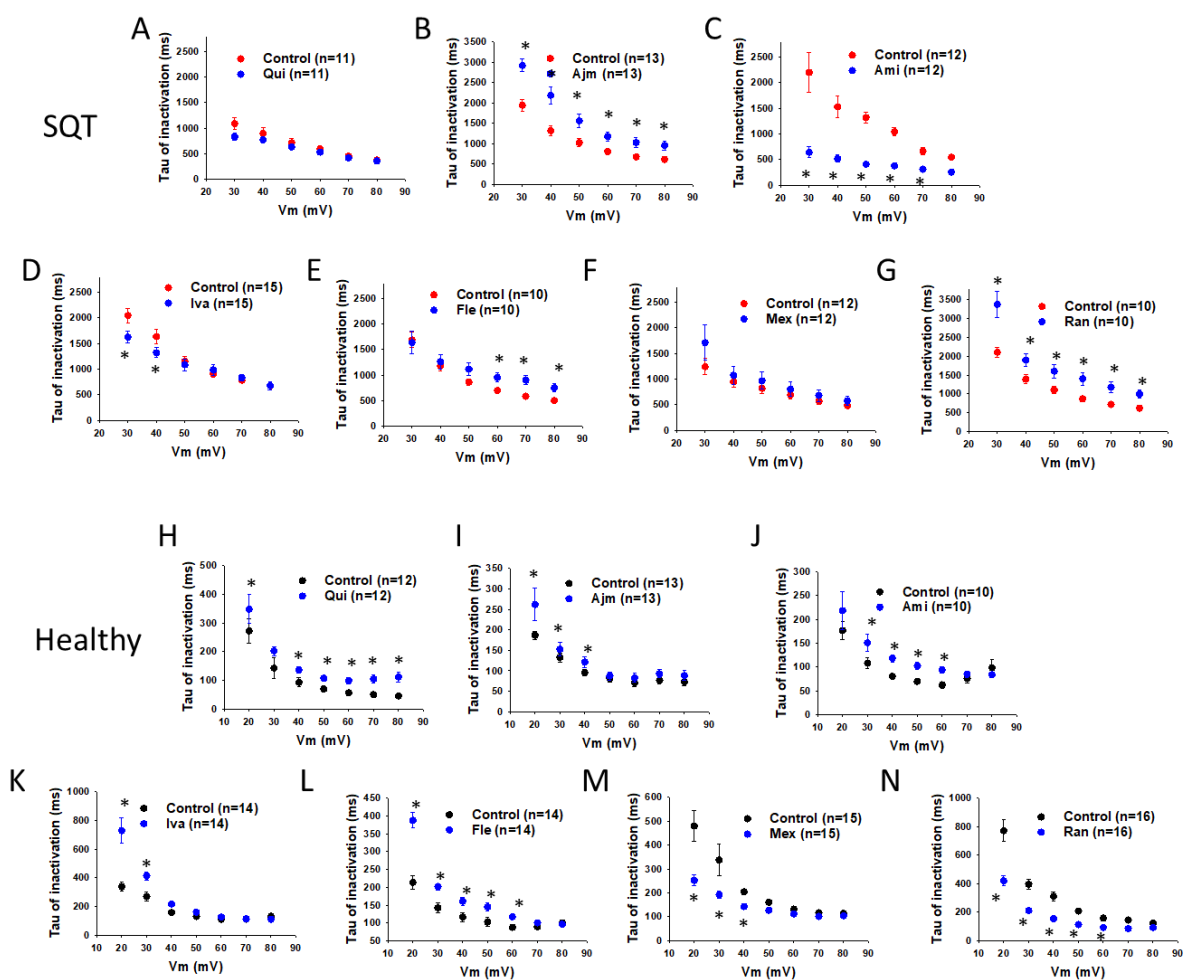
Figure 25. Drug effects on the time constant of I_{Kr} inactivation in healthy and SQTS1-hiPSC-CMs. To evaluate drug effects on the fast phase of inactivation, I_{Kr} was induced by a 1 s-long pre-pulse from -80 mV to 80 mV for activation and inactivation of channels, then returned to -120 mV for 20 ms for recovery of channels, and then 500 ms test-pulses from 20

mV to 80 mV (10 mV increments) were started, as shown in figure 17. Currents induced by test pulses were fitted by single exponential decay to obtain the time constant (Tau) of I_{Kr} fast inactivation. (A)-(G) Mean values of Tau of I_{Kr} inactivation in SQTS1-hiPSC-CMs before (Control) and after application of quinidine (Qui, 10 µM), ajmaline (Ajm, 30 µM), amiodarone (Ami, 10 µM), ivabradine (Iva, 10 µM), flecainide (Fle, 30 µM), mexiletine (Mex, 100 µM) and ranolazine (Ran, 30 µM). (H)-(N) Mean values of Tau of I_{Kr} inactivation in healthy donor hiPSC-CMs before (Control) and after application of each drug. Shown are mean ± SEM, n represents the number of cells. The statistical significance was determined by paired t-test, *$p < 0.05$ versus Control.

Due to the possibility that the shift of activation or inactivation curves may change the window current, we analyzed drug effects on the I_{Kr} window current. In SQTS1-hiPSC-CMs, quinidine, ivabradine, ajmaline and mexiletine decreased the I_{Kr} window current, while amiodarone, flecainide and ranolazine showed no effect (figure 26 A-G). In healthy hiPSC-CMs, quinidine, ajmaline and mexiletine, but not ivabradine, ranolazine, amiodarone and flecainide, decreased the window current (figure 26 H-N). Notably, the window current in SQTS1-hiPSC-CMs is larger than that in healthy donor hiPSC-CMs (figure 26 O).
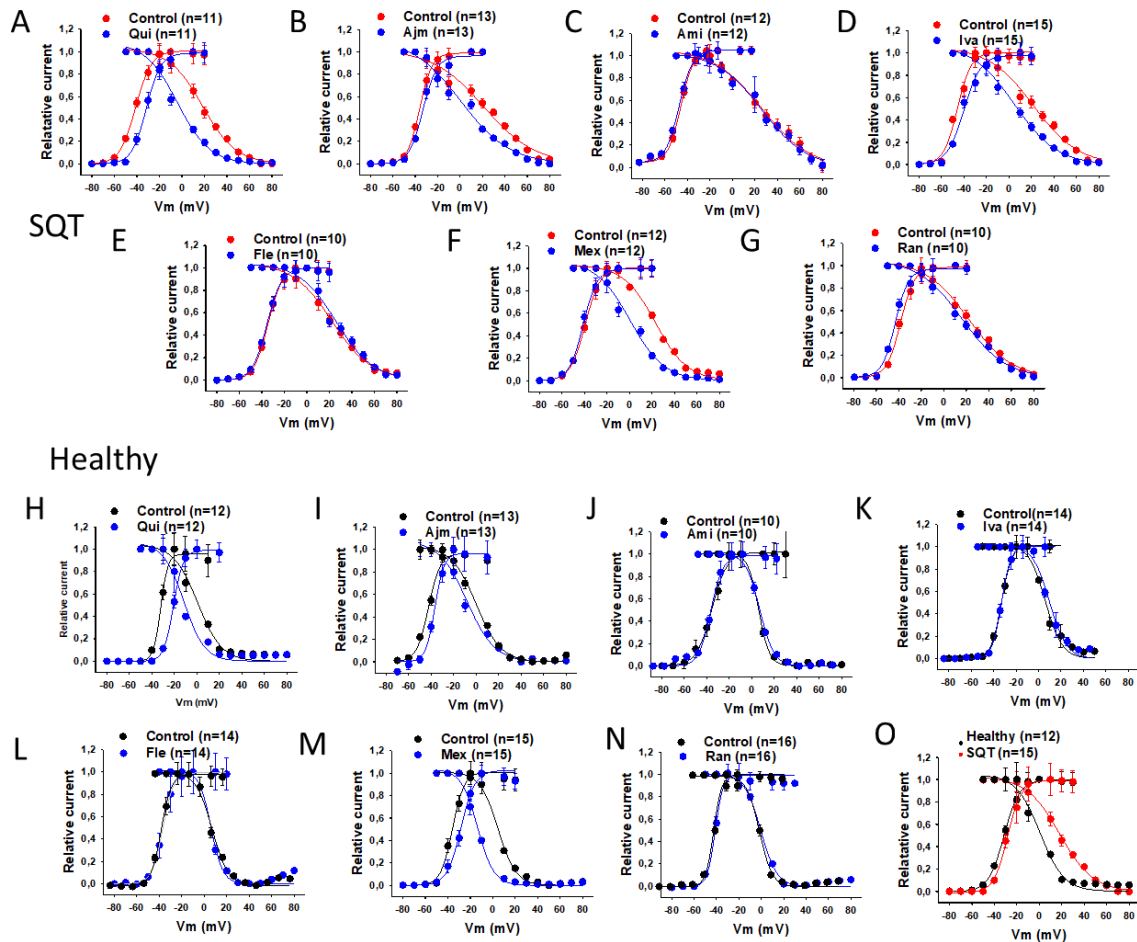
Figure 26. Drug effects on window currents of I_Kr in healthy and SQTS1-hiPSC-CMs. The activation and inactivation curves were plotted in the same figure. The window current was defined as the current under the crossover of activation and inactivation curves. For comparison, the window currents in absence (black and red symbols and lines) and presence (blue symbols and lines) of drugs were overlapped in the same plot. (A)-(G) Widow currents in SQTS1-hiPSC-CMs before (Control) and after application of quinidine (Qui, 10 µM), ajmaline (Ajm, 30 µM), amiodarone (Ami, 10 µM), ivabradine (Iva, 10 µM), flecainide (Fle, 30 µM), mexiletine (Mex, 100 µM) and ranolazine (Ran, 30 µM). (H)-(N) Widow currents in healthy donor hiPSC-CMs before (Control) and after application of each drug. (O) Window currents in healthy donor and SQTS1-hiPSC-CMs before application of drug.

To assess drug effect on the I_Kr recovery, the time constant (Tau) of tail currents reflecting the recovery of hERG channels was analyzed (figure 27 A-B). In healthy donor hiPSC-CMs, the Tau value of recovery was increased by quinidine, ivabradine and ranolazine, decreased by amiodarone but not significantly changed by ajmaline, flecainide and mexiletine (figure 27 A). In SQTS1-hiPSC-CMs, ajmaline, amiodarone and mexiletine decreased the Tau value of recovery, whereas flecainide and quinidine

increased it (figure 27 B). Ivabradine and ranolazine did not change the Tau of recovery (figure 27 B).
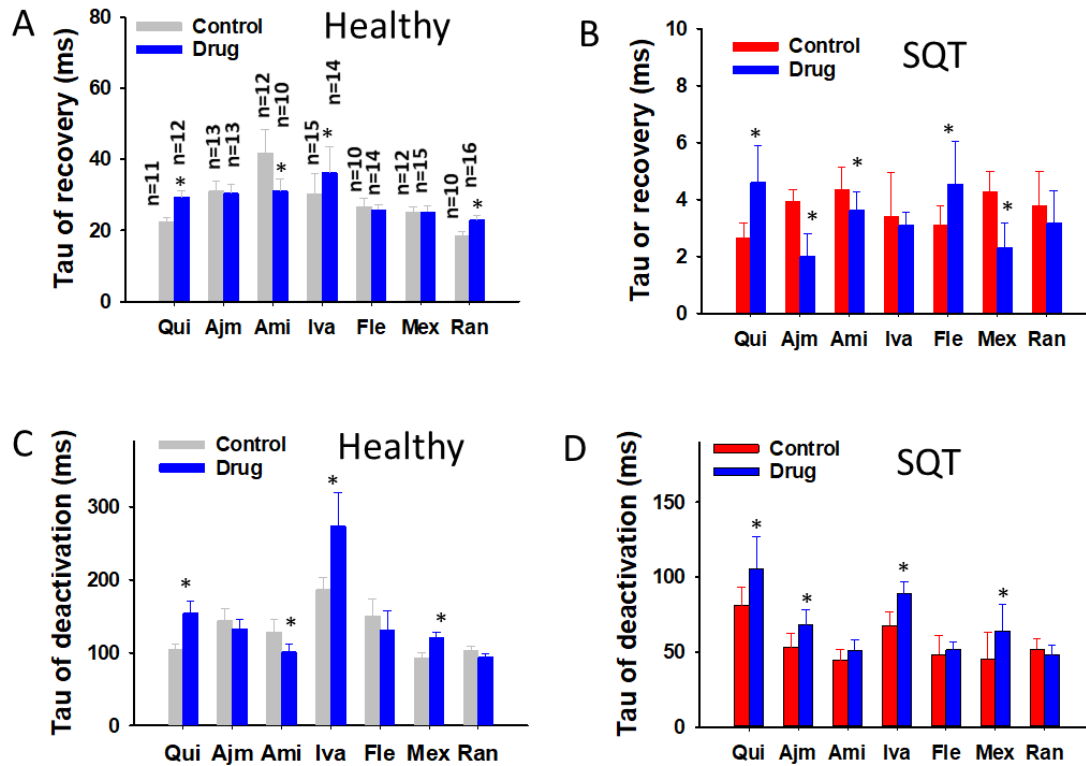
Figure 27. Drug effects on time constants of I_{Kr} recovery and deactivation in healthy and SQTS1-hiPSC-CMs. The time constant (Tau) of recovery and deactivation was analyzed as described in figure 18 and 19. (A) Mean values of Tau of I_{Kr} recovery from inactivation at -60 mV in healthy hiPSC-CMs before (Control) and after application of quinidine (Qui, 10 μM), ajmaline (Ajm, 30 μM), amiodarone (Ami, 10 μM), ivabradine (Iva, 10 μM), flecainide (Fle, 30 μM), mexiletine (Mex, 100 μM) and ranolazine (Ran, 30 μM). (B) Mean values of Tau of I_{Kr} recovery from inactivation at -60 mV in SQTS1-hiPSC-CMs before (Control) and after application of each drug. (C) Mean values of Tau of I_{Kr} deactivation at -80 mV in healthy donor hiPSC-CMs before (Control) and after application of each drug. (D) Mean values of Tau of I_{Kr} deactivation at -80 mV in SQTS1-hiPSC-CMs before (Control) and after application of each drug. Shown are mean ± SEM, n represents the number of cells. The n-numbers given in A are for A-D. The statistical significance was determined by paired t-test, *p<0.05 versus Control.

Finally, the deactivation of I_{Kr} was analyzed in hiPSC-CMs (figure 27 C-D). In healthy donor hiPSC-CMs, amiodarone decreased the time constant (Tau) of deactivation, whereas ivabradine, quinidine and mexiletine increased it (figure 27 C). Ajmaline,

flecainide and ranolazine showed no effect on the channel deactivation (figure 27 C). In SQTS1-hiPSC-CMs, quinidine, ajmaline, ivabradine and mexiletine increased the Tau of deactivation of I_{Kr}, but amiodarone, flecainide and ranolazine did not change it (figure 27 D).

4. DISCUSSION

4.1. Clinical relevance of study

The study investigated changes of cellular electrical activity in hiPSC-CMs carrying the mutation N588K in hERG channels and the mutation-related changes of the regulation of hERG channels by some environmental factors and antiarrhythmic drugs. The main findings are that: 1) the hERG channel current (I_{Kr}) was enhanced, the APD was shortened and arrhythmic events were increased in SQTS1 patient-hiPSC-CMs carrying the hERG channel mutation; 2) the activation and inactivation of hERG channels were attenuated, while the recovery from inactivation and the deactivation were enhanced in SQTS1 patient-hiPSC-CMs; 3) acidosis, high frequency, hyperthermia, LPS and ROS influenced hERG channel current and gating kinetics in SQTS1 patient-hiPSC-CMs and these effects differed from that in healthy donor hiPSC-CMs; 4) the effect of LPS on hERG channels was mediated by a NADPH oxidase-ROS-PKC pathway and enhanced in SQTS1-hiPSC-CMs compared to healthy donor cells; 5) quinidine, ajmaline, ivabradine, mexiletine but not amiodarone, flecainide and ranolazine prolonged APD and reduced arrhythmic events in SQTS1-hiPSC-CMs; 6) the drug effects on hERG channel current and gating kinetics in SQTS1-hiPSC-CMs differed from that in healthy donor hiPSC-CMs.

Although SQTS is a rare disease, it can cause life-threatening arrhythmias, especially in young persons. The mechanisms by which arrhythmias occur in SQTS-patients are still not clearly clarified. Therefore, optimal therapy for SQTS is still lacking. So far, the implantable cardioverter defibrillator (ICD) is recommended as the first choice for preventing life-threatening arrhythmias in SQTS-patients [2]. However, ICD is not applicable or suitable for some patients, who therefore require drug therapy. Up to date, only a limited number of drugs were tested in small number of SQTS-patients and only quinidine was shown to be effective for prolonging QT interval or reducing occurrence

of arrhythmias [116]. Quinidine is not acceptable or contradicted in some patients due to its severe side effect. Thus, more effective drugs are needed for the treatment of SQTS. In search for new effective alternatives, a detailed investigation of the underlying mechanisms of arrhythmogenesis in SQTS patients may provide help. The pathogenic role of N588K for SQTS1 has been confirmed by different studies including a gene editing study [117]. Although it has been known that this mutation causes an inactivation defect, which can contribute to the enhancement of I_{Kr} (gain-of-function), whether the mutation also change other gating parameters of hERG channel in cardiomyocytes is not clear. The fact that the SQTS-patient with the gene mutation suffered from arrhythmias only under certain condition suggests roles of co-factors for the occurrence of arrhythmias. Whether environmental factors modulate wild-type (healthy) and N588K-hERG channel differentially has not been investigated. This study, using hiPSC-CMs generated from an SQTS1-patient, investigated the mechanisms behind changes of hERG channel currents and the modulations of hERG channels by some environmental factors and drugs, focusing their difference between cells obtained from healthy donors and the patient. Therefore, the study may put new insights into the arrhythmogenesis of SQTS, especially SQTS1 with the N588K hERG mutation. It may help search for new effective drugs for SQTS-treatment.

4.2. Possible mechanisms underlying arrhythmias in SQTS1-hiPSC-CMs

The main phenotype features of SQTS are shortened QT interval and arrhythmias. The former is persistent, the latter is conditional, suggesting that short QT interval is not the only and direct cause for the occurrence of arrhythmias, but rather a substrate for arrhythmias. It is well-known that QT-prolongation (long-QT syndrome) can cause arrhythmias and the mechanism has been well investigated. QT prolongation in ECG means APD prolongation in cardiomyocytes. The prolonged APD can augment opening of calcium channels at phase 2. The enhanced Ca^{2+} influx can stimulate the Na^+/Ca^{2+} exchanger, generating an inward current (3 Na^+ influx versus 1 Ca^{2+} efflux). The inward Ca^{2+} and Na^+/Ca^{2+} exchanger currents can cause depolarizations even when the membrane potential has not been repolarized to resting potential. This phenomenon is called early afterdepolarization (EAD). EAD can cause torsades de pointes, tachycardia or other forms of arrhythmias [118, 119]. In SQTS, however, APD is shortened, suggesting different mechanisms for the arrhythmogenesis in SQTS.

When APD is shortened, the resting phase (interval between two APs) is prolonged, which increases the chance for occurrence of extra depolarizations. The extra depolarizations that appear before the next normal AP occurs are called delayed afterdepolarization (DAD). DADs arise from the resting potential after full repolarization of an action potential (phase 4) and they may reach threshold for activation and induce extra excitations [119]. DAD can be caused by elevated cytosolic Ca^{2+} concentrations, classically seen with digoxin toxicity [120]. The overload of Ca^{2+} in the sarcoplasmic reticulum (SR) can increase spontaneous Ca^{2+} release after repolarization. The elevated intracellular Ca^{2+} may trigger the Na^+/Ca^{2+}-exchanger, resulting in a net inward current. In addition, high intracellular Ca^{2+} can also activate non-specific cation channels, generating inward currents [119]. The inward currents generate the DAD, which may trigger arrhythmias. This means that DAD can be one mechanism for the arrhythmogenesis in SQTS. In our study, more DAD events and trigger activities (clusters of DAD or EAD) were observed in SQTS1-hiPSC-CMs, which is in agreement with this concept. The open question, however, is how DAD are triggered in SQTS1 patient cells.

A Ca^{2+} overload needs a substrate or trigger such as APD-prolongation or drugs that can elevate the intracellular Ca^{2+} level. Both were lacking in our hiPSC-CMs at base line (without any trigger), but still some cells displayed DADs. The reason for DADs in SQTS1-hiPSC-CMs at base line is not clear. One possibility could be the consequence of ion channel remodeling resulting from the changes in SQTS1-cells. We know that normal APs warrant normal cardiac functions, either the electrical or the mechanical. The AP is determined by both inward and outward currents conducted through different ion channels. A change of one or some currents can change APs and hence cardiac function, which may cause compensatory reaction in cells. In SQTS1-hiPSC-CMs, the N588K mutation in hERG gene caused a gain-of-function and increased I_{Kr} and hence shortened APD. It could be possible that these alterations caused a compensatory reaction in cells. Since an increase in inward current can prolong APD, it is possible that some intracellular signaling or ion channels were remodelled in favor of increasing the inward current. If the inward currents are large enough, especially when phase 3 is shortened, DADs may appear. Which signaling or ion channels are remodelled and responsible for DADs in SQTS1-hiPSC-CMs needs to explored in future studies.

Of note, EADs were also detected in SQTS1-hiPSC-CMs in absence or presence of epinephrine even though APD was shortened. We know that EAD usually appears when APD is prolonged, which favors opening of Ca channels. In other words, APD-shortening should reduce opening of Ca^{2+} channels and reduced the chance of EADs. The reason for the observed EADs in SQTS1-hiPSC-CMs could be the observed abnormal Ca^{2+} release at phase 3 of APs which subsequently caused EADs. The reason for this abnormal Ca^{2+} release in SQTS1-hiPSC-CMs is still unclear and needs to be revealed in future studies.

Beside EAD and DAD, re-entry can be another mechanism for arrhythmogenesis in SQTS. Shinnawi et al. established 2-dimensional hiPSC-CM modeling approach to investigate the tissue's electrophysiological properties in hiPSC-CMs from an SQTS1-patient [117]. To this end, they induced arrhythmias in the different hiPSC-CM groups through a systematic electrical programmed stimulation approach. Using this protocol, they could robustly induce sustained re-entrant arrhythmias in the SQTS-hiPSC-CMs, indicating that re-entry may be an important mechanism for the occurrence of arrhythmias in SQTS as well. As our study is based on single-cell measurements we cannot investigate re-entry induced arrhythmias in our model system

Although DAD, EAD and re-entry all might contribute to the occurrence of arrhythmias, the APD-shortening is the basic and most important substrate for arrhythmogenesis in SQTS. Hence, exploring mechanisms underlying the APD/QT-shortening is of importance for preventing and treating arrhythmias in SQTS. Previous studies showed the N588K mutation led to inactivation defect of hERG channels and enhanced I_{Kr} [121], which can explain the APD/QT-shortening in SQTS-patients. However, several questions remain open. First, the inactivation defect and gain-of-function was detected in non-cardiac cells. Whether the mutation causes the same changes in cardiomyocytes is not known. Second, the gating kinetics were not fully investigated before. Whether the mutation changed hERG gating kinetics besides inactivation was not clearly addressed. One aim of the current study is to address these two issues. In our SQTS1-hiPSC-CMs, I_{Kr} was enhanced and the inactivation of I_{Kr} was largely reduced by a large shift of the inactivation curve to a more positive potential. These data, from cardiomyocyte like cells, now confirmed the previously reported data. In addition, we found that due to the N588K mutation in cardiomyocytes like hiPSC-CMs, the time-course of inactivation was slowed, the activation was reduced (activation

shifted to a more positive potential, time to peak prolonged), whereas the recovery from inactivation and the deactivation of hERG channel were accelerated. The slowed inactivation and accelerated recovery from inactivation may contribute to the enhanced I_{Kr}. The reduced speed and right-shift of the activation suggest that I_{Kr} may be enhanced mainly when the membrane potential is depolarized to high potentials. As a slow deactivation of I_{Kr} may exert a protective effect against premature arrhythmogenic depolarizations like EADs or DADs [122, 123], the accelerated deactivation may reduce the outward current at the end of phase 3 or beginning of phase 4 for counteracting the inward currents at the same time and hence increase the chance of the occurrence of DAD or EAD in SQTS1 patient cells.

4.3. Possible roles and mechanism of environmental factors for arrhythmias in SQTS1-hiPSC-CMs

Besides genetic factors, non-genetic (environmental) factors are important for the arrhythmogenesis of SQTS as arrhythmias appear only under certain circumstances. In SQTS-patients, arrhythmias occur usually at rest or at night, indicating that a trigger, probably changes of adrenergic/muscarinic stimulation, plays an important role. In a recent study, it was detected that carbachol (CCh) triggered arrhythmic events [124]. Herein, epinephrine (Epi) increased arrhythmic events in SQTS1 patient but not healthy donor hiPSC-CMs, confirming the importance of a trigger for the occurrence of arrhythmias in SQTS. The trigger effect of Epi can be apprehended as it can increase Ca^{2+} influx by activating L-type Ca channels, which is a well-known mechanism for positive inotropic effect of adrenergic stimulation on cardiomyocytes. By contrast, how CCh triggered arrhythmias in SQTS1-hiPSC-CMs is difficult to understand. When CCh was applied to hiPSC-CMs, no effect on APs or I_{Kr} was observed, which cannot explain the arrhythmia-inducing effect of CCh. One possibility is that CCh may influence other channel currents. In our previous study, we checked CCh effect on inward (I_{Na}, I_{Ca}, I_{NCX}) and outward currents (I_{to}, I_{Ks}, I_{K1}, I_{KATP}, I_{SK1-3}, I_{SK4}), which can influence APs, and no effect was detected [99]. Another possibility is that CCh may change Ca^{2+} handling and cause abnormal Ca^{2+} release from the SR in SQTS1 patient but not healthy donor cells. The abnormal Ca^{2+} release could cause DADs and triggered arrhythmias. Indeed, in our study, Ca^{2+} transient measurements detected abnormal Ca^{2+} transients (DAD-like or EAD-like), which displayed as arrhythmic events, in SQTS1-hiPSC-CMs. This

suggests that CCh-triggered arrhythmias might at least partially result from dysfunctional Ca^{2+} handling.

Besides adrenergic/muscarinic stimulation, other factors including high temperature (e.g., fever), pH value (e.g., acidosis), inflammation or oxidative stress may contribute to the occurrence of arrhythmias. Therefore, it was interesting to examine whether those environmental factors can be potential triggers for arrhythmias in SQTS patient cells. To this end, we investigated the effects of those factors on APs and hERG channel current and gating kinetics in healthy donor and SQTS1 patient cells to figure out whether the mutation of N588K renders hERG channel more sensitive to such environmental factors.

In acidosis (pH=6.0), APs were shortened and I_{Kr} was reduced in both healthy donor and SQTS1-hiPSC-CMs. The AP shortening and I_{Kr} reduction induced by acidosis were consistent with previously reported data [125-127]. Hirayama et al found that in the low pH solution at 6.4, APD was markedly shortened and the amplitude of I_{Cl-Ca} (Ca^{2+}-activated Cl^- channel current) was increased at all membrane potentials and concluded that the APD-shortening caused by acidosis resulted from the activation of Ca^{2+}-activated Cl^- currents[125]. Terai et al investigated the effect of external acidosis on hERG current expressed in Xenopus oocytes. They found that the steady-state activation was shifted by about 20 mV in a depolarized (more positive potential) direction with a change from pH(o) 7.6 to 6.0, while steady-state inactivation was not significantly changed. The activation time constants were increased, the deactivation and recovery time constants were decreased, while those of inactivation showed no significant change [126]. The results indicated that external acidosis suppressed hERG current mainly by shifting the voltage-dependence of the activation and deactivation kinetics, and partly by decreasing slope conductance [126]. Du et al found that hERG channel current (I_{hERG}) recorded in hERG-expressing Chinese Hamster Ovary cells using action potential clamp was rapidly suppressed by reducing external pH from 7.4 to 6.3; steady state I_{hERG} activation curve was shifted by $\sim$+6 mV; the voltage-dependence of I_{hERG} inactivation was little-altered; fast and slow time-constants of I_{hERG} deactivation were smaller across a range of voltages at pH 6.3 than at pH 7.4; a modest acceleration of the time-course of recovery of I_{hERG} from inactivation was observed, but time-course of activation was unaffected [127]. These data as well as our own data, which show an inhibition of I_{Kr}, cannot explain the APD-shortening because the I_{Kr}-inhibition should

prolong APD. The APD-shortening in acidosis resulted probably from changes of other channel currents. Of note, changes of APs and I_{Kr} and I_{Kr} gating kinetics in our healthy and SQTS1 patient cells are similar, implying that the mutation of N588K may not increase the risk of acidosis-triggered arrhythmias in SQTS patients.

Fever can trigger arrhythmias in some patients, especially in some patients with Brugada syndrome. To check whether fever might be a potential trigger for SQTS, the effects of temperature variation on I_{Kr} were investigated in healthy donor and SQTS1-hiPSC-CMs. Thus, to mimic fever conditions, I_{Kr} was recorded at 40°C. As expected, at 40°C, I_{Kr} was enhanced. Our results differed from previously reported data from isolated rat cardiomyocytes. The disparity may result from species and gene mutation differences.   It was reported that compared with culture at 37°C, culture at 40°C decreased the hERG expression and I_{Kr} and thus prolonged the APD [128]. Another study investigated the effect of fever in I_{Kr} in LQT-2 patients with A558P and F640V missense mutation in the hERG channel [114]. In that study, the ECG displayed a prolongation of QTc with fever in both patients. When WT, A558P, and WT+A558P hERG channels were expressed in HEK293 cells, A558P proteins showed a trafficking-deficient phenotype and the co-expression of WT+A558P displayed a dominant-negative effect, thus selectively accelerating the rate of channel inactivation and reducing the temperature-dependent increase of current compared to the WT current. The temperature induced increase in WT+A558P current was smaller than that in the WT current, leading to larger current density differences at higher temperatures. A similar temperature-dependent phenotype was seen for co-expression of the trafficking-deficient LQT-2 F640V mutation. The authors thus postulated that the weak increase in the hERG current density in WT-mutant co-assembled channels contributes to the development of QTc prolongation and arrhythmias at higher temperatures and concluded that fever is a potential trigger for arrhythmias in LQT-2 patients [114]. In agreement with this concept, we detected that the I_{Kr} enhancement by higher temperatures in SQTS1 patient cells were larger than that in healthy donor cells. In addition, we found that higher temperatures accelerated the time to peak, shifted the activation curve to more negative, the inactivation curve to more positive potential, and accelerated the recovery of I_{Kr} in healthy donor as well as SQTS patient cells. Nevertheless, the effects of hyperthermia on activation and inactivation curves in SQTS patient cells were larger than in healthy donor cells, indicating that the N588K mutation renders hERG channels more sensitive to fever, and hence that fever may

be another potential trigger for SQTS. Whether fever prolong or shorten APD/QTc may be determined by mutations in hERG channels or the total effects of higher temperature on a variety of channels contributing to the APD.

Malignant tachy- and brady-arrhythmia in myocarditis patients have been observed for quite a long time, indicating that inflammation might induce arrhythmic events as well [129]. Different factors in inflammatory responses, such as endotoxin, cytokines and C-reactive protein (CRP) may affect the electrophysiology of cardiomyocytes, either directly or indirectly [129]. To examine whether inflammation is a possible trigger for arrhythmias in SQTS, we investigated the effects of LPS treatment on I_{Kr} in healthy donor and SQTS1-hiPSC-CMs. LPS treatment enhanced I_{Kr} in both healthy donor and SQTS1-hiPSC-CMs, but importantly, the effect of LPS treatment was more pronounced in SQTS1 patient than that in healthy donor cells., Divergent effects of LPS treatment were reported from studies using different animal models. A study in a pig model showed that LPS induced a shortening of the APD that resulted from a decrease in I_{Ca} and an increase in I_K [130]. Another study observed that LPS induced a prolongation of action potential associated with enhanced Ca^{2+} efflux via the Na^+/Ca^{2+} exchanger in isolated rat cardiomyocytes [131]. Wondergem et al found that LPS prolonged the APD and suppressed I_{Kr} in atrial HL-1 mouse cardiomyocytes [132]. In our study, using hiPSC-CMs, we found that LPS shifted the activation curve of I_{Kr} to more negative and the inactivation curve to more positive potentials. These data are in accordance with the enhanced I_{Kr} after LPS treatment. Moreover, LPS treatment accelerated I_{Kr} deactivation in SQTS1 patient but not in healthy donor cells. The enhanced I_{Kr} likely shortens APD/QT and in addition, the acceleration of I_{Kr} deactivation may facilitate the occurrence of DAD. Therefore, our data indicate, that inflammation may be indeed a trigger for arrhythmias in SQTS1 patients, at least in those carrying the N588K mutation.

It is well known that reactive oxygen species (ROS) play critical roles in cell signaling. ROS is involved in different pathological process, including inflammation, neurodegeneration, diabetes, atherosclerosis and aging. The phenomenon that LPS can increase ROS production in cardiomyocytes has been widely described [133, 134]. ROS may also be involved in the process of ion channel regulation via direct or indirect modulation. It was reported that ROS increased the peak sodium current in rat muscle afferent DRG neurons through an unknown mechanism [135]. Another study

demonstrated that an increased ROS production was associated with the reduction of peak I_{Na} in HEK cells and cardiomyocytes [136]. To investigate the role of ROS in LPS-induced changes of I_{Kr} in hiPSC-CMs, we assessed the effects of NAC, a strong reducing agent, and H_2O_2, a main content of ROS in cells. Indeed, NAC attenuated and H_2O_2 mimicked the effects of LPS on I_{Kr}. In addition, H_2O_2 exerted effects on I_{Kr} gating kinetics, similar to the effects of LPS treatment. These data indicate that ROS likely mediate the effects of LPS treatment on I_{Kr}. A study reported that H_2O_2 exposure significantly prolonged the APD due to significantly decreased I_{to} and I_{K1} resulting in frequent early afterdepolarizations (EADs) in mouse cardiomyocytes [137]. In accordance, another study detected that an increased ROS production is associated with APD-prolongation in mouse cardiomyocytes [138]. Also, Chen et al observed a marked attenuation of I_{Kr} and a significant prolongation of APD by simulating ischemia/reperfusion (I/R) with sodium dithionite ($Na_2S_2O_4$) in ventricular myocytes of guinea pigs. The authors showed that the I_{Kr} amplitude was inhibited by 64% and the APD was increased by 87%. The inhibition of I_{Kr} was attributed to ROS overproduction during I/R, which indicate that the inhibition of I_{Kr} is one of the underlying mechanisms of the prolongation of the QT interval and the APD in I/R [139]. Taking together, those studies demonstrated that ROS can prolong APD by affecting ion channel currents including I_{Kr}, which differs from the results of our study in hiPSC-CMs. The discrepancy may result from species or tissue difference. However, our study revealed that the mutation N588K enhanced the effect of ROS effect on I_{Kr}, suggesting the effects ROS may vary in different patients carrying different gene mutations. To explore the source of ROS occurring from LPS treatment, we examined the effect of DPI, an inhibitor of NADPH oxidases, important enzymes for ROS generation. In fact, DPI prevented effect of LPS treatment on I_{Kr}, suggesting that NADPH oxidases might mediate the effects of LPS treatment, at least in hiPSC-CMs.

Protein kinase A (PKA) as well as protein kinase C (PKC) were reported to regulate I_{Kr}, and thus their involvement in the effect of LPS treatment on I_{Kr} was assessed. Chelerythrine, an alkaloid which besides multiple other effects inhibits PKC but not PKA, attenuated the effect of LPS treatment, whereas H89, a strong inhibitor of PKA with only minor influence on PKC, did not. These data argue for an involvement of PKC in the regulation of I_{Kr} by LPS in hiPSC-CMs. In accordance, phorbol-12-myristate-13-acetate (PMA), a PKC activator, mimicked the effect of LPS on I_{Kr} in a chelerythrine sensitive manner. Considering that both PKC and ROS participated in the effect LPS

treatment on I_{Kr}, we tried to explore whether ROS is a downstream or upstream factor of PKC within the cascade. As chelerythrine suppressed the effect of H_2O_2, a ROS substitute, but the antioxidant N-acetylcysteine (NAC) failed to alter of the stimulation of I_{Kr} by PMA, the data indicate that the PKC activation occurs downstream of ROS production. Taken together, our study demonstrated that LPS treatment can enhance I_{Kr} in hiPSC-CMs likely via a pathway involving NAPDH, ROS and PKC.

To explore the mechanism for loss of rate adaptation of APD/QTc in SQTS, we analyzed I_{Kr} at different frequencies. We detected a larger enhancement of I_{Kr} at high (3Hz) frequency in healthy donor hiPSC-CMs compared to SQTS1-hiPSC-CMs. This difference might explain the loss of rate adaptation in SQTS. Normally, when heart beat increases, the APD/QTc will shorten in order to warrant regular beats. This phenomenon is called rate adaptation. The high frequency increases I_{Kr} that can shorten the APD and hence facilitates the rate adaptation in healthy cardiomyocytes. However, in cardiomyocytes, carrying the N588K mutation (SQTS1- hiPSC-CMs) the increase of I_{Kr} was less pronounced, thus the APD was less shortened, which in turn would affect the rate adaptation in a diseased heart. The reason for the reduced I_{Kr} increase at high frequency in SQTS1-hiPSC-CMs is likely due to the accelerated deactivation caused by N588K mutation detected in SQTS1-cells. We know that I_{Kr} deactivates very slow in healthy donor (wild-type) cells. At high frequency, not all channels are completely deactivated, thus the residual currents likely accumulate and hence increase the current at phase 3 of APs which shortens the APD. In contrast, in the N588K mutant-cells, the deactivation is much faster, and in consequence much less residual current can accumulate. In agreement, a smaller enhancement of I_{Kr} at high frequency was observed in SQTS1-cells. Since at high frequency (3 Hz or higher), the time frame for measuring I_{Kr} is too short (totally<333 ms) for detecting differences between healthy donor and SQTS1 cells regarding the effects of high frequency on the channel gating, especially the recovery from inactivation and the deactivation, the data with respect to gating kinetics at high frequency were not analyzed in the current study.

4.4. Mechanisms of differential drug effects

To explore whether the SQTS1- hiPSC-CM model offer the possibility to evaluate of the effects of known antiarrhythmic drugs effects on hERG channels with gene mutation, we established a cellular arrhythmia model by challenging cells with

epinephrine and then characterized the influence of different drugs. Indeed, quinidine, ajmaline, ivabradine and mexiletine, but not amiodarone, flecainide or ranolazine, prolonged the APD and decreased the probability for arrhythmic events in SQTS1-cells. In healthy donor cells, I_{Kr} was inhibited by almost all of the tested drugs to a similar extent. Only amiodarone was less effective. In SQTS1 cells, however, the inhibitory effect of all drugs was reduced. Especially the inhibition by amiodarone, mexiletine, flecainide and ranolazine, was largely affected, whereas quinidine, ajmaline and ivabradine still displayed an inhibitory effect of more than 40%. This might explain why these drugs still showed antiarrhythmic effects. Albeit we observed that the suppression of the N588K-hERG channel current amplitude by all drugs is different from that of the wild type hERG current, whether those drugs exhibit different effects on N588K-hERG channel gating kinetics, still needs to be addressed.

Quinidine is an antiarrhythmic drug with a known I_{Kr}-blocking property, but severe side effects limit its clinical application. Yet, when it was demonstrated to be effective for SQTS-treatment, the interests of physicians and researchers in this dug was reinstated. It was observed that the mutation N588K rendered hERG channel resistant to many antiarrhythmic drugs including classical I_{Kr} blockers, with quinidine as an exception. In addition, different from other drugs that inhibit only inactivated I_{Kr} channels, quinidine inhibits I_{Kr} conducted by both activated and inactivated channels. The N588K mutation leads to an inactivation defect and hence decrease the effects of inactivation-affecting drugs [44, 140]. However, our study has added novel information: we found that besides known inactivation defect, the activation was also attenuated, the recovery and deactivation were accelerated in SQTS1-cells with N588K. In addition, we observed that the quinidine effects on activation (time to peak and V0.5 of activation), on inactivation (the tau of inactivation and V0.5 of inactivation), on the recovery from inactivation and the deactivation as well as on the window current of the hERG channel were similar in healthy donor and SQTS1-hiPSC-CMs, which may also be an explanation for the efficacy of quinidine. These data demonstrate that not only the inactivation defect but also changes in other gating kinetics caused by the N588K mutation contribute to differential drug efficacy, at least in our model.

The class Ia anti-arrhythmic drug ajmaline is commonly used in ECG diagnosis to unmask the phenotypic changes of Brugada syndrome (BrS). Ajmaline attenuates several currents, including I_{Na}, I_{to} and I_{Kr} [141, 142]. This suggests that ajmaline might bear

the potential for treating patient carrying the SQTS1 mutation. In our study, ajmaline suppressed I_{Kr}, prolonged APDs and decreased the occurrence of arrhythmic events in SQTS1-hiPSC-CMs. In HEK293 cells and Xenopus oocytes recombinantly expressing hERG channels, ajmaline suppressed I_{Kr}, but the mutations Y652A and F656A attenuated the efficacy of ajmaline [143]. Ajmaline shifted the activation curve to more hyperpolarized potentials but did not significantly change I_{Kr} inactivation, although it decreased Tau of the inactivation [143]. The influence of the N588K on the efficacy of ajmaline was, however, not assessed in that study. Here, we obtained new data about the influence of ajmaline on the gating kinetics of WT- and N588K-hERG channels in hiPSC-CMs. The influence of ajmaline on I_{Kr} activation (time to peak and V0.5 of activation), on inactivation (Tau of inactivation and V0.5 of inactivation) and on the window current are similar in healthy donor and SQTS1-hiPSC-CMs, whereas an alteration on the recovery and the deactivation by ajmaline could only be detected in SQTS1-hiPSC-CMs.

In the clinical setting, amiodarone alone failed to prolong QTc, but it prolonged QTc in an SQTS-patient when it was used together with metoprolol [20]. Hence, whether SQTS patients benefit from treatment with amiodarone is still unclear. In our study, amiodarone did not prolong APD and did not suppress the occurrence of arrhythmic events. Although it is known that amiodarone can inhibit I_{Kr}, the influence of amiodarone on the gating kinetics of hERG channels carrying the N588K mutation was not investigated before. Hence, no data were available to understand why quinidine but not amiodarone exerts beneficial effects in SQTS1-patients. Our study revealed a possible reason, i.e., that quinidine decreased the window current, slowed the recovery and deactivation, whereas amiodarone displayed no or opposite effects on those parameters.

Ivabradine prolonged the QT interval and reduced the occurrence of arrhythmias in a rabbit model of SQTS [144]. Ivabradine as a funny channel (I_f) inhibitor exerts no negative inotropic effects and can maintain stable hemodynamics. It is clinically used to reduce heart rate in patients with heart failure not tolerating β-adrenoceptor antagonist treatment. Ivabradine can also inhibit I_{Kr} [145]. In a previous study, hERG channels, either WT or mutant, were expressed in HEK cells and the influence of ivabradine on the channels was assessed [146]. The authors reported that ivabradine suppressed wild-type as well as mutant hERG channel currents. Whereas the N588K and S624A mutations

altered the efficacy of ivabradine weakly, the Y652A and F656A mutation had a more severe influence. Further, it was shown that ivabradine shifted the activation and inactivation curve to a more hyperpolarized potential without any effect on the time constant of inactivation of the wild-type hERG channel. In our study, we found that the inhibitory effect of ivabradine on I_{Kr} was reduced and the inactivation curve was shifted to a more hyperpolarized potential in SQTS1-cells, which data are in agreement with the previous study. However, we observed that ivabradine shifted the activation curve to a more depolarized potential, which is different from the results of the Melgari study. Further, we detected that ivabradine increased the time to peak, decreased Tau of the inactivation and increased Tau of the deactivation in healthy donor and SQTS1-cells. It decreased the window current in SQTS1-cells but not in healthy donor cells, and increased Tau of the recovery in healthy donor cells but not in SQTS1-cells.

Mexiletine was reported to reduce arrhythmias in a rabbit model of SQTS [147]. In our study, we also detected beneficial effects of mexiletine, showing APD-prolonging and arrhythmia-suppressing effects in the SQTS1-hiPSC-CMs. It is known that mexiletine inhibited recombinantly expressed I_{Kr}, but its effect on I_{Kr} and channel gating in cardiomyocytes has not been studied. In a study of Gualdani et al, wild-type and mutant hERG channels were expressed in HEK and CHO cells and mexiletine effects were investigated [148]. The study showed that 1) mexiletine suppressed I_{Kr} in a time- and voltage-dependent way; 2) the inhibition was attenuated by the Y652A and F656A mutations; 3) mexiletine decreased Tau of the activation but increased Tau of the deactivation, implying that it accelerates the activation and slows the deactivation; 4) mexiletine did not alter the channel inactivation. However, the effects of mexiletine on N588K-hERG gating were not assessed in that study. Our data revealed that the effect of mexiletine was largely attenuated in SQTS1-hiPSC-CMs. Mexiletine decreased time to peak in both healthy donor and SQTS1-hiPSC-CMs, indicating an acceleration of activation, which date are in agreement with the Gualdani´s study. Mexiletine also decelerated the deactivation which is also in agreement with the previous study. In contrast to the data reported by Gualdini and colleagues, mexiletine accelerated the inactivation in both healthy donor and SQTS1-hiPSC-CMs. This difference between our data and those reported previous study is most likely caused by use of recombinant expression models in the older study and to the use of cardiomyocyte like hiPSC-CMs herein which express the hERG channels at levels similar to that in native

cardiomyocytes. In addition, in our hands, mexiletine accelerated the recovery and reduced the window current, which data have not been reported so far.

Flecainide was reported to prolong the APD and the refractory period but was unable to decrease the occurrence of ventricular arrhythmias in a rabbit model of SQTS [149]. In a clinical study, flecainide treatment slightly prolonged the QT interval [24]. In our model, it reduced I_{Kr} to a minor extent, but showed no effect on the APD and the occurrence of arrhythmic events in SQTS1-hiPSC-CMs. In an earlier study, it was observed that flecainide decreased I_{Kr} of recombinantly expressed hERG channels in HEK293 cells, but the N588K mutation prevented this effect of flecainide [150]. In this study, flecainide failed to change the inactivation curve but increased Tau of the inactivation of WT-hERG channels [150]. Flecainide also shifted the activation curve to a more hyperpolarized potential without effect on Tau of the deactivation of WT-hERG channels [151]. Flecainide effects on N588K-hERG gating are still unknown. In our model we detected that 1) the effect of flecainide was decreased in SQTS1-hiPSC-CMs, 2) the time to peak of I_{Kr} was increased in healthy donor but not in SQTS1-hiPSC-CMs and 3) the inactivation curve was shifted to a more hyperpolarized potential in healthy donor but not in SQTS1-hiPSC-CMs. Flecainide showed no effect on the I_{Kr} window current. It slowed the recovery of I_{Kr} without an effect on the I_{Kr} deactivation in SQTS1-cells. Taken together, flecainide displayed a week inhibitory effect on I_{Kr} due to its week effect on inactivation and window current. Thus, in SQTS1-cells flecainide displayed no antiarrhythmic effects which might explain its failure in the treatment of SQTS-patients.

Ranolazine, an inhibitor of the late sodium current, is an antianginal drug with beneficial effects in heart failure patients and additional antiarrhythmic effects [152, 153]. It displayed potent antiarrhythmic effect in the rabbit model of SQTS [154]. Ranolazine was also reported to inhibit I_{Kr} in dog cardiomyocytes [155, 156]. In HEK293 cells expressing wild-type and mutant hERG channels, ranolazine reduced I_{Kr} and its effect was attenuated by several mutants including N588K [157]. In the presence of ranolazine the activation curve of wild-type I_{Kr} was shifted to a more hyperpolarized potential [157, 158]. It was also reported that ranolazine decreased Tau of the inactivation, but did not alter Tau of the recovery of I_{Kr} of recombinantly expressed hERG channels in HEK293 cells [158]. Additional effects of ranolazine on other I_{Kr} gating parameters have not been reported. The current study investigated the effects of ranolazine on the activation, inactivation,

recovery and deactivation of I_{Kr} in both healthy donor and SQTS1-cells. We detected that both the activation and inactivation curves were shifted in the same direction and hence the window current was not changed. The time to peak and Tau of the deactivation were similar in healthy donor and SQTS1-cells, whereas Tau of the inactivation and recovery was differentially attenuated by ranolazine in healthy donor and SQTS1-cells.

In summary, all the tested drugs inhibited the I_{Kr} in both healthy donor and SQTS1-cells. The inhibitory effect of each drug was reduced in SQTS1-hiPSC-CMs, although to a different extent, indicating the importance of hERG gene mutations for individual drug effects. Although the tested drugs showed different effects on the hERG channel gating kinetics in healthy donor and SQTS1-cells, we detected important properties: 1) quinidine, ajmaline, ivabradine and mexiletine but not amiodarone, flecainide and ranolazine decreased the window current in SQTS1-cells, 2) quinidine, ajmaline, ivabradine and mexiletine but not amiodarone, flecainide and ranolazine decelerated the deactivation of I_{Kr}. Given that quinidine, ajmaline, ivabradine and mexiletine but not amiodarone, flecainide and ranolazine had APD-prolonging and antiarrhythmic effects in SQTS1-cells, we assume that the window current-reducing and deactivation-slowing effect may allow for antiarrhythmic therapy in SQTS1-paptients carrying the hERG N588K mutation. Since it is possible that effects of individual drugs on other channel currents besides I_{Kr} may also contribute to the antiarrhythmic effects observed in SQTS1-hiPSC-CMs and side effects cannot anticipate in our model, the potential use of quinidine, ajmaline, ivabradine and mexiletine in SQTS1 patients needs to be verified in clinical studies.

4.5. Study limitations

Cells from only one SQTS1-patient and three healthy donors were used for this study. Individual differences should be considered when interpreting the data from this study. However, AP parameters and I_{Kr} in hiPSC-CMs from the three healthy donors were very similar, indicating that the interindividual variability of hiPSC-CMs generated in our lab is not large. Since it is difficult to recruit SQTS-patients carrying the same mutation, the study used cells from a single patient only. Moreover, in the present study, isogenic control cells were lacking. Taking data from the literature into account, it is highly likely that the differences detected between healthy donor and SQTS1-hiPSC-

CMs resulted from the hERG mutation. Nevertheless, the CRISPR/Cas9-mediated genome editing technology to introduce the mutation into healthy donor cells on the one hand and to correct the N588K mutation in SQTS1-hiPSC-CMs on the other hand should be performed in future experiments to clarify this issue. Furthermore, the immature hiPSC-CMs possess similarities but also differences comparing with adult human cardiomyocytes. The possibility that some factors or drugs exert effects on I_{Kr} in mature cardiomyocytes different from that in hiPSC-CMs cannot be excluded.

In addition, the concentration of the drugs used in the study was higher than those occurring in the blood stream of patients under therapy. Although, it is possible that lower concentration of an individual drug is needed to exert same or similar effects in vivo than on hiPSC-CMs in culture, the exploration of effective concentrations of these drugs for SQTS patient treatment need to be clinically evaluated, also with regard to the possibility of severe side effects.

4.6. Conclusions

From the results we conclude that (1) the hERG mutation N588K changes hERG channel gating kinetics and causes a gain-of-function of hERG channels, leading to APD-shortening and the SQTS phenotype; (2) the mutation alters the effects of some environmental factors and drugs on APs and hERG channel current or gating; (3) inflammation and fever can be potential trigger for arrhythmias in SQTS patients and (4) window current-reduction as well as a deceleration of the deactivation are likely critical properties of antiarrhythmic drugs for their potential use in SQTS1-paptients carrying the hERG-N588K mutation. Thus, our findings may help to understand the pathogenesis of SQTS and allow for the search for potential drug candidates to treat SQTS1-patients.

5. SUMMARY

Background-Short QT syndrome (SQTS) is a rare, inheritable heart disease representing abbreviated corrected QT interval (QTc) and sudden cardiac death (SCD). The short QT syndrome type 1 (SQTS1) is linked to hERG channel mutations. An optimal therapy for SQTS is still lacking. An implantable cardioverter defibrillator (ICD) is recommended as first choice for the treatment, but it is not applicable to every patient. Therefore, drug therapy is required for some, especially young patients. So far, only a small number of drugs has been tested in SQTS-patients and only quinidine has been shown to be effective. Searching new effective drugs for SQTS is of clinical importance. In spite of rapid progress in searching for genetic factors in SQTS, a convincing proof of genotype-phenotype correlation remains lacking for most SQTS forms. Functional roles of most gene mutations or variants associated with SQTS have not clarified. Of note, only a small part of SQTS-patients has been proved to carry the disease-associated gene mutation and arrhythmias appear only under certain conditions even in patients carrying a clear pathogenic mutation, suggesting roles of environmental factors. Studies regarding roles of environmental factors in occurrence of arrhythmias of SQTS remain spars. Whether and how the SQTS-associated mutation influence effects of environmental factors in cardiac electrophysiology are unknown. It is known that N588K in hERG can change drug affinity, but it is not known if it can change the drug effects on channel gating kinetics in cardiomyocytes.

Aims-The study was designed to assess the changes of hERG channel current and gating kinetics caused by genetic mutation and some environmental factors and drugs using healthy donor and SQTS1-cardiomyocytes carrying the N588K mutation.

Methods-Human-induced pluripotent stem cell-derived cardiomyocytes (hiPSC-CMs) from three healthy donors and an SQTS1-patient carrying the N588K mutation were generated and patch clamp, single cell contraction and calcium transient measurement techniques were used in these cells for the study.

Results-The hiPSC-CMs from the SQTS1-patient (SQTS1-hiPSC-CMS) showed enhanced hERG channel current (I_{Kr}), shortened action potential duration (APD) and arrhythmic events, the main features of SQTS. Both the activation and inactivation of I_{Kr} were attenuated. Time constants of activation and inactivation were increased and

the curves of activation and inactivation were shifted to more positive potentials, whereas the recovery from the inactivation and the deactivation of I_{Kr} were accelerated in SQTS1-hiPSC-CMs. Hyperthermia (40°C), Lipopolysaccharide (LPS) and reactive oxygen species (ROS) increased I_{Kr} with shifts of the activation and inactivation curves. The alterations in SQTS1-hiPSC-CMs were larger than that in healthy donor hiPSC-CMs. The effect LPS on I_{Kr} could be blocked by diphenyleneiodonium, N-acetylcysteine and chelerythine, suggesting that the effect of LPS treatment was mediated by an activation of NADPH oxidase/ROS/PKC involving pathway. High frequency (3Hz) electrical stimulation increased I_{Kr} in healthy donor but not in SQTS1-hiPSC-CMs, which may be one reason for the loss of frequency-adaptation in SQTS. Stimulation with isoprenaline and carbachol had no effect on I_{Kr}. Acidosis (pH6) inhibited I_{Kr} similarly in healthy donor and SQTS1-hiPSC-CMs. Ajmaline, amiodarone, ivabradine, flecainide, quinidine, mexiletine and ranolazine inhibited the hERG channel current (I_{Kr}) less effective in SQTS1-cells when compared with healthy donor cells. Quinidine and mexiletine decreased, but ajmaline, amiodarone, ivabradine and ranolazine increased the time to peak of I_{Kr} similarly in healthy donor and SQTS1-hiPSC-CMs. With respect to the shift of the activation and inactivation curves, the tested drugs showed differential effects in healthy donor and SQTS1-cells. Quinidine, ajmaline, ivabradine and mexiletine but not amiodarone, flecainide and ranolazine decreased the window current in SQTS1-cells. Quinidine, ajmaline, ivabradine and mexiletine affected the time constant of the recovery from inactivation differentially, but all of these drugs decelerated the deactivation of I_{Kr} in SQTS1-hiPSC-CMs.

Conclusion-Both the genetic and non-genetic factors can modulate hERG channel gating. The N588K mutation enhances the effect of hyperthermia, LPS, ROS and some drugs on hERG channel gating. Inflammation and fever may thus be potential triggers for the occurrence of arrhythmias in SQTS. Apparently, the window current-reduction and the deceleration of the deactivation of hERG channels may be critical properties for antiarrhythmic drugs such as ajmaline, ivabradine, quinidine and mexiletine to suppress the occurrence of arrhythmic events in SQTS1-hiPSC-CMs.

6. REFERENCES

1.   Gussak I, Brugada P, Brugada J, Wright RS, Kopecky SL, Chaitman BR, Bjerregaard P. Idiopathic short QT interval: a new clinical syndrome? Cardiology 2000;**94**(2):99-102.

2.   Campuzano O, Sarquella-Brugada G, Cesar S, Arbelo E, Brugada J, Brugada R. Recent Advances in Short QT Syndrome. Front Cardiovasc Med 2018;**5**:149.

3.   Guerrier K, Kwiatkowski D, Czosek RJ, Spar DS, Anderson JB, Knilans TK. Short QT Interval Prevalence and Clinical Outcomes in a Pediatric Population. Circ Arrhythm Electrophysiol 2015;**8**(6):1460-4.

4.   Iribarren C, Round AD, Peng JA, Lu M, Klatsky AL, Zaroff JG, Holve TJ, Prasad A, Stang P. Short QT in a cohort of 1.7 million persons: prevalence, correlates, and prognosis. Ann Noninvasive Electrocardiol 2014;**19**(5):490-500.

5.   El-Battrawy I, Schlentrich K, Besler J, Liebe V, Schimpf R, Lang S, Odening KE, Wolpert C, Zhou X, Borggrefe M, Akin I. Sex-differences in short QT syndrome: A systematic literature review and pooled analysis. Eur J Prev Cardiol 2020;**27**(12):1335-1338.

6.   Jorgensen IN, Skakkebaek A, Andersen NH, Pedersen LN, Hougaard DM, Bojesen A, Trolle C, Gravholt CH. Short QTc interval in males with klinefelter syndrome-influence of CAG repeat length, body composition, and testosterone replacement therapy. Pacing Clin Electrophysiol 2015;**38**(4):472-82.

7.   Akdis D, Saguner AM, Shah K, Wei C, Medeiros-Domingo A, von Eckardstein A, Luscher TF, Brunckhorst C, Chen HSV, Duru F. Sex hormones affect outcome in arrhythmogenic right ventricular cardiomyopathy/dysplasia: from a stem cell derived cardiomyocyte-based model to clinical biomarkers of disease outcome. Eur Heart J 2017;**38**(19):1498-1508.

8.   Mazzanti A, Kanthan A, Monteforte N, Memmi M, Bloise R, Novelli V, Miceli C, O'Rourke S, Borio G, Zienciuk-Krajka A, Curcio A, Surducan AE, Colombo M, Napolitano C, Priori SG. Novel insight into the natural history of short QT syndrome. J Am Coll Cardiol 2014;**63**(13):1300-1308.

9.   Brugada J, Gussak I, Brugada P. Short QT syndrome: a predictable story. Cardiology 2014;**128**(3):231-3.

10.   Suzuki H, Hoshina S, Ozawa J, Sato A, Minamino T, Aizawa Y, Saitoh A. Short QT syndrome in a boy diagnosed on screening for heart disease. Pediatr Int 2014;**56**(5):774-6.

11.   Gollob MH, Blier L, Brugada R, Champagne J, Chauhan V, Connors S, Gardner M, Green MS, Gow R, Hamilton R, Harris L, Healey JS, Hodgkinson K, Honeywell C, Kantoch M, Kirsh J, Krahn A, Mullen M, Parkash R, Redfearn D, Rutberg J, Sanatani S, Woo A. Recommendations for the use of genetic testing in the clinical evaluation of inherited cardiac arrhythmias associated with sudden cardiac death: Canadian Cardiovascular Society/Canadian Heart Rhythm Society joint position paper. Can J Cardiol 2011;**27**(2):232-45.

12.   Priori SG, Wilde AA, Horie M, Cho Y, Behr ER, Berul C, Blom N, Brugada J, Chiang CE, Huikuri H, Kannankeril P, Krahn A, Leenhardt A, Moss A, Schwartz PJ, Shimizu W, Tomaselli G, Tracy C. HRS/EHRA/APHRS expert consensus statement on the diagnosis and management of patients with inherited primary arrhythmia syndromes: document endorsed by HRS, EHRA, and APHRS in May 2013 and by ACCF, AHA, PACES, and AEPC in June 2013. Heart Rhythm 2013;**10**(12):1932-63.

13.   Priori SG, Blomstrom-Lundqvist C, Mazzanti A, Blom N, Borggrefe M, Camm J, Elliott PM, Fitzsimons D, Hatala R, Hindricks G, Kirchhof P, Kjeldsen K, Kuck KH, Hernandez-Madrid A, Nikolaou N, Norekval TM, Spaulding C, Van Veldhuisen DJ, Group ESCSD. 2015 ESC Guidelines for the management of patients with ventricular arrhythmias and the prevention of sudden cardiac death: The Task Force for the Management of Patients with Ventricular Arrhythmias and the Prevention of Sudden Cardiac Death of the European Society of Cardiology (ESC). Endorsed by: Association for European Paediatric and Congenital Cardiology (AEPC). Eur Heart J 2015;**36**(41):2793-2867.

14.   Dewi IP, Dharmadjati BB. Short QT syndrome: The current evidences of diagnosis and management. J Arrhythm 2020;**36**(6):962-966.

15.   El-Battrawy I, Muller J, Zhao Z, Cyganek L, Zhong R, Zhang F, Kleinsorge M, Lan H, Li X, Xu Q, Huang M, Liao Z, Moscu-Gregor A, Albers S, Dinkel H, Lang S, Diecke S, Zimmermann WH, Utikal J, Wieland T, Borggrefe M, Zhou X, Akin I. Studying Brugada Syndrome With an SCN1B Variants in Human-Induced Pluripotent Stem Cell-Derived Cardiomyocytes. Front Cell Dev Biol 2019;**7**:261.

16.   Migliore F, Silvano M, Zorzi A, Bertaglia E, Siciliano M, Leoni L, De Franceschi P, Iliceto S, Corrado D. Implantable cardioverter defibrillator therapy in young patients with cardiomyopathies and channelopathies: a single Italian centre experience. J Cardiovasc Med (Hagerstown) 2016;**17**(7):485-93.

17.   Schimpf R, Wolpert C, Bianchi F, Giustetto C, Gaita F, Bauersfeld U, Borggrefe M. Congenital short QT syndrome and implantable cardioverter defibrillator treatment: inherent risk for inappropriate shock delivery. J Cardiovasc Electrophysiol 2003;**14**(12):1273-7.

18.   Abriel H, Rougier JS. beta-blockers in congenital short-QT syndrome as ion channel blockers. J Cardiovasc Electrophysiol 2013;**24**(10):1172-4.

19.   Mizobuchi M, Enjoji Y, Yamamoto R, Ono T, Funatsu A, Kambayashi D, Kobayashi T, Nakamura S. Nifekalant and disopyramide in a patient with short QT syndrome: evaluation of pharmacological effects and electrophysiological properties. Pacing Clin Electrophysiol 2008;**31**(9):1229-32.

20.   Giustetto C, Schimpf R, Mazzanti A, Scrocco C, Maury P, Anttonen O, Probst V, Blanc JJ, Sbragia P, Dalmasso P, Borggrefe M, Gaita F. Long-term follow-up of patients with short QT syndrome. J Am Coll Cardiol 2011;**58**(6):587-95.

21.   Mazzanti A, Maragna R, Vacanti G, Kostopoulou A, Marino M, Monteforte N, Bloise R, Underwood K, Tibollo V, Pagan E, Napolitano C, Bellazzi R, Bagnardi V, Priori SG. Hydroquinidine Prevents Life-Threatening Arrhythmic Events in Patients With Short QT Syndrome. J Am Coll Cardiol 2017;**70**(24):3010-3015.

22.   El-Battrawy I, Besler J, Liebe V, Schimpf R, Tülümen E, Rudic B, Lang S, Wolpert C, Zhou X, Akin I, Borggrefe M. Long-Term Follow-Up of Patients With Short QT Syndrome: Clinical Profile and Outcome. J Am Heart Assoc 2018;**7**(23):e010073.

23.   El-Battrawy I, Besler J, Li X, Lan H, Zhao Z, Liebe V, Schimpf R, Lang S, Wolpert C, Zhou X, Akin I, Borggrefe M. Impact of Antiarrhythmic Drugs on the Outcome of Short QT Syndrome. Front Pharmacol 2019;**10**:771.

24.   Gaita F, Giustetto C, Bianchi F, Schimpf R, Haissaguerre M, Calo L, Brugada R, Antzelevitch C, Borggrefe M, Wolpert C. Short QT syndrome: pharmacological treatment. J Am Coll Cardiol 2004;**43**(8):1494-9.

25.   Hong K, Hu J, Yu J, Brugada R. Concomitant Brugada-like and short QT electrocardiogram linked to SCN5A mutation. Eur J Hum Genet 2012;**20**(11):1189-92.

26.   Hancox JC, Whittaker DG, Du C, Stuart AG, Zhang H. Emerging therapeutic targets in the short QT syndrome. Expert Opin Ther Targets 2018;**22**(5):439-451.

27.   Thorsen K, Dam VS, Kjaer-Sorensen K, Pedersen LN, Skeberdis VA, Jurevičius J, Treinys R, Petersen I, Nielsen MS, Oxvig C, Morth JP, Matchkov VV, Aalkjær C, Bundgaard H, Jensen HK. Loss-of-activity-mutation in the cardiac chloride-bicarbonate exchanger AE3 causes short QT syndrome. Nat Commun 2017;**8**(1):1696.

28.   Thorsen K, Dam VS, Kjaer-Sorensen K, Pedersen LN, Skeberdis VA, Jurevicius J, Treinys R, Petersen I, Nielsen MS, Oxvig C, Morth JP, Matchkov VV, Aalkjaer C, Bundgaard H, Jensen HK. Loss-of-activity-mutation in the cardiac chloride-bicarbonate exchanger AE3 causes short QT syndrome. Nat Commun 2017;**8**(1):1696.

29.   Campuzano O, Fernandez-Falgueras A, Lemus X, Sarquella-Brugada G, Cesar S, Coll M, Mates J, Arbelo E, Jorda P, Perez-Serra A, Del Olmo B, Ferrer-Costa C, Iglesias A, Fiol V, Puigmule M, Lopez L, Pico F, Brugada J, Brugada R. Short QT Syndrome: A Comprehensive Genetic Interpretation and Clinical Translation of Rare Variants. J Clin Med 2019;**8**(7).

30.   Brugada R, Hong K, Dumaine R, Cordeiro J, Gaita F, Borggrefe M, Menendez TM, Brugada J, Pollevick GD, Wolpert C, Burashnikov E, Matsuo K, Wu YS, Guerchicoff A, Bianchi F, Giustetto C, Schimpf R, Brugada P, Antzelevitch C. Sudden death associated with short-QT syndrome linked to mutations in HERG. Circulation 2004;**109**(1):30-5.

31.   Hu D, Li Y, Zhang J, Pfeiffer R, Gollob MH, Healey J, Harrell DT, Makita N, Abe H, Sun Y, Guo J, Zhang L, Yan G, Mah D, Walsh EP, Leopold HB, Giustetto C, Gaita F, Zienciuk-Krajka A, Mazzanti A, Priori SG, Antzelevitch C, Barajas-Martinez H. The Phenotypic Spectrum of a Mutation Hotspot Responsible for the Short QT Syndrome. JACC Clin Electrophysiol 2017;**3**(7):727-743.

32.   Sun Y, Quan XQ, Fromme S, Cox RH, Zhang P, Zhang L, Guo D, Guo J, Patel C, Kowey PR, Yan GX. A novel mutation in the KCNH2 gene associated with short QT syndrome. J Mol Cell Cardiol 2011;**50**(3):433-41.

33.   Bellocq C, van Ginneken AC, Bezzina CR, Alders M, Escande D, Mannens MM, Baro I, Wilde AA. Mutation in the KCNQ1 gene leading to the short QT-interval syndrome. Circulation 2004;**109**(20):2394-7.

34.   Harrell DT, Ashihara T, Ishikawa T, Tominaga I, Mazzanti A, Takahashi K, Oginosawa Y, Abe H, Maemura K, Sumitomo N, Uno K, Takano M, Priori SG, Makita N. Genotype-dependent differences in age of manifestation and arrhythmia complications in short QT syndrome. Int J Cardiol 2015;**190**:393-402.

35.   Lee HC, Rudy Y, Liang H, Chen CC, Luo CH, Sheu SH, Cui J. Pro-arrhythmogenic Effects of the V141M KCNQ1 Mutation in Short QT Syndrome and Its Potential Therapeutic Targets: Insights from Modeling. J Med Biol Eng 2017;**37**(5):780-789.

36.   Wu ZJ, Huang Y, Fu YC, Zhao XJ, Zhu C, Zhang Y, Xu B, Zhu QL, Li Y. Characterization of a Chinese KCNQ1 mutation (R259H) that shortens repolarization and causes short QT syndrome 2. J Geriatr Cardiol 2015;**12**(4):394-401.

37. Priori SG, Pandit SV, Rivolta I, Berenfeld O, Ronchetti E, Dhamoon A, Napolitano C, Anumonwo J, di Barletta MR, Gudapakkam S, Bosi G, Stramba-Badiale M, Jalife J. A novel form of short QT syndrome (SQT3) is caused by a mutation in the KCNJ2 gene. Circ Res 2005;**96**(7):800-7.

38. Hattori T, Makiyama T, Akao M, Ehara E, Ohno S, Iguchi M, Nishio Y, Sasaki K, Itoh H, Yokode M, Kita T, Horie M, Kimura T. A novel gain-of-function KCNJ2 mutation associated with short-QT syndrome impairs inward rectification of Kir2.1 currents. Cardiovasc Res 2012;**93**(4):666-73.

39. Deo M, Ruan Y, Pandit SV, Shah K, Berenfeld O, Blaufox A, Cerrone M, Noujaim SF, Denegri M, Jalife J, Priori SG. KCNJ2 mutation in short QT syndrome 3 results in atrial fibrillation and ventricular proarrhythmia. Proc Natl Acad Sci U S A 2013;**110**(11):4291-6.

40. Xia M, Jin Q, Bendahhou S, He Y, Larroque MM, Chen Y, Zhou Q, Yang Y, Liu Y, Liu B, Zhu Q, Zhou Y, Lin J, Liang B, Li L, Dong X, Pan Z, Wang R, Wan H, Qiu W, Xu W, Eurlings P, Barhanin J, Chen Y. A Kir2.1 gain-of-function mutation underlies familial atrial fibrillation. Biochem Biophys Res Commun 2005;**332**(4):1012-9.

41. Staff PCB. Correction: Atrial arrhythmogenicity of KCNJ2 mutations in short QT syndrome: Insights from virtual human atria. PLoS Comput Biol 2019;**15**(6):e1007145.

42. Antzelevitch C, Pollevick GD, Cordeiro JM, Casis O, Sanguinetti MC, Aizawa Y, Guerchicoff A, Pfeiffer R, Oliva A, Wollnik B, Gelber P, Bonaros EP, Jr., Burashnikov E, Wu Y, Sargent JD, Schickel S, Oberheiden R, Bhatia A, Hsu LF, Haissaguerre M, Schimpf R, Borggrefe M, Wolpert C. Loss-of-function mutations in the cardiac calcium channel underlie a new clinical entity characterized by ST-segment elevation, short QT intervals, and sudden cardiac death. Circulation 2007;**115**(4):442-9.

43. Templin C, Ghadri JR, Rougier JS, Baumer A, Kaplan V, Albesa M, Sticht H, Rauch A, Puleo C, Hu D, Barajas-Martinez H, Antzelevitch C, Luscher TF, Abriel H, Duru F. Identification of a novel loss-of-function calcium channel gene mutation in short QT syndrome (SQTS6). Eur Heart J 2011;**32**(9):1077-88.

44. McPate MJ, Duncan RS, Hancox JC, Witchel HJ. Pharmacology of the short QT syndrome N588K-hERG K+ channel mutation: differential impact on selected class I and class III antiarrhythmic drugs. Br J Pharmacol 2008;**155**(6):957-66.

45. Zhao Z, Li X, El-Battrawy I, Lan H, Zhong R, Xu Q, Huang M, Liao Z, Lang S, Zimmermann WH, Cyganek L, Wieland T, Akin I, Zhou XB, Borggrefe M. Drug Testing in Human-Induced Pluripotent Stem Cell-Derived Cardiomyocytes From a Patient With Short QT Syndrome Type 1. Clin Pharmacol Ther 2019;**106**(3):642-651.

46. Bauer CK, Schwarz JR. Ether-à-go-go K(+) channels: effective modulators of neuronal excitability. J Physiol 2018;**596**(5):769-783.

47. Benzer S. BEHAVIORAL MUTANTS OF Drosophila ISOLATED BY COUNTERCURRENT DISTRIBUTION. Proc Natl Acad Sci U S A 1967;**58**(3):1112-9.

48. Warmke J, Drysdale R, Ganetzky B. A distinct potassium channel polypeptide encoded by the Drosophila eag locus. Science 1991;**252**(5012):1560-2.

49. Warmke JW, Ganetzky B. A family of potassium channel genes related to eag in Drosophila and mammals. Proc Natl Acad Sci U S A 1994;**91**(8):3438-42.

50. Wimmers S, Wulfsen I, Bauer CK, Schwarz JR. Erg1, erg2 and erg3 K channel subunits are able to form heteromultimers. Pflugers Arch 2001;**441**(4):450-5.

51.   Schönherr R, Gessner G, Löber K, Heinemann SH. Functional distinction of human EAG1 and EAG2 potassium channels. FEBS Lett 2002;**514**(2-3):204-8.

52.   Lin TF, Lin IW, Chen SC, Wu HH, Yang CS, Fang HY, Chiu MM, Jeng CJ. The subfamily-specific assembly of Eag and Erg K+ channels is determined by both the amino and the carboxyl recognition domains. J Biol Chem 2014;**289**(33):22815-22834.

53.   Farrelly AM, Ro S, Callaghan BP, Khoyi MA, Fleming N, Horowitz B, Sanders KM, Keef KD. Expression and function of KCNH2 (HERG) in the human jejunum. Am J Physiol Gastrointest Liver Physiol 2003;**284**(6):G883-95.

54.   Rosati B, Marchetti P, Crociani O, Lecchi M, Lupi R, Arcangeli A, Olivotto M, Wanke E. Glucose- and arginine-induced insulin secretion by human pancreatic beta-cells: the role of HERG K(+) channels in firing and release. Faseb j 2000;**14**(15):2601-10.

55.   Lastraioli E, Guasti L, Crociani O, Polvani S, Hofmann G, Witchel H, Bencini L, Calistri M, Messerini L, Scatizzi M, Moretti R, Wanke E, Olivotto M, Mugnai G, Arcangeli A. herg1 gene and HERG1 protein are overexpressed in colorectal cancers and regulate cell invasion of tumor cells. Cancer Res 2004;**64**(2):606-11.

56.   Wang H, Zhang Y, Cao L, Han H, Wang J, Yang B, Nattel S, Wang Z. HERG K+ channel, a regulator of tumor cell apoptosis and proliferation. Cancer Res 2002;**62**(17):4843-8.

57.   Sanguinetti MC, Jiang C, Curran ME, Keating MT. A mechanistic link between an inherited and an acquired cardiac arrhythmia: HERG encodes the IKr potassium channel. Cell 1995;**81**(2):299-307.

58.   Trudeau MC, Warmke JW, Ganetzky B, Robertson GA. HERG, a human inward rectifier in the voltage-gated potassium channel family. Science 1995;**269**(5220):92-5.

59.   Keating MT, Sanguinetti MC. Molecular and cellular mechanisms of cardiac arrhythmias. Cell 2001;**104**(4):569-80.

60.   Curran ME, Splawski I, Timothy KW, Vincent GM, Green ED, Keating MT. A molecular basis for cardiac arrhythmia: HERG mutations cause long QT syndrome. Cell 1995;**80**(5):795-803.

61.   Anderson CL, Delisle BP, Anson BD, Kilby JA, Will ML, Tester DJ, Gong Q, Zhou Z, Ackerman MJ, January CT. Most LQT2 mutations reduce Kv11.1 (hERG) current by a class 2 (trafficking-deficient) mechanism. Circulation 2006;**113**(3):365-73.

62.   Guo J, Massaeli H, Xu J, Jia Z, Wigle JT, Mesaeli N, Zhang S. Extracellular K+ concentration controls cell surface density of IKr in rabbit hearts and of the HERG channel in human cell lines. J Clin Invest 2009;**119**(9):2745-57.

63.   Torres AM, Bansal PS, Sunde M, Clarke CE, Bursill JA, Smith DJ, Bauskin A, Breit SN, Campbell TJ, Alewood PF, Kuchel PW, Vandenberg JI. Structure of the HERG K+ channel S5P extracellular linker: role of an amphipathic alpha-helix in C-type inactivation. J Biol Chem 2003;**278**(43):42136-48.

64.   Spector PS, Curran ME, Zou A, Keating MT, Sanguinetti MC. Fast inactivation causes rectification of the IKr channel. J Gen Physiol 1996;**107**(5):611-9.

65.   Smith PL, Baukrowitz T, Yellen G. The inward rectification mechanism of the HERG cardiac potassium channel. Nature 1996;**379**(6568):833-6.

66.   Fan JS, Jiang M, Dun W, McDonald TV, Tseng GN. Effects of outer mouth mutations on hERG channel function: a comparison with similar mutations in the Shaker channel. Biophys J 1999;**76**(6):3128-40.

67.   Liu J, Zhang M, Jiang M, Tseng GN. Structural and functional role of the extracellular s5-p linker in the HERG potassium channel. J Gen Physiol 2002;**120**(5):723-37.

68.   Yellen G. The moving parts of voltage-gated ion channels. Q Rev Biophys 1998;**31**(3):239-95.

69.   Vandenberg JI, Walker BD, Campbell TJ. HERG K+ channels: friend and foe. Trends Pharmacol Sci 2001;**22**(5):240-6.

70.   Mitcheson JS, Chen J, Lin M, Culberson C, Sanguinetti MC. A structural basis for drug-induced long QT syndrome. Proc Natl Acad Sci U S A 2000;**97**(22):12329-33.

71.   Jiang M, Zhang M, Maslennikov IV, Liu J, Wu DM, Korolkova YV, Arseniev AS, Grishin EV, Tseng GN. Dynamic conformational changes of extracellular S5-P linkers in the hERG channel. J Physiol 2005;**569**(Pt 1):75-89.

72.   Dun W, Jiang M, Tseng GN. Allosteric effects of mutations in the extracellular S5-P loop on the gating and ion permeation properties of the hERG potassium channel. Pflugers Arch 1999;**439**(1-2):141-9.

73.   Korolkova YV, Bocharov EV, Angelo K, Maslennikov IV, Grinenko OV, Lipkin AV, Nosyreva ED, Pluzhnikov KA, Olesen SP, Arseniev AS, Grishin EV. New binding site on common molecular scaffold provides HERG channel specificity of scorpion toxin BeKm-1. J Biol Chem 2002;**277**(45):43104-9.

74.   Splawski I, Shen J, Timothy KW, Lehmann MH, Priori S, Robinson JL, Moss AJ, Schwartz PJ, Towbin JA, Vincent GM, Keating MT. Spectrum of mutations in long-QT syndrome genes. KVLQT1, HERG, SCN5A, KCNE1, and KCNE2. Circulation 2000;**102**(10):1178-85.

75.   Itoh H, Sakaguchi T, Ashihara T, Ding WG, Nagaoka I, Oka Y, Nakazawa Y, Yao T, Jo H, Ito M, Nakamura K, Ohe T, Matsuura H, Horie M. A novel KCNH2 mutation as a modifier for short QT interval. Int J Cardiol 2009;**137**(1):83-5.

76.   Redpath CJ, Green MS, Birnie DH, Gollob MH. Rapid genetic testing facilitating the diagnosis of short QT syndrome. Can J Cardiol 2009;**25**(4):e133-5.

77.   Shu L, Zhang W, Su G, Zhang J, Liu C, Xu J. Modulation of HERG K+ channels by chronic exposure to activators and inhibitors of PKA and PKC: actions independent of PKA and PKC phosphorylation. Cell Physiol Biochem 2013;**32**(6):1830-44.

78.   Cockerill SL, Tobin AB, Torrecilla I, Willars GB, Standen NB, Mitcheson JS. Modulation of hERG potassium currents in HEK-293 cells by protein kinase C. Evidence for direct phosphorylation of pore forming subunits. J Physiol 2007;**581**(Pt 2):479-93.

79.   Thomas D, Zhang W, Karle CA, Kathöfer S, Schöls W, Kübler W, Kiehn J. Deletion of protein kinase A phosphorylation sites in the HERG potassium channel inhibits activation shift by protein kinase A. J Biol Chem 1999;**274**(39):27457-62.

80.   Cui J, Melman Y, Palma E, Fishman GI, McDonald TV. Cyclic AMP regulates the HERG K(+) channel by dual pathways. Curr Biol 2000;**10**(11):671-4.

81.   Chen J, Sroubek J, Krishnan Y, Li Y, Bian J, McDonald TV. PKA phosphorylation of HERG protein regulates the rate of channel synthesis. Am J Physiol Heart Circ Physiol 2009;**296**(5):H1244-54.

82.   Ramström C, Chapman H, Viitanen T, Afrasiabi E, Fox H, Kivelä J, Soini S, Korhonen L, Lindholm D, Pasternack M, Törnquist K. Regulation of HERG (KCNH2) potassium channel surface expression by diacylglycerol. Cell Mol Life Sci 2010;**67**(1):157-69.

83.   Shi YQ, Yan M, Liu LR, Zhang X, Wang X, Geng HZ, Zhao X, Li BX. High Glucose Represses hERG K+ Channel Expression through Trafficking Inhibition. Cell Physiol Biochem 2015;**37**(1):284-96.

84.   Lin J, Lin S, Choy PC, Shen X, Deng C, Kuang S, Wu J, Xu W. The regulation of the cardiac potassium channel (HERG) by caveolin-1. Biochem Cell Biol 2008;**86**(5):405-15.

85.   Munoz C, Saxena A, Pakladok T, Bogatikov E, Wilmes J, Seebohm G, Föller M, Lang F. Stimulation of HERG channel activity by β-catenin. PLoS One 2012;**7**(8):e43353.

86.   Lamothe SM, Song W, Guo J, Li W, Yang T, Baranchuk A, Graham CH, Zhang S. Hypoxia reduces mature hERG channels through calpain up-regulation. Faseb j 2017;**31**(11):5068-5077.

87.   Jiang M, Dun W, Tseng GN. Mechanism for the effects of extracellular acidification on HERG-channel function. Am J Physiol 1999;**277**(4):H1283-92.

88.   Zhou Q, Bett GC. Regulation of the voltage-insensitive step of HERG activation by extracellular pH. Am J Physiol Heart Circ Physiol 2010;**298**(6):H1710-8.

89.   Zhou Z, Gong Q, Ye B, Fan Z, Makielski JC, Robertson GA, January CT. Properties of HERG channels stably expressed in HEK 293 cells studied at physiological temperature. Biophys J 1998;**74**(1):230-41.

90.   Wang J, Della Penna K, Wang H, Karczewski J, Connolly TM, Koblan KS, Bennett PB, Salata JJ. Functional and pharmacological properties of canine ERG potassium channels. Am J Physiol Heart Circ Physiol 2003;**284**(1):H256-67.

91.   Ramalho D, Freitas J. Drug-induced life-threatening arrhythmias and sudden cardiac death: A clinical perspective of long QT, short QT and Brugada syndromes. Rev Port Cardiol 2018;**37**(5):435-446.

92.   Schimpf R, Veltmann C, Papavassiliu T, Rudic B, Göksu T, Kuschyk J, Wolpert C, Antzelevitch C, Ebner A, Borggrefe M, Brandt C. Drug-induced QT-interval shortening following antiepileptic treatment with oral rufinamide. Heart Rhythm 2012;**9**(5):776-81.

93.   Shah RR. Drug-induced QT interval shortening: potential harbinger of proarrhythmia and regulatory perspectives. Br J Pharmacol 2010;**159**(1):58-69.

94.   Evans MJ, Kaufman MH. Establishment in culture of pluripotential cells from mouse embryos. Nature 1981;**292**(5819):154-6.

95.   Thomson JA, Itskovitz-Eldor J, Shapiro SS, Waknitz MA, Swiergiel JJ, Marshall VS, Jones JM. Embryonic stem cell lines derived from human blastocysts. Science 1998;**282**(5391):1145-7.

96.   Takahashi K, Yamanaka S. Induction of pluripotent stem cells from mouse embryonic and adult fibroblast cultures by defined factors. Cell 2006;**126**(4):663-76.

97.   Takahashi K, Tanabe K, Ohnuki M, Narita M, Ichisaka T, Tomoda K, Yamanaka S. Induction of pluripotent stem cells from adult human fibroblasts by defined factors. Cell 2007;**131**(5):861-72.

98.   Narazaki G, Uosaki H, Teranishi M, Okita K, Kim B, Matsuoka S, Yamanaka S, Yamashita JK. Directed and systematic differentiation of cardiovascular cells from mouse induced pluripotent stem cells. Circulation 2008;**118**(5):498-506.

99.   Zhao Z, Lan H, El-Battrawy I, Li X, Buljubasic F, Sattler K, Yücel G, Lang S, Tiburcy M, Zimmermann WH, Cyganek L, Utikal J, Wieland T, Borggrefe M, Zhou XB, Akin I. Ion Channel Expression and Characterization in Human Induced Pluripotent Stem Cell-Derived Cardiomyocytes. Stem Cells Int 2018;**2018**:6067096.

100.   Sinnecker D, Goedel A, Dorn T, Dirschinger RJ, Moretti A, Laugwitz KL. Modeling long-QT syndromes with iPS cells. J Cardiovasc Transl Res 2013;**6**(1):31-6.

101.   Moretti A, Bellin M, Welling A, Jung CB, Lam JT, Bott-Flügel L, Dorn T, Goedel A, Höhnke C, Hofmann F, Seyfarth M, Sinnecker D, Schömig A, Laugwitz KL. Patient-specific induced pluripotent stem-cell models for long-QT syndrome. N Engl J Med 2010;**363**(15):1397-409.

102.   El-Battrawy I, Albers S, Cyganek L, Zhao Z, Lan H, Li X, Xu Q, Kleinsorge M, Huang M, Liao Z, Zhong R, Rudic B, Muller J, Dinkel H, Lang S, Diecke S, Zimmermann WH, Utikal J, Wieland T, Borggrefe M, Zhou X, Akin I. A cellular model of Brugada syndrome with SCN10A variants using human-induced pluripotent stem cell-derived cardiomyocytes. Europace 2019;**21**(9):1410-1421.

103.   Liang P, Sallam K, Wu H, Li Y, Itzhaki I, Garg P, Zhang Y, Vermglinchan V, Lan F, Gu M, Gong T, Zhuge Y, He C, Ebert AD, Sanchez-Freire V, Churko J, Hu S, Sharma A, Lam CK, Scheinman MM, Bers DM, Wu JC. Patient-Specific and Genome-Edited Induced Pluripotent Stem Cell-Derived Cardiomyocytes Elucidate Single-Cell Phenotype of Brugada Syndrome. J Am Coll Cardiol 2016;**68**(19):2086-2096.

104.   El-Battrawy I, Zhao Z, Lan H, Cyganek L, Tombers C, Li X, Buljubasic F, Lang S, Tiburcy M, Zimmermann WH, Utikal J, Wieland T, Borggrefe M, Zhou XB, Akin I. Electrical dysfunctions in human-induced pluripotent stem cell-derived cardiomyocytes from a patient with an arrhythmogenic right ventricular cardiomyopathy. Europace 2018;**20**(Fi1):f46-f56.

105.   Xia S, Wang X, Yue P, Li Y, Zhang D. Establishment of induced pluripotent stem cell lines from a family of an ARVC patient receiving heart transplantation in infant age carrying compound heterozygous mutations in DSP gene. Stem Cell Res 2020;**48**:101977.

106.   Shah D, Virtanen L, Prajapati C, Kiamehr M, Gullmets J, West G, Kreutzer J, Pekkanen-Mattila M, Heliö T, Kallio P, Taimen P, Aalto-Setälä K. Modeling of LMNA-Related Dilated Cardiomyopathy Using Human Induced Pluripotent Stem Cells. Cells 2019;**8**(6).

107.   Wu H, Yang H, Rhee JW, Zhang JZ, Lam CK, Sallam K, Chang ACY, Ma N, Lee J, Zhang H, Blau HM, Bers DM, Wu JC. Modelling diastolic dysfunction in induced pluripotent stem cell-derived cardiomyocytes from hypertrophic cardiomyopathy patients. Eur Heart J 2019;**40**(45):3685-3695.

108.   Borchert T, Hübscher D, Guessoum CI, Lam TD, Ghadri JR, Schellinger IN, Tiburcy M, Liaw NY, Li Y, Haas J, Sossalla S, Huber MA, Cyganek L, Jacobshagen C, Dressel R, Raaz U, Nikolaev VO, Guan K, Thiele H, Meder B, Wollnik B, Zimmermann WH, Lüscher TF, Hasenfuss G, Templin C, Streckfuss-Bömeke K. Catecholamine-Dependent β-Adrenergic Signaling in a Pluripotent Stem Cell Model of Takotsubo Cardiomyopathy. J Am Coll Cardiol 2017;**70**(8):975-991.

109.   Yücel G, Zhao Z, El-Battrawy I, Lan H, Lang S, Li X, Buljubasic F, Zimmermann WH, Cyganek L, Utikal J, Ravens U, Wieland T, Borggrefe M, Zhou XB, Akin I. Lipopolysaccharides induced inflammatory

responses and electrophysiological dysfunctions in human-induced pluripotent stem cell derived cardiomyocytes. Sci Rep 2017;**7**(1):2935.

110.   Plociennikowska A, Hromada-Judycka A, Dembinska J, Roszczenko P, Ciesielska A, Kwiatkowska K. Contribution of CD14 and TLR4 to changes of the PI(4,5)P2 level in LPS-stimulated cells. J Leukoc Biol 2016;**100**(6):1363-1373.

111.   Lu Y, Liu J, Liu Y, Qin Y, Luo Q, Wang Q, Duan H. TLR4 plays a crucial role in MSC-induced inhibition of NK cell function. Biochem Biophys Res Commun 2015;**464**(2):541-7.

112.   Cyganek L, Tiburcy M, Sekeres K, Gerstenberg K, Bohnenberger H, Lenz C, Henze S, Stauske M, Salinas G, Zimmermann WH, Hasenfuss G, Guan K. Deep phenotyping of human induced pluripotent stem cell-derived atrial and ventricular cardiomyocytes. JCI Insight 2018;**3**(12).

113.   Tiburcy M, Zimmermann WH. Modeling myocardial growth and hypertrophy in engineered heart muscle. Trends Cardiovasc Med 2014;**24**(1):7-13.

114.   Amin AS, Herfst LJ, Delisle BP, Klemens CA, Rook MB, Bezzina CR, Underkofler HA, Holzem KM, Ruijter JM, Tan HL, January CT, Wilde AA. Fever-induced QTc prolongation and ventricular arrhythmias in individuals with type 2 congenital long QT syndrome. J Clin Invest 2008;**118**(7):2552-61.

115.   Cai H, Griendling KK, Harrison DG. The vascular NAD(P)H oxidases as therapeutic targets in cardiovascular diseases. Trends Pharmacol Sci 2003;**24**(9):471-8.

116.   Schimpf R, Wolpert C, Gaita F, Giustetto C, Borggrefe M. Short QT syndrome. Cardiovasc Res 2005;**67**(3):357-66.

117.   Shinnawi R, Shaheen N, Huber I, Shiti A, Arbel G, Gepstein A, Ballan N, Setter N, Tijsen AJ, Borggrefe M, Gepstein L. Modeling Reentry in the Short QT Syndrome With Human-Induced Pluripotent Stem Cell-Derived Cardiac Cell Sheets. J Am Coll Cardiol 2019;**73**(18):2310-2324.

118.   El-Sherif N, Turitto G, Boutjdir M. Congenital Long QT syndrome and torsade de pointes. Ann Noninvasive Electrocardiol 2017;**22**(6).

119.   Fozzard HA. Afterdepolarizations and triggered activity. Basic Res Cardiol 1992;**87 Suppl 2**:105-13.

120.   Wilson D, Ermentrout B, Němec J, Salama G. A model of cardiac ryanodine receptor gating predicts experimental Ca(2+)-dynamics and Ca(2+)-triggered arrhythmia in the long QT syndrome. Chaos 2017;**27**(9):093940.

121.   Cordeiro JM, Brugada R, Wu YS, Hong K, Dumaine R. Modulation of I(Kr) inactivation by mutation N588K in KCNH2: a link to arrhythmogenesis in short QT syndrome. Cardiovasc Res 2005;**67**(3):498-509.

122.   Hancox JC, Levi AJ, Witchel HJ. Time course and voltage dependence of expressed HERG current compared with native "rapid" delayed rectifier K current during the cardiac ventricular action potential. Pflugers Arch 1998;**436**(6):843-53.

123.   Lu Y, Mahaut-Smith MP, Varghese A, Huang CL, Kemp PR, Vandenberg JI. Effects of premature stimulation on HERG K(+) channels. J Physiol 2001;**537**(Pt 3):843-51.

124.   El-Battrawy I, Lan H, Cyganek L, Zhao Z, Li X, Buljubasic F, Lang S, Yucel G, Sattler K, Zimmermann WH, Utikal J, Wieland T, Ravens U, Borggrefe M, Zhou XB, Akin I. Modeling Short QT

Syndrome Using Human-Induced Pluripotent Stem Cell-Derived Cardiomyocytes. J Am Heart Assoc 2018;**7**(7).

125. Hirayama Y, Kuruma A, Hiraoka M, Kawano S. Calcium-activated CL- current is enhanced by acidosis and contributes to the shortening of action potential duration in rabbit ventricular myocytes. Jpn J Physiol 2002;**52**(3):293-300.

126. Terai T, Furukawa T, Katayama Y, Hiraoka M. Effects of external acidosis on HERG current expressed in Xenopus oocytes. J Mol Cell Cardiol 2000;**32**(1):11-21.

127. Du CY, Adeniran I, Cheng H, Zhang YH, El Harchi A, McPate MJ, Zhang H, Orchard CH, Hancox JC. Acidosis impairs the protective role of hERG K(+) channels against premature stimulation. J Cardiovasc Electrophysiol 2010;**21**(10):1160-9.

128. Zhao Y, Wang T, Guo J, Yang T, Li W, Koichopolos J, Lamothe SM, Kang Y, Ma A, Zhang S. Febrile temperature facilitates hERG/IKr degradation through an altered K(+) dependence. Heart Rhythm 2016;**13**(10):2004-11.

129. Vonderlin N, Siebermair J, Kaya E, Köhler M, Rassaf T, Wakili R. Critical inflammatory mechanisms underlying arrhythmias. Herz 2019;**44**(2):121-129.

130. Aoki Y, Hatakeyama N, Yamamoto S, Kinoshita H, Matsuda N, Hattori Y, Yamazaki M. Role of ion channels in sepsis-induced atrial tachyarrhythmias in guinea pigs. Br J Pharmacol 2012;**166**(1):390-400.

131. Monnerat-Cahli G, Alonso H, Gallego M, Alarcón ML, Bassani RA, Casis O, Medei E. Toll-like receptor 4 activation promotes cardiac arrhythmias by decreasing the transient outward potassium current (Ito) through an IRF3-dependent and MyD88-independent pathway. J Mol Cell Cardiol 2014;**76**:116-25.

132. Wondergem R, Graves BM, Li C, Williams DL. Lipopolysaccharide prolongs action potential duration in HL-1 mouse cardiomyocytes. Am J Physiol Cell Physiol 2012;**303**(8):C825-33.

133. Shang F, Zhao L, Zheng Q, Wang J, Xu Z, Liang W, Liu H, Liu S, Zhang L. Simvastatin inhibits lipopolysaccharide-induced tumor necrosis factor-alpha expression in neonatal rat cardiomyocytes: The role of reactive oxygen species. Biochem Biophys Res Commun 2006;**351**(4):947-52.

134. Huang J, Peng W, Zheng Y, Hao H, Li S, Yao Y, Ding Y, Zhang J, Lyu J, Zeng Q. Upregulation of UCP2 Expression Protects against LPS-Induced Oxidative Stress and Apoptosis in Cardiomyocytes. Oxid Med Cell Longev 2019;**2019**:2758262.

135. Wang HJ, Li YL, Zhang LB, Zucker IH, Gao L, Zimmerman MC, Wang W. Endogenous reactive oxygen species modulates voltage-gated sodium channels in dorsal root ganglia of rats. J Appl Physiol (1985) 2011;**110**(5):1439-47.

136. Liu M, Liu H, Dudley SC, Jr. Reactive oxygen species originating from mitochondria regulate the cardiac sodium channel. Circ Res 2010;**107**(8):967-74.

137. Trum M, Islam MMT, Lebek S, Baier M, Hegner P, Eaton P, Maier LS, Wagner S. Inhibition of cardiac potassium currents by oxidation-activated protein kinase A contributes to early afterdepolarizations in the heart. Am J Physiol Heart Circ Physiol 2020;**319**(6):H1347-h1357.

138. Santos-Miranda A, Joviano-Santos JV, Ribeiro GA, Botelho AFM, Rocha P, Vieira LQ, Cruz JS, Roman-Campos D. Reactive oxygen species and nitric oxide imbalances lead to in vivo and in vitro

arrhythmogenic phenotype in acute phase of experimental Chagas disease. PLoS Pathog 2020;**16**(3):e1008379.

139. Chen Y, Yin C, Yang Y, Fan Z, Shang J, Tan W. Inhibition of rapid delayed rectifier potassium current (I(Kr)) by ischemia/reperfusion and its recovery by vitamin E in ventricular myocytes. J Electrocardiol 2017;**50**(4):437-443.

140. Perrin MJ, Kuchel PW, Campbell TJ, Vandenberg JI. Drug binding to the inactivated state is necessary but not sufficient for high-affinity binding to human ether-à-go-go-related gene channels. Mol Pharmacol 2008;**74**(5):1443-52.

141. Miller DC, Harmer SC, Poliandri A, Nobles M, Edwards EC, Ware JS, Sharp TV, McKay TR, Dunkel L, Lambiase PD, Tinker A. Ajmaline blocks INa and IKr without eliciting differences between Brugada syndrome patient and control human pluripotent stem cell-derived cardiac clusters. Stem Cell Res 2017;**25**:233-244.

142. Bebarova M, Matejovic P, Pasek M, Simurdova M, Simurda J. Effect of ajmaline on transient outward current in rat ventricular myocytes. Gen Physiol Biophys 2005;**24**(1):27-45.

143. Kiesecker C, Zitron E, Lück S, Bloehs R, Scholz EP, Kathöfer S, Thomas D, Kreye VA, Katus HA, Schoels W, Karle CA, Kiehn J. Class Ia anti-arrhythmic drug ajmaline blocks HERG potassium channels: mode of action. Naunyn Schmiedebergs Arch Pharmacol 2004;**370**(6):423-35.

144. Frommeyer G, Weller J, Ellermann C, Kaese S, Kochhauser S, Lange PS, Dechering DG, Eckardt L. Antiarrhythmic properties of ivabradine in an experimental model of Short-QT- Syndrome. Clin Exp Pharmacol Physiol 2017;**44**(9):941-945.

145. Lees-Miller JP, Guo J, Wang Y, Perissinotti LL, Noskov SY, Duff HJ. Ivabradine prolongs phase 3 of cardiac repolarization and blocks the hERG1 (KCNH2) current over a concentration-range overlapping with that required to block HCN4. J Mol Cell Cardiol 2015;**85**:71-8.

146. Melgari D, Brack KE, Zhang C, Zhang Y, El Harchi A, Mitcheson JS, Dempsey CE, Ng GA, Hancox JC. hERG potassium channel blockade by the HCN channel inhibitor bradycardic agent ivabradine. J Am Heart Assoc 2015;**4**(4).

147. Frommeyer G, Garthmann J, Ellermann C, Dechering DG, Kochhauser S, Reinke F, Kobe J, Wasmer K, Eckardt L. Broad antiarrhythmic effect of mexiletine in different arrhythmia models. Europace 2017.

148. Gualdani R, Tadini-Buoninsegni F, Roselli M, Defrenza I, Contino M, Colabufo NA, Lentini G. Inhibition of hERG potassium channel by the antiarrhythmic agent mexiletine and its metabolite m-hydroxymexiletine. Pharmacol Res Perspect 2015;**3**(5):e00160.

149. Milberg P, Tegelkamp R, Osada N, Schimpf R, Wolpert C, Breithardt G, Borggrefe M, Eckardt L. Reduction of dispersion of repolarization and prolongation of postrepolarization refractoriness explain the antiarrhythmic effects of quinidine in a model of short QT syndrome. J Cardiovasc Electrophysiol 2007;**18**(6):658-64.

150. Melgari D, Zhang Y, El Harchi A, Dempsey CE, Hancox JC. Molecular basis of hERG potassium channel blockade by the class Ic antiarrhythmic flecainide. J Mol Cell Cardiol 2015;**86**:42-53.

151. Paul AA, Witchel HJ, Hancox JC. Inhibition of the current of heterologously expressed HERG potassium channels by flecainide and comparison with quinidine, propafenone and lignocaine. Br J Pharmacol 2002;**136**(5):717-29.

152.   Frommeyer G, Schmidt M, Clauss C, Kaese S, Stypmann J, Pott C, Eckardt L, Milberg P. Further insights into the underlying electrophysiological mechanisms for reduction of atrial fibrillation by ranolazine in an experimental model of chronic heart failure. Eur J Heart Fail 2012;**14**(12):1322-31.

153.   Burashnikov A, Belardinelli L, Antzelevitch C. Atrial-selective sodium channel block strategy to suppress atrial fibrillation: ranolazine versus propafenone. J Pharmacol Exp Ther 2012;**340**(1):161-8.

154.   Frommeyer G, Ellermann C, Dechering DG, Kochhäuser S, Bögeholz N, Güner F, Leitz P, Pott C, Eckardt L. Ranolazine and Vernakalant Prevent Ventricular Arrhythmias in an Experimental Whole-Heart Model of Short QT Syndrome. J Cardiovasc Electrophysiol 2016;**27**(10):1214-1219.

155.   Antzelevitch C, Belardinelli L, Wu L, Fraser H, Zygmunt AC, Burashnikov A, Di Diego JM, Fish JM, Cordeiro JM, Goodrow RJ, Jr., Scornik F, Perez G. Electrophysiologic properties and antiarrhythmic actions of a novel antianginal agent. J Cardiovasc Pharmacol Ther 2004;**9 Suppl 1**:S65-83.

156.   Schram G, Zhang L, Derakhchan K, Ehrlich JR, Belardinelli L, Nattel S. Ranolazine: ion-channel-blocking actions and in vivo electrophysiological effects. Br J Pharmacol 2004;**142**(8):1300-8.

157.   Du C, Zhang Y, El Harchi A, Dempsey CE, Hancox JC. Ranolazine inhibition of hERG potassium channels: drug-pore interactions and reduced potency against inactivation mutants. J Mol Cell Cardiol 2014;**74**(100):220-30.

158.   Rajamani S, Shryock JC, Belardinelli L. Rapid kinetic interactions of ranolazine with HERG K+ current. J Cardiovasc Pharmacol 2008;**51**(6):581-9.

7. CURRICULUM VITAE

PERSONAL DETAILS

Family name and first name:	Li, Xin
Birthday:	09.01.1987
Place of birth:	Sichuan China
Father:	Li, Xiao
Mather:	Xin, Dongyan
Spouse:	Zhang, Huimin

SCHOOL EDUCATION

09.2002-06.2005	Nanchong Senior High School, Nanchong, China

UNIVERSITY EDUCATION

09.2005-07.2009	Southwest University, Chongqing, China Bachelor
09.2010-07.2013	Chongqing Medical University, Chongqing, China Master
05.2017-Now	First Department of Medicine, Medical Faculty Mannheim, University of Heidelberg PhD (Dr. sc. hum) student

PROFESSIONAL EXPERIENCE

07.2013-Now	Chengdu University of Traditional Chinese Medicine, Chengdu, China Assistant

8. ACKNOWLEDGEMENTS

9. PUBLICATIONS (*co-first author)

1. Huang M*, Liao Z*, **Li X***, Yang Z, Fan X, Li Y, Zhao Z, Lang S, Cyganek L, Zhou X, Akin I, Borggrefe M, El-Battrawy I. Effects of Antiarrhythmic Drugs on hERG Gating in Human-Induced Pluripotent Stem Cell-Derived Cardiomyocytes From a Patient With Short QT Syndrome Type 1. *Front Pharmacol.* 2021 May 7;12:675003. doi: 10.3389/fphar.2021.675003. eCollection 2021

2. Zhao Z*, **Li X***, El-Battrawy I, Lan H, Zhong R, Xu Q, Huang M, Liao Z, Lang S, Zimmermann WH, Cyganek L, Wieland T, Akin I, Zhou XB, Borggrefe M. Drug Testing in Human-Induced Pluripotent Stem Cell-Derived Cardiomyocytes From a Patient With Short QT Syndrome Type 1. *Clin Pharmacol Ther.* **2019** Sep;106(3):642-651. doi: 10.1002/cpt.1449. Epub 2019 May 13. PMID: 30947366

3. Wiedmann F, Beyersdorf C, Zhou XB, Kraft M, Paasche A, Jávorszky N, Rinné S, Sutanto H, Büscher A, Foerster KI, Blank A, El-Battrawy I, **Li X**, Lang S, Tochtermann U, Kremer J, Arif R, Karck M, Decher N, van Loon G, Akin I, Borggrefe M, Kallenberger S, Heijman J, Haefeli WE, Katus HA, Schmidt C. Treatment of atrial fibrillation with doxapram: TASK-1 potassium channel inhibition as a novel pharmacological strategy. *Cardiovasc Res.* 2021 May 24:cvab177. doi: 10.1093/cvr/cvab177. Online ahead of print.

4. Huang M, Fan X, Yang Z, Cyganek L, **Li X**, Yuecel G, Lan H, Li Y, Wendel A, Lang S, Bieback K, El-Battrawy I, Zhou X, Akin I, Borggrefe M. Alpha 1-adrenoceptor signalling contributes to toxic effects of catecholamine on electrical properties in cardiomyocytes. *Europace.* 2021 Feb 19:euab008. doi: 10.1093/europace/euab008. Online ahead of print.

5. Lan H, Xu Q, El-Battrawy I, Zhong R, **Li X**, Lang S, Cyganek L, Borggrefe M, Zhou X, Akin I. Ionic Mechanisms of Disopyramide Prolonging Action Potential Duration in Human-Induced Pluripotent Stem Cell-Derived Cardiomyocytes From a Patient With Short QT Syndrome Type 1. *Front Pharmacol.* 2020 Oct 12;11:554422. doi: 10.3389/fphar.2020.554422. eCollection 2020..

6. Buljubasic F, El-Battrawy I, Lan H, Lomada SK, Chatterjee A, Zhao Z, **Li X**, Zhong R, Xu Q, Huang M, Liao Z, Lang S, Cyganek L, Zhou X, Wieland T,

Borggrefe M, Akin I. <u>Nucleoside Diphosphate Kinase B Contributes to Arrhythmogenesis in Human-Induced Pluripotent Stem Cell-Derived Cardiomyocytes from a Patient with Arrhythmogenic Right Ventricular Cardiomyopathy.</u> *J Clin Med.* **2020 Feb** 10;9(2):486. doi: 10.3390/jcm9020486. PMID: 32050722

7. El-Battrawy I, Müller J, Zhao Z, Cyganek L, Zhong R, Zhang F, Kleinsorge M, Lan H, **Li X**, Xu Q, Huang M, Liao Z, Moscu-Gregor A, Albers S, Dinkel H, Lang S, Diecke S, Zimmermann WH, Utikal J, Wieland T, Borggrefe M, Zhou X, Akin I. <u>Studying Brugada Syndrome With an SCN1B Variants in Human-Induced Pluripotent Stem Cell-Derived Cardiomyocytes.</u> *Front Cell Dev Biol.* **2019 Nov** 1;7:261. doi: 10.3389/fcell.2019.00261. eCollection 2019. PMID: 31737628

8. Schmidt C, Wiedmann F, Beyersdorf C, Zhao Z, El-Battrawy I, Lan H, Szabo G, **Li X**, Lang S, Korkmaz-Icöz S, Rapti K, Jungmann A, Ratte A, Müller OJ, Karck M, Seemann G, Akin I, Borggrefe M, Zhou XB, Katus HA, Thomas D. <u>Genetic Ablation of TASK-1 (Tandem of P Domains in a Weak Inward Rectifying K$^+$ Channel-Related Acid-Sensitive K$^+$ Channel-1) (K$_{2P}$3.1) K$^+$ Channels Suppresses Atrial Fibrillation and Prevents Electrical Remodeling.</u> *Circ Arrhythm Electrophysiol.* **2019 Sep;**12(9):e007465. doi: 10.1161/CIRCEP.119.007465. Epub 2019 Sep 13. PMID: 31514528

9. El-Battrawy I, Albers S, Cyganek L, Zhao Z, Lan H, **Li X**, Xu Q, Kleinsorge M, Huang M, Liao Z, Zhong R, Rudic B, Müller J, Dinkel H, Lang S, Diecke S, Zimmermann WH, Utikal J, Wieland T, Borggrefe M, Zhou X, Akin I. <u>A cellular model of Brugada syndrome with SCN10A variants using human-induced pluripotent stem cell-derived cardiomyocytes.</u> *Europace.* **2019 Sep** 1;21(9):1410-1421. doi: 10.1093/europace/euz122. PMID: 31106349

10. El-Battrawy I, Besler J, **Li X**, Lan H, Zhao Z, Liebe V, Schimpf R, Lang S, Wolpert C, Zhou X**,** Akin I, Borggrefe M. <u>Impact of Antiarrhythmic Drugs on the Outcome of Short QT Syndrome.</u> *Front Pharmacol.* **2019 Aug** 2;10:771. doi: 10.3389/fphar.2019.00771. eCollection 2019. PMID: 31427960

11. Sattler K, El-Battrawy I, Zhao Z, Schrottenberg C, Yücel G, Lan H, **Li X**, Lang S, Zimmermann WH, Cyganek L, Utikal J, Wieland T, Ravens U, Bieback K, Borggrefe M, Zhou X, Akin I. <u>Serum of patients with acute myocardial</u>

infarction prevents inflammation in iPSC-cardiomyocytes. *Sci Rep*. **2019 Apr** 4;9(1):5651. doi: 10.1038/s41598-019-42079-z. PMID: 30948775

12. El-Battrawy I, Lan H, Cyganek L, Zhao Z, **Li X**, Buljubasic F, Lang S, Yücel G, Sattler K, Zimmermann WH, Utikal J, Wieland T, Ravens U, Borggrefe M, Zhou XB, Akin I. Modeling Short QT Syndrome Using Human-Induced Pluripotent Stem Cell-Derived Cardiomyocytes. *J Am Heart Assoc*. 2018 Mar 24;7(7):e007394. doi: 10.1161/JAHA.117.007394.

13. El-Battrawy I, Zhao Z, Lan H, Cyganek L, Tombers C, **Li X**, Buljubasic F, Lang S, Tiburcy M, Zimmermann WH, Utikal J, Wieland T, Borggrefe M, Zhou XB, Akin I. Electrical dysfunctions in human-induced pluripotent stem cell-derived cardiomyocytes from a patient with an arrhythmogenic right ventricular cardiomyopathy. *Europace*. 2018 Jun 1;20(FI1):f46-f56. doi: 10.1093/europace/euy042.

14. El-Battrawy I, Zhao Z, Lan H, **Li X**, Yücel G, Lang S, Sattler K, Schünemann JD, Zimmermann WH, Cyganek L, Utikal J, Wieland T, Bieback K, Bauer R, Ratte A, Pribe-Wolferts R, Rapti K, Nowak D, Wittig J, Thomas D, Most P, Katus HA, Ravens U, Schmidt C, Borggrefe M, Zhou XB, Müller OJ, Akin I. Ion Channel Dysfunctions in Dilated Cardiomyopathy in Limb-Girdle Muscular Dystrophy. *Circ Genom Precis Med*. 2018 Mar;11(3):e001893. doi: 10.1161/CIRCGEN.117.001893.

15. Zhao Z, Lan H, El-Battrawy I, **Li X**, Buljubasic F, Sattler K, Yücel G, Lang S, Tiburcy M, Zimmermann WH, Cyganek L, Utikal J, Wieland T, Borggrefe M, Zhou XB, Akin I. Ion Channel Expression and Characterization in Human Induced Pluripotent Stem Cell-Derived Cardiomyocytes. *Stem Cells Int*. 2018 Jan 8;2018:6067096. doi: 10.1155/2018/6067096. eCollection 2018.

16. El-Battrawy I, Zhao Z, Lan H, Schünemann JD, Sattler K, Buljubasic F, Patocskai B, **Li X**, Yücel G, Lang S, Nowak D, Cyganek L, Bieback K, Utikal J, Zimmermann WH, Ravens U, Wieland T, Borggrefe M, Zhou XB, Akin I. Estradiol protection against toxic effects of catecholamine on electrical properties in human-induced pluripotent stem cell derived cardiomyocytes. *Int J Cardiol*. 2018 Mar 1;254:195-202. doi: 10.1016/j.ijcard.2017.11.007. Epub 2018 Jan 28. PMID: 29407091

17. Yücel G, Zhao Z, El-Battrawy I, Lan H, Lang S, **Li X**, Buljubasic F, Zimmermann WH, Cyganek L, Utikal J, Ravens U, Wieland T, Borggrefe M,

Zhou XB, Akin I. Lipopolysaccharides induced inflammatory responses and electrophysiological dysfunctions in human-induced pluripotent stem cell derived cardiomyocytes. *Sci Rep*. 2017 Jun 7;7(1):2935. doi: 10.1038/s41598-017-03147-4.